Master Thesis, Department of Geosciences

Timescales of surface-to-tropopause transport in the tropics, using Flexpart

Eivind Grøtting Wærsted

UNIVERSITY OF OSLO
FACULTY OF MATHEMATICS AND NATURAL SCIENCES

Timescales of surface-to-tropopause transport in the tropics, using Flexpart

Eivind Grøtting Wærsted

Master Thesis in Geosciences

Discipline: Meteorology and Oceanography

Department of Geosciences

Faculty of Mathematics and Natural Sciences

University of Oslo

June 1, 2015

Abstract

The timescales of transport from the surface to the tropical tropopause layer (TTL) was studied using the Lagrangian transport model Flexpart. The model was driven by the ERA-Interim reanalysis from the European Center for Medium-Range Weather Forecasts (ECMWF). Trajectories were released each month in the period 1. June 2002 - 1. May 2013 at 15 km and 17 km over the whole tropics and simulated 90 days backward in time. The age of air at 15 km and 17 km relative to the last contact with the boundary layer (BL) was computed using a constant BL-height of 1 km above sea level. The aim of the study was to give a detailed description of the tropospheric age of air in the TTL, mainly motivated by the importance of transport timescales for the entry of short-lived compounds to the stratosphere.

Several sensitivity studies were carried out. The most important of these were the sensitivity to the use of the convection scheme in Flexpart. In the run without the convection scheme, the median age at 15 km was 17 day longer, and at 17 km 25 days longer, than in the runs using the convection scheme. In particular, the fraction of the air at 17 km younger than 10 days decreased with an order of magnitude, from 11.1 % to 0.9 %.

For 30°S - 30°N as a whole, the median age was 26 days at 15 km and 50 days at 17 km. A seasonal cycle in the age was found at both altitudes. The seasonal cycle was most pronounced at 17 km, where the median age varied by ∼14 days during the year, being highest in August and lowest in May. At both altitudes, the air was younger near the main convective areas in the tropics, such as the Intertropical Convergence Zone (ITCZ), with less young air approaching the subtropics. The air was particularly young above the tropical western Pacific; the median age there was only 16 days at 15 km and 30 days at 17 km. The air at both 15 km and 17 km was found to originate from the BL above the main convective regions in the tropics. In particular, the West and Central Pacific stood for 40-50 % of the BL-origins.

The age decreased over the period, both at 15 km and 17 km. The decrease in the annual median age during 2003-2012 was 2.0 days per decade at 15 km and 9.7 days per decade at 17 km (for 30°S - 30°N). Much of this decrease appeared to have taken place around 2009.

Interannual variability in the age above the tropical Pacific in December-February (DJF) was found to be related to the El Niño-Southern Oscillation (ENSO). The air was younger above the Pacific in El Niño and older in La Niña. A shift in the BL-origins above the Pacific ocean, eastward in El Niño and westward in La Niña, was also found.

Contents

Chapter 1

Introduction

The stratosphere is an important part of the atmosphere mainly due to the ozone layer, which absorbs UV-radiation from the sun that is harmful to plants and animals. The ozone layer is affected by halogens in the stratosphere, which act as catalysts for breaking down ozone (Jacob, 1999). Contrary to the long-lived man-made Clourofluorocarbons, so-called very short-lived substances (VSLS) containing halogens have life-times ranging from days to 6 months. Various VSLS are emitted from anthropogenic activity or natural processes, especially in the ocean. Due to their short lifetimes, and the solubility of their degradation products, which are rapidly removed by wash-out in the troposphere, the VSLS will only affect the stratosphere if transported from their location of emission to the stratosphere on short enough timescales (Montzka et al., 2010). The study of the timescales of the atmospheric transport from the surface to the stratosphere is therefore of interest.

The tropical tropopause is the main entrance region for air to the stratosphere, which was first suggested by Brewer (1949). The troposphere-to-stratosphere transport (TST) in the tropics is therefore of particular interest. Newell and Gould-Stewart (1981) lanced the stratospheric fountain theory: that the stratospheric entry is further confined to the West Pacific, Maritime Continent and, in Northern Hemisphere (NH) summer, the Indian monsoon region. The dryness of the stratosphere requires very low temperatures during TST, and these were only observed at the tropical tropopause in these regions. Later studies have found that these regions of coldest tropopause is indeed the dominating entry region to the stratosphere (Bonazzola and Haynes, 2004; Fueglistaler et al., 2005), and is highly collocated with the locations of the deepest convection (Gettelman et al., 2002).

In order to study transit times of air from the surface to the stratosphere, transport models can be utilized (Jacob, 1999). These models rely on a proper representation of the atmospheric processes of transport (advection, convection, mixing), which will not be perfectly correct on all scales. The results of transport models therefore have uncertainties.

An alternative approach is to use in situ measurements of atmospheric trace gases from air-craft campaigns to deduce where the air is coming from, and how old it is relative to the that source. For example, Park et al. (2007) used a "CO_2 tracer clock" approach, taking advantage of the seasonal cycle in surface CO_2 concentrations, which causes a rapid rise in the concentrations in January and February. Using air-craft measurements at several altitudes, they described the age of air relative to surface contact as function of height, by comparing the profile of CO_2 mixing ratios to the surface value. Although such measurement-based studies are limited in their spatial and temporal coverage, they are important for verifying and supplementing the results of studies based on transport models.

Several Eulerian and Lagrangian[1] modelling studies have estimated the transit times from

[1]The difference between the Eulerian and Lagrangian approach will be explained in Section 3.1.1.

the surface[2] to the tropical tropopause. Rex et al. (2014), using backward trajectories, estimated the tropospheric residence times for air entering the stratosphere in NH winter to be 20-100 days, a right-skewed distribution with a mode at 30-40 days. Berthet et al. (2007) found that ∼20 % of the air near the tropical tropopause was younger than 30 days. The Eulerian study of Patra et al. (2009) found the mean age of air to be around 60-100 days in regions of stratospheric entry at 100 hPa in the tropics. The transit times of TST are thus in the order of 1-3 months.

For the application to the transfer of VSLS to the stratosphere, it is the shortest timescales that are of most interest. Trajectory studies using an e-folding decrease of the modelled tracer have therefore been performed to investigate how much of the tracer can reach the stratosphere. Pisso et al. (2010) modelled trajectories released at the surface carrying a tracer with an e-folding decay time of 20 days. They found that the fraction of the original tracer that entered the stratosphere was highly sensitive to the geographical location it was released. The surface origins of the air entering the stratosphere is thus another important aspect, as they determine where surface emissions of short-lived compounds will be most important for the stratosphere. The locations where air undergoing TST was last near the surface have been investigated by other trajectory studies, such as Berthet et al. (2007) and Rex et al. (2014). They found that the main convective areas in the tropics are dominating the origins, indicating that deep convection is of importance for the transport. In particular, the West Pacific is a prominent source region, and in NH summer also the Indian Monsoon region. Equatorial Africa and South America appear as secondary maxima, and there are also contributions from other parts of the Intertropical Convergence Zone (ITCZ).

The studies on transport from the surface to the tropause mentioned above consider the timescales, but often this is only indirectly presented through fractions reaching the stratosphere in a given time (Berthet et al., 2007; Levine et al., 2007; Pisso et al., 2010). Many of the studies also lack the coverage of different years and seasons. Berthet et al. (2007) limited their study to 4 years and released trajectories only in the Norhtern Hemisphere. Pisso et al. (2010) only used January and July 2001, while Rex et al. (2014) had more years but only studied the transport in NH winter. A weakness with the studies of Berthet et al. (2007) and Rex et al. (2014) is that the vertical transport of air by convection on subgrid-scale, which is not resolved by global datasets (Berthet et al., 2007), was not parameterized. The current literature therefore cannot provide the climatological timescales of surface-to-tropopause transport in the tropics when subgrid-scale convective transport is accounted for, or the magnitudes of the seasonal and interannual variability of these timescales. A more detailed study on the age of the air in the tropical tropopause layer (TTL) is currently missing and is the scope of this study.

In this thesis, the timescales of the transport of air from the atmospheric boundary layer (BL) to altitudes in the TTL well above the level of main convective outflow are studied. The geographical locations where the air reaching these altitudes was last near the surface are also investigated. These characteristics, and their seasonal cycle and interannual variability, are studied for the period 2002-2013.

The Lagrangian transport model Flexpart is used to track air parcels in the TTL backward in time to their BL origins. This model includes parameterizations of subgrid-scale convective transport and turbulent mixing and is driven by the ERA-Interim reanalysis.

The thesis is structured as following: The theory about atmospheric circulation and transport modeling is given in Chapter 2. A presentation of the Flexpart model, the ERA-Interim reanalysis and how the model runs are set up and analysed, is provided in Chapter 3. Sensitivity studies of various aspects of the experimental setup are presented in Chapter 4. In Chapter 5, the results are presented and discussed, and the conclusions are given in Chapter 6.

[2]The lower level used varies between studies, depending on the modelling approach. It can be the surface, the atmospheric boundary layer (BL) top or a level in the middle troposphere. However, the timescales of the studies are still comparable, since vertical transport in the lower troposphere is much faster than near the tropopause (Patra et al., 2009).

Chapter 2

Theory

In this chapter, the background for the atmospheric circulation and transport processes relevant for this thesis will be presented. The vertical structure of the atmosphere and the phenomenon deep convection is introduced in Section 2.1. Section 2.2 describes the large-scale features of the tropospheric circulation in the tropics, and also shortly the stratospheric circulation. Section 2.3 describes the transport to the stratosphere through the tropical tropopause layer and the role of convection for this transport.

2.1 Vertical structure of the atmosphere

The atmosphere is conventionally separated into layers according to chemical and radiative properties, as explained by Marshall and Plumb (2008). The troposphere (lowest ∼15 km) and the stratosphere (∼15-50 km) are the two lowest of these layers, and together they contain more than 99 % of the atmospheric mass, with the majority in the troposphere. Solar radiation is mainly absorbed at the surface of the Earth, heating the troposphere from below. In the stratosphere, the absorption of the ultraviolet part of the solar radiation by ozone constitutes a heating source for the stratosphere. Between these two heating layers, less solar radiation is absorbed. This leads to a decrease in temperature with height in the troposphere, and an increases with height in the stratosphere. The border between the two is called the tropopause (see Figure 2.1). There are different tropopause definitions used for different purposes and at different latitudes (Ivanova, 2013). For the tropopause in the tropics, the cold point tropopause (CPT), which is the altitude of the observed temperature minimum in a vertical profile, is commonly used.

In the troposphere, especially in the tropics, there are frequently fast vertical motions referred to as convection (Wallace and Hobbs, 2006). In the rest of this section, the convection in the troposphere will be introduced.

2.1.1 Static stability

The theory on static stability is described by Wallace and Hobbs (2006). In essence, an air column is statically unstable when lighter warm air underlies denser cold air, so that exchanging them will lower their common mass center. However, due to the compressibility of air, stability considerations cannot be based on pure temperature comparisons. Because the atmosphere is in hydrostatic balance, the pressure decreases with height. If an air parcel rises, the decrease in pressure will cause it to expand and do work on the environment. The energy needed for the expansion cools the parcel. Conversely, a descending parcel will be warmed. For fast motions, this process is adiabatic[1], and if no water phase changes occur, the cooling rate with ascent follows the dry adiabatic lapse rate (∼9.8 K/km). An air column will therefore only be unstable

[1] In an adiabatic process, the exchange between the air parcel and the surroundings happens only through work

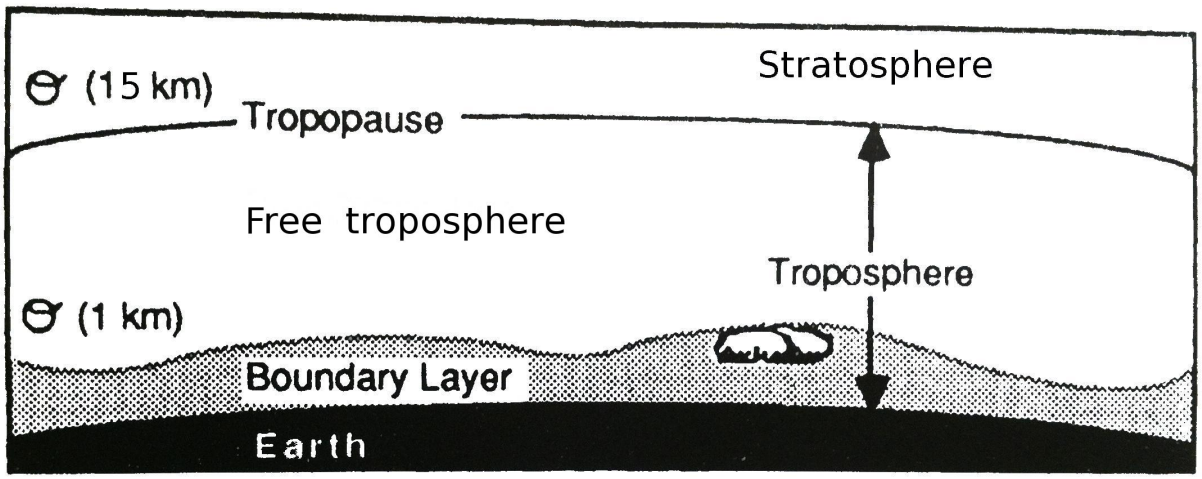

Figure 2.1: The vertical structure of the atmosphere. Modified from Stull (1988).

if the ambient temperature falls off more rapidly with height than the adiabatic lapse rate. When an air column becomes unstable, it will mix in the vertical to stabilize itself, and these vertical motions, induced by buoyancy, is called *convection*.

The potential temperature, θ, is a useful quantity when studying stability. It is the temperature an air parcel obtains if moved *adiabatically* to a reference pressure level (without any latent heat release, see below) and is therefore conserved in (dry) adiabatic processes. An air column is unstable if the potential temperature decreases with height, and the more rapidly θ increases with height, the more stable is the air column.

In moist conditions the stability theory described above is modified by the heat associated with phase changes of water. In addition to sensible heat exchange by BL turbulence, energy is also transported away from the surface by evaporation. Evaporation of liquid water to vapor requires heat, which is taken from the surface. Because the saturation pressure of water vapor increases strongly with temperature, a moist rising air parcel can eventually be cooled to saturation as it expands adiabatically. Further lifting after saturation is reached will cause condensation of vapor onto cloud droplets[2], which releases the same amount of heat as was taken for evaporation. This is called latent heat release, because the energy transferred from the surface is "hidden" in the vapor until it is released during condensation. Due to this heating, the saturated air parcel will increase its θ while rising and cool less than a dry parcel. The rate at which a saturated rising parcel cools is called the *saturated* adiabatic lapse rate. If the ambient temperature decreases less with height than the saturated adiabatic lapse rate, the rising parcel will become warmer than the environment and continue to rise from its own buoyancy; this is called *conditionally unstable* conditions.

2.1.2 Atmospheric boundary layer

The lowest part of the troposphere is called the planetary boundary layer (BL) (Stull, 1988). This is the layer whose dynamics and chemical composition is rapidly affected by the surface of the Earth (in timescales of an hour or less). The thickness of the BL is typically 1 km, but is quite variable both in space and time, ranging between about 100 m and 3 km. Turbulent motions, generated by buoyancy or suface wind stress, is the most important mechanism for vertical transport of heat, moisture and tracers in the BL. The BL can be unstable or stable. An unstable boundary layer occurs when the surface is warmer than the air, so that buoyancy drives rapid vertical motions. In these conditions the BL can be well-mixed in timescales as short as 10-15 minutes. When the surface is colder than the air, the BL becomes stable. This happens during clear nights above land or when warm air is advected over a colder surface. In

[2]If the air is colder than 0°C, ice particles may also form

these conditions turbulence is inhibited. The vertical mixing timescale is therefore longer, and can be as much as 30 hours. At the top of the BL, there is normally a stable layer (capping inversion) which acts like a lid to vertical motion, so that the air in the BL most of the time is relatively isolated from the troposphere above the BL, which is called the free troposphere.

Due to heating at the surface, the BL in the tropics is often unstable, but due to the stable layer at the top of the BL, the convective mixing is confined to the BL most of the time. However, when enough moisture and heating is provided from below, the air may eventually break through the stable layer. The free troposphere above is often conditionally unstable, allowing the ascending saturated plumes of air to continue to rise throughout the troposphere, forming a vast cumulonimbus cloud and heavy precipitation. If the convection extends all the way to the upper troposphere, where stability increases approaching the tropopause, it is called *deep* convection.

2.1.3 Deep convection

In this section the phenomenon deep convection is described, based on Wallace and Hobbs (2006) unless otherwise cited.

An idealized description of convection is shown in the thermodynamic diagram in Figure 2.2. The vertical profile[3] of temperature is provided as well as the humidity at the surface, and one assumes that a surface air parcel starts to rise adiabatically. As long as the air parcel is not saturated, it will cool according to the dry adiabatic lapse rate. Once it has left the mixed layer in the BL, it becomes colder than the environment, and it therefore depends on some external forcing for continued ascent. This could be provided by an approaching front, topographic lifting or some other phenomenon. If continuing to rise, the air parcel eventually cools to saturation. The level where this occurs is called the lifting condensation level (LCL). In further ascent, cooling is less rapid, following the saturated adiabatic lapse rate. If the surroundings are conditionally unstable, as in Figure 2.2, the temperature difference between the parcel and the environment will decrease and at some level become zero. This level is called the level of free convection (LFC). Further ascent will make the parcel warmer than the environment, and it is thus no longer depending on an external source of lifting, but continues to rise from its own buoyancy until it reaches a layer where the atmosphere is sufficiently stable so that ambient temperatures become warmer than the rising parcel. This level is called the level of neutral buoyancy (LNB), and from here, further ascent will be inhibited.

The thermodynamic chart used in Figure 2.2 has the property that the area between the curves correspond to the potential energy of buoyancy. Between the surface and the LFC, the potential energy of the rising air parcel is increasing, because the parcel is denser than the environment. The energy required to lift the parcel this distance is called the convective inhibition (CIN). Once above the LFC, potential energy is released in the lifting because the parcel is lighter than the environment. The potential energy released between the LFC and the LNB is called the convective available potential energy (CAPE). This energy will be transformed to kinetic energy in the rising air, so that the air parcel has a high vertical velocity when reaching the LNB and may *overshoot* this level, i.e. rising considerably higher before the negative buoyancy above the LNB has immobilized it.

The above description neglects many important characteristics of convection which alter how high the rising air can reach. A rising plume of buoyant air will induce turbulence at its boundaries, and considerable amounts of surronding air will entrain into it. This air is colder and dryer than the plume, and causes further cooling by evaporation of cloud droplets. The buoyancy in the rising air is therefore reduced so that the effective LNB is lower than its theoretical altitude. The distance that the updraft may overshoot the LNB is also reduced due to the frictional drag on the plume, which prevents all the CAPE to be transformed into kinetic energy.

[3]Note that the y-axis in Figure 2.2 corresponds approximately to the altitude due to the hydrostatic balance.

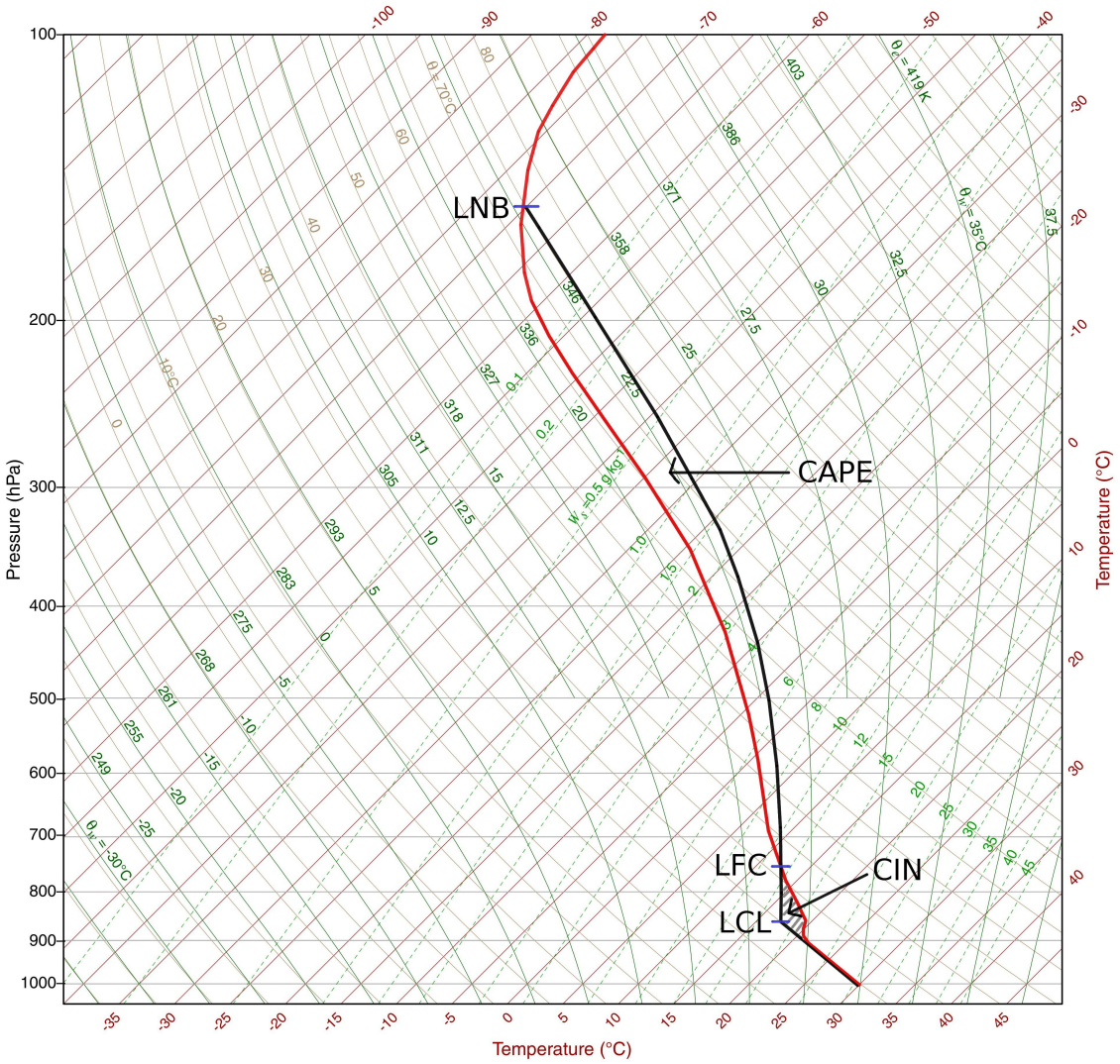

Figure 2.2: Thermodynamic diagram showing the dry adiabats (gold), saturated adiabats (green, solid) and isophlets of water vapor saturation mixing ratio (green dotted) as function of temperature and pressure. The red line is a (made up) example of a tropical temperature profile. The black lines illustrates the development of a deep convective updraft, with important levels and quantities indicated. See text for details. (Courtesy of Jennifer Adams, COLA (modified))

The structure of deep convection is also more complex than one rising plume. Within the updraft there are also areas of downward motion. These downdrafts are induced by the negative buoyancy of entrained air from the environment and the weight of precipitation particles. Moreover, convective systems often appear in bands or clusters, where many single cells of convection interact with each other. This is particularly the case when a vertical wind shear exists, so that the downdrafts and updrafts of a system are displaced from each other. The cold downdrafts can then activate new cells by colliding into warm surface air and providing the buoyant lift needed for that air to overcome its CIN. Outside of convective systems the air subsides, to compensate for the net upward mass flux within the convection, and the adiabatic heating of descent is compensated by radiative cooling. The areas of subsidence are usually much larger than the areas of convective updrafts, so that the subsidence vertical velocity is much weaker than the vigorous up- and downdrafts within the convective clouds.

Deep convection in the tropics usually reaches up to about 12-13 km, but the strongest convection can reach sevaral kilometers above these levels, and overshooting cells may even penetrate the tropopause in some rare events (Section 2.3.1). At the level where buoyant ascent

ceases (LNB), the air spreads out in the horizontal, forming an anvil-shaped cloud. This cloud will eventually be diluted and evaporate, but it can stay in the upper troposphere for some time as a cirrus cloud.

To sum up, in order for deep convection to occur, the free troposphere must be conditionally unstable and the surface air has to be sufficiently warm and moist. A mechanism for lifting the air through its CIN is also required. If the heating and evaporation from the surface is strong, the CIN diminishes and deep convection is triggered more easily.

Deep convection and SST

The relationship between the sea surface temperature (SST) and deep convection above the tropical oceans is a topic of scientific interest. The ocean surface efficiently absorbs solar radiation and is a source of both heat and moisture for the BL over the ocean. Deep convection is rarely observed where SST $< 26°$C and becomes more frequent as SST approaches 29°C (Zhang, 1993). However, less convection is observed when SSTs are even higher than this. This has been attributed to the cooling mechanism associated with latent heat transfer by convection, so that the highest SSTs can be regarded as a result of the lack of deep convection (Waliser and Graham, 1993). Thus, there is a distinct coupling between convection and SST: while high SST can trigger convection, the presence of convective activity also limits the level of SST. More recently, Sabin et al. (2013) has pointed out that there are different regimes of the SST-convection relationship. In warm pool areas, such as the West Pacific, they found the SST-gradient to be most important for the convection by producing a low-level convergence of moisture fluxes, so that the area of maximum SST is less convectively active than the edges of the warm pool. In the ITCZ, however, an increase in convection with SST for all values of SST was found. Here, the flow from the north and south converge above the warmest waters.

2.2 General circulation of the atmosphere

The general circulation of the atmosphere is driven by the incoming solar radiation (Marshall and Plumb, 2008). Because the atmosphere is relatively transparent to this radiation, most of the energy is absorbed at the surface, thus heating the atmosphere from below. Due to the fact that warm air is less dense than cold air, the atmospheric column eventually becomes unstable, and vertical motions are induced to stabilize the air. Moreover, low latitudes receive more insolation than higher latitudes, so that a meridional temperature gradient exists, which implies meridional gradients in pressure. These pressure gradients, in interplay with effects of the Earth's rotation, topographic forcing, turbulent drag from the boundary layer and latent heat exchanges, create the large-scale horizontal circulation systems of the atmosphere. The circulation acts to transport energy from the areas absorbing much solar radiation (the surface at low latitudes) to the areas where less solar radiation is absorbed (upper troposphere and high latitudes), with the effect that these areas have lower and higher temperatures, respectively, than they would have had in a pure radiative equilibrium.

2.2.1 Tropical tropospheric circulation

The tropical tropospheric circulation is now described, based on Hartmann (1994) unless otherwise cited. The main components of the tropical circulation are depicted in Figure 2.3. The Intertropical Convergence Zone (ITCZ) is a belt of large-scale low-level convergence and ascent encircling the Earth near the equator. The ITCZ forms where the surface air is most heated, and therefore migrates to the north and south in an annual cycle due to the seasonal shift in the latitude where the sun is in zenith. The ITCZ is a rather narrow band over the Atlantic and East Pacific oceans, while it is much wider in the western Pacific and Indian ocean. From the western Pacific, there is also a second branch of convergence extending southeastward, which is called the South Pacific Convergence Zone (SPCZ) (Waliser and Gautier, 1993). The ITCZ

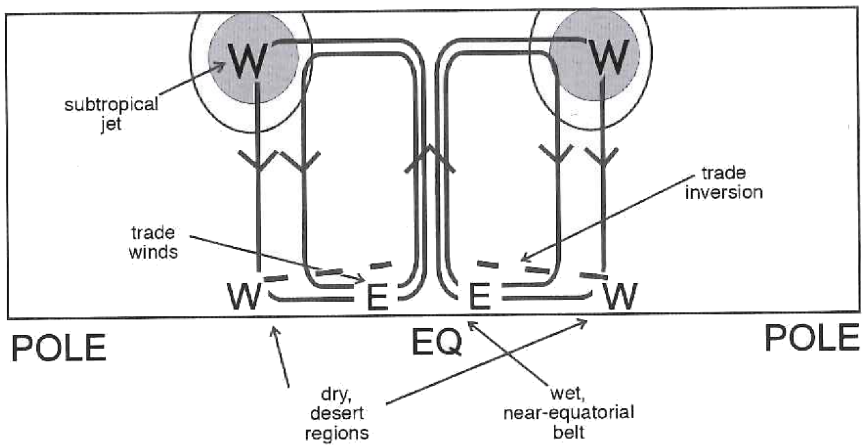

Figure 2.3: Illustration of the annual mean meridional circulation in the tropics. Arrows depict the Hadley cells. 'E' indicates easterly and 'W' westerly winds (Marshall and Plumb, 2008).

is charaterized by rising cells of deep convection, formation of vast cumulonimbus clouds and heavy rainfall. In the upper troposphere, air detrained from the convection travels poleward and descends at about ∼20-30° of latitude in both hemispheres. These regions of large-scale descent are dry, and they are called the subtropics. The upper-level outflow lowers the surface pressure in the ITCZ, so that air in the lower troposphere flows back to the equator. This return flow is deflected by the rotation of the Earth and forms the easterly trade winds. Thus, there is a closed circulation between the tropics and subtropics, which is driven by the solar heating. This circulation is called the Hadley cell. There is one Hadley cell in each hemisphere, but the cell extending into the winter hemisphere is the strongest one.

Due to the absence of friction in the upper troposphere, poleward traveling air in the upper branch of the Hadley cell conserves its angular momentum and its motion is shifted to the east relative to the Earth's surface. There are therefore strong westerly winds in the upper troposphere above the subtropics, which are called the subtropical jets. Poleward of the subtropics are the extratropics, where low and high pressure eddies in the storm tracks of the mid-latitude westerlies ensure that heat is transported on to the higher latitudes.

At continent-ocean transitional borders within the tropical belt, there is often a monsoon circulation. In a period of the summer season, the surface wind blows from the ocean to the continent and there is much convective activity over land, while the conditions are dry in the winter. The monsoons exist because the surface of the ocean requires much more energy to warm than land surfaces. This is due to both the higher heat capacity of water than soils and that the ocean is a fluid, allowing the heat to mix several tens of meters down into the sea. Because of this, the oceans warm less during summer and cool less during winter than land surfaces. In monsoon regions, the air above the continent therefore becomes more buoyant than the air above the ocean, and the deep convection and precipitation of the ITCZ moves to the continent, in some cases exhibiting a considerably larger seasonal migration than the solar zenith latitude. The low-level winds go from the ocean to the continent, providing moisture for the heavy precipitation over land. Conversely, in the winter season the land is cooled more than the ocean, the wind is offshore and the continent is dry. The strongest monsoon regions on Earth are located over India and East Asia, but there are also monsoons over other continents in the tropics.

2.2.2 Tropical tropopause layer

The tropical tropopause layer (TTL) is a transition layer where the radiative, chemical and dynamical properties change gradually from those typical of the troposphere to those typical of the stratosphere (Fueglistaler et al., 2009). Figure 2.4 shows a schematic of the TTL. The

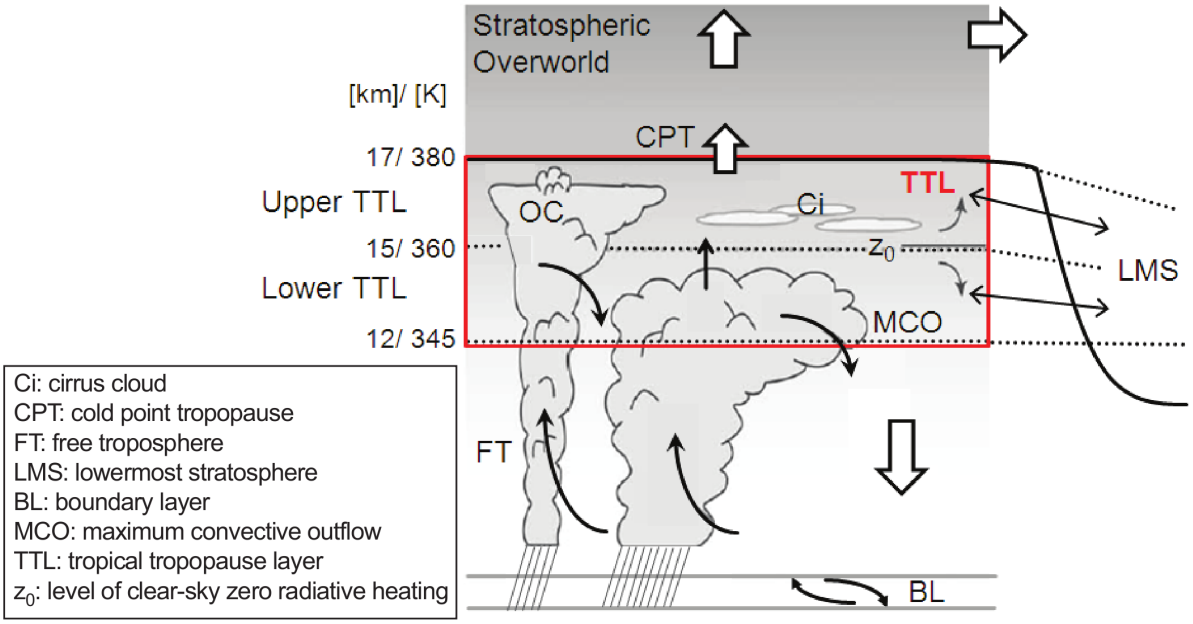

Figure 2.4: Schematic of the tropical tropopause layer (TTL), with approximate altitude and potential temperature of important levels. The thick black line is the tropopause. See text for details. Figure taken from Montzka et al. (2010).

definition applied here is the same as the World Meteorological Organization (WMO) used for the ozone assessment report (Montzka et al., 2010). The lower boundary is the level of maximum convective outflow, at about 12-13 km (∼200 hPa), and the upper boundary is the cold point tropopause (CPT), which in the tropics is climatologically located at ∼380 K potential temperature (17 km, 100 hPa) (Holton et al., 1995). The CPT height in the tropics varies to some extent in time and space, though, and in particular it is about 0.5 km lower in NH summer than in NH winter (Seidel et al., 2001). In the meridional direction the TTL is bounded by the subtropical jets (see Section 2.2.1), where strong zonal winds inhibit meridional transport (Fueglistaler et al., 2009).

The Level of Zero Radiative Heating (LZRH), at about 15 km altitude (∼125 hPa), is an important level which divides the TTL into a lower and an upper part (Figure 2.4). Below this level, radiative cooling prevails, so that air outside convective clouds will sink (Gettelman et al., 2004). The upward transport in the lower TTL is therefore dependent on convection and is thus largely tropospherically controlled. Above the LZRH the net radiation is positive, and the air therefore rises without the aid of latent heat release. The rising is associated with the mechanism of the BDC, and the upper TTL is therefore more stratospherically controlled (Fueglistaler et al., 2009).

2.2.3 Stratospheric circulation

The stratospheric circulation is described by Holton et al. (1995). Unlike the troposphere, in which radiative cooling is compensated by the latent heating in the weather systems, the stratosphere is close to radiative equilibrium. The vertical motions in the stratosphere are weak, but there is an important meridional circulation cell also in the stratosphere, which extends all the way from the tropics to each pole. This circulation is called the Brewer-Dobson circulation (BDC) and is depicted in Figure 2.5. In the stratosphere, air rises in the tropics, accompanied by radiative heating, and sinks at high latitudes, where it is subjected to radiative cooling. The main entrance for air to the stratosphere is thus the tropical tropopause layer (described in Section 2.2.2). In the extratropics, the air is transported back into the troposphere through stratospheric intrusions which deform and mix with tropospheric air due to instabilities in the

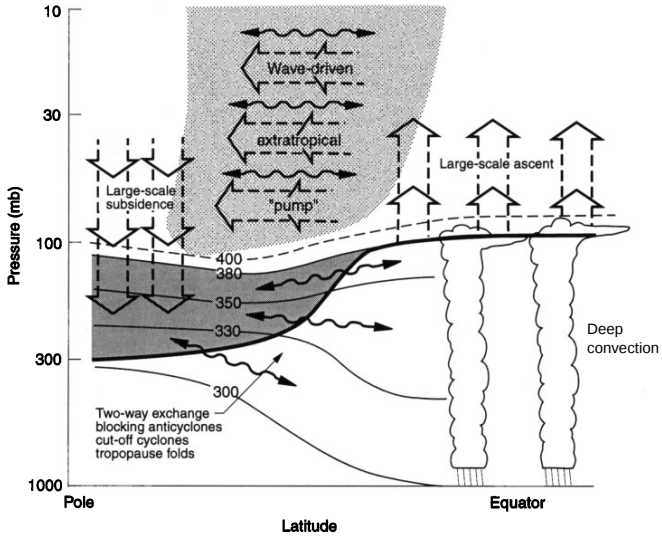

Figure 2.5: The large-scale dynamics of stratosphere-troposphere exchange: The tropopause (thick line) and isentropes (thin lines) are indicated. Thick arrows depict the BDC, while thin, wavy arrows illustrate two-way adiabatic processes exchanging air between the lowermost stratosphere and the troposphere. From Holton et al. (1995).

flow.

The BDC is driven by Rossby waves generated at mid-latitudes, which propagate up into the stratosphere, where they break and release their momentum, forcing the stratospheric air poleward. By mass conservation, air must rise in the tropics and descend at high latitudes. The circulation is stronger in the winter hemisphere because the wind profile at mid-latitudes are more favorable for upward Rossby wave propagation in the winter season. Due to more topography in the Northern Hemisphere (NH) winter than in the Southern Hemisphere (SH), the wave-driving is especially strong in NH winter. The BDC is therefore about twice as strong in NH winter as in NH summer.

The tropopause is higher in the tropics than in the extratropics, also in terms of potential temperature (see Figure 2.5). The isentropes between about 340 K and 380 K cross the tropopause in the sub- and extratropics, and adiabatic transport between the lower stratosphere and the troposphere is therefore possible. This has motivated the division of the stratosphere into an overworld, indicating the stratosphere above 380 K (≈CPT in the tropics), and the (extratropical) lowermost stratosphere (LMS) below 380 K outside the tropics (Figure 2.5). While transport between the LMS and the TTL can happen adiabatically, the transport to (from) the overworld requires slow radiative heating (cooling).

2.2.4 El Niño-Southern Oscillation

The El Niño-Southern Oscillation (ENSO), which is a strong phenomenon of climate variability on sub-decadal timescales (Marshall and Plumb, 2008), will now be introduced. It occurs due to coupled ocean-atmosphere dynamics in the equatorial Pacific ocean, causing changes in ocean sea surface temperatures (SST) and atmospheric circulation patterns, which affect the temperature and rainfall patterns in large areas of the Earth. ENSO has also been found to be important for the interannual variability of the TTL (e.g. Krüger et al. (2008); Levine et al. (2008)). The introduction on ENSO given here builds on Marshall and Plumb (2008) unless otherwise cited.

The normal conditions in the equatorial Pacific are illustrated in Figure 2.6a. The easterly wind stress from the trade winds causes upwelling of cold water near the equator. Due to the ocean boundaries, the thermocline is deeper in the west, inhibiting upwelling, so that the surface water becomes especially warm there, and it is referred to as the West Pacific warm pool.

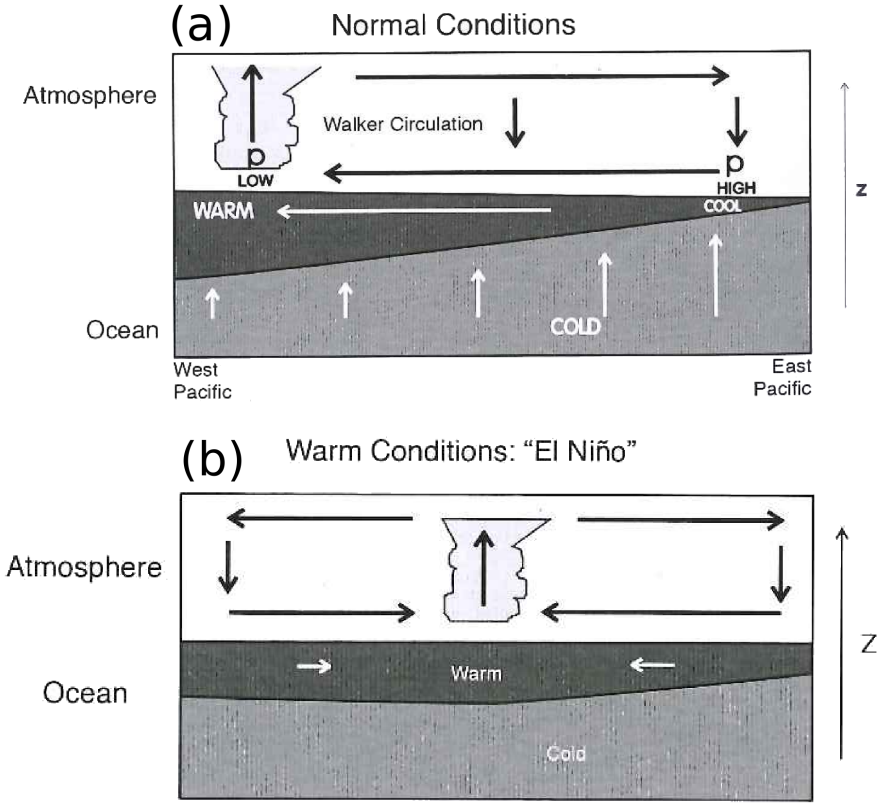

Figure 2.6: Illustration of ENSO. (a) Normal conditions in the equatorial Pacific. (b) El Niño conditions. From Marshall and Plumb (2008).

Because of the high SST, this area experiences very much deep convection (see Section 2.1.3) in all seasons. In the East Pacific, the SST is lower and there is much less convection. This gives rise to a zonal circulation cell across the tropical Pacific known as the Walker circulation. Air rises above the warm pool, flows eastward across the Pacific, descends in the east and flows back to the western Pacific at low-levels. This easterly return flow causes an increase in the trade winds so that the wind stress on the ocean surface increases, thus strengthening the ocean process creating the warm pool. So a positive feedback mechanism exists between the ocean and atmosphere in the tropical Pacific, and this allows for amplifications in the anomalies described below.

The state of the tropical Pacific undergoes irregular fluctuations in the order of a few years. In the ENSO warm phase, called El Niño, the warm pool is shifted eastward into the Central Pacific, and the equatorial upwelling of cold water weakens in the east (Figure 2.6b). The SSTs get higher in most of the equatorial Pacific, but the largest anomalies occur in the east. This anomalous state of the ocean lasts for a few month, usually culminating around Christmas. The opposite phase is called La Niña, or the cold phase, and is an enhancement of the normal circulation pattern. Under these conditions the equatorial upwelling is stronger and the East and Central Pacific have lower SSTs than usual.

El Niño and La Niña events develop through coupling between the tropical ocean and atmosphere. The atmospheric part of the phenomenon is called the Southern Oscillation. It is characterized by variations in sea level pressure (SLP), which are anticorrelated between the western and eastern tropical Pacific. Under average conditions, the SLP is low over the warm pool and higher in the Central and East Pacific. During an El Niño event, the trade winds weaken and may even reverse in the west, as convection is shifted east with the shift in the warm pool. A lowering of SLP and an increase in rainfall thus occur in the Central and East Pacific, while there is less than normal convection and precipitation and unusually high SLP in

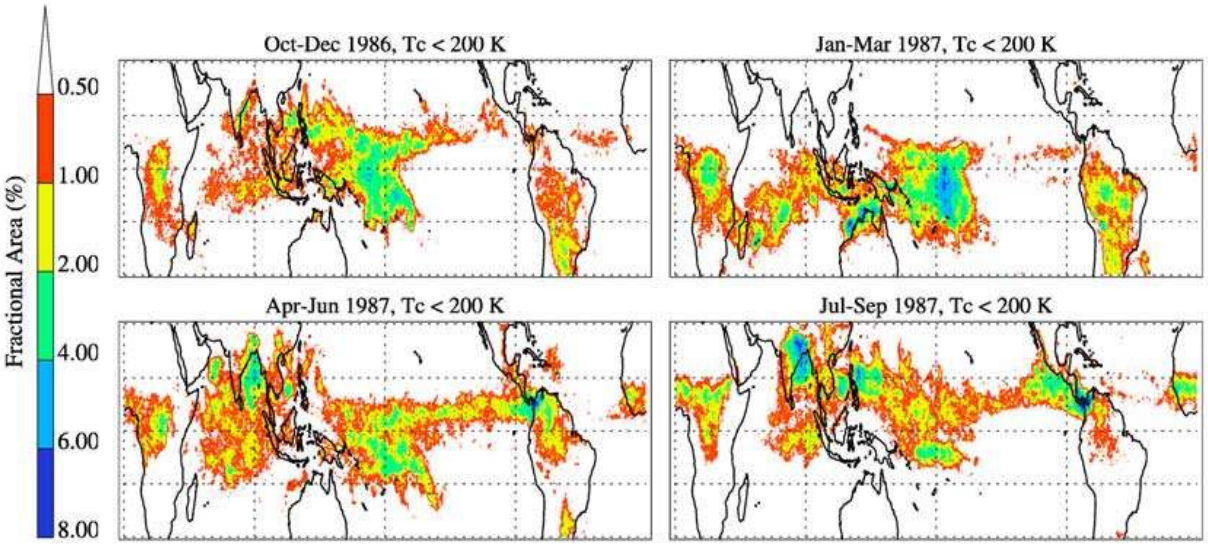

Figure 2.7: Geographical distribution of cloud top area observed colder than 200 K (1986-87), using IR brightness temperature measurements from satellite. Figure taken from Gettelman et al. (2004), and based on the work of Gettelman et al. (2002).

the west. In La Niña, the Walker circulation increases in strength, and the SLP is even lower than normal in the west and higher than normal in the east.

A strong anticorrelation in the SLP time series occurs be between Darwin (131°E, 12°S) and Tahiti (149°W, 17°S), and the pressure difference between these two locations is therefore used for describing the Soutern Oscillation. The index is called the Southern Oscillation Index (SOI) and is defined as:

$$\text{SOI} \equiv 10 \cdot \frac{\Delta P - \overline{\Delta P}}{\sigma}, \tag{2.1}$$

where $\Delta P = SLP_{Tahiti} - SLP_{Darwin}$ is the pressure difference between the two places, and $\overline{\Delta P}$ and σ is the climatological mean and standard deviation of this difference. The time series of SOI for the experimental period in this study (2002-2013) is shown in Figure 5.18.

In recent decades, a different type of El Niño has been observed to occur more frequently (Yeh et al., 2009). This new type is called El Niño Modoki, the warm-pool El Niño or the Central Pacific El Niño. It differs from the traditional El Niño by the high SSTs shifting less east, so that the SST anomalies are highest in the Central Pacific, while the East Pacific experiences a relatively small increase in SST. The El Niño Modoki was rarely observed before 1990, but since then it has occured more frequently than the traditional type of El Niño. The two types have been shown to give different, and sometimes opposing, effects on the weather systems of the regions surrounding the Pacific ocean (Yeh et al., 2009; Zhang et al., 2011).

2.3 Troposphere-to-stratosphere transport

2.3.1 Convective transport to the TTL

Gettelman et al. (2004) studied the radiation balance in the TTL. From radiosonde data, using a variety of radiative transfer models, the LZRH was found to be located at around 15 km altitude in the tropics (Gettelman et al., 2004). They further argued that only convection with cloud tops colder than 200 K are able to inject air above the LZRH. In Figure 2.7, the geographical distribution of cloud area colder than 200 K is shown. Gettelman et al. (2002) calculated the cloud top temperatures using cloud infrared (IR) brightness temperature data measured from satellite. Cloud tops colder than 200 K were found to occur most frequently over the West and Central Pacific in NH winter, over Panama in July-September and over the Ganges river

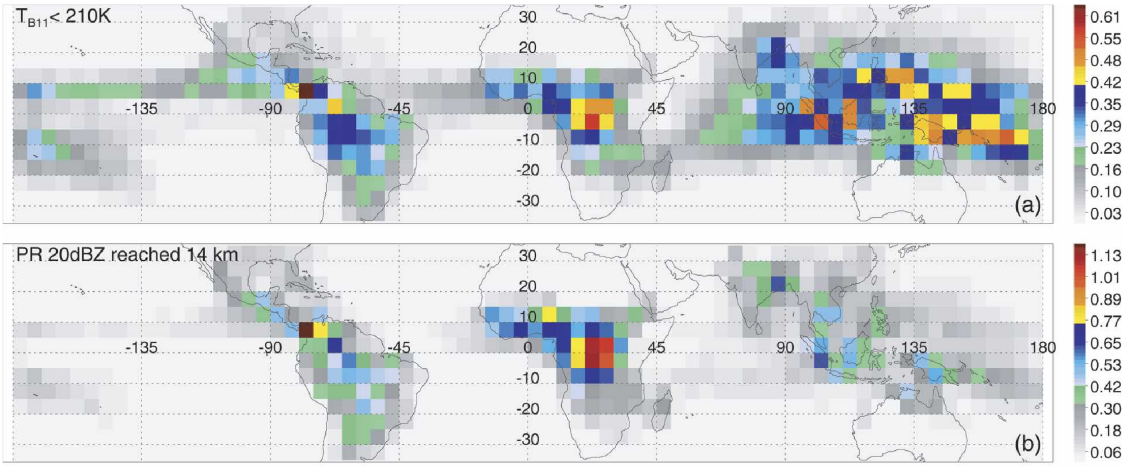

Figure 2.8: Global distribution of the relative contribution (in %) of different areas to the total area where cloud brightness temperature is below 210 K (a) and to the total area where the PR signal of 20 dBZ reaches 14 km (b). From Liu et al. (2007).

valley during the Asian summer monsoon. However, even in these areas, these events were only observed up to 5 % of the time (Gettelman et al., 2004). The authors also argued that the LZRH will be located well above the main convective outflow, because the moisture and cloudiness associated with the convection will cause radiative cooling.

Gettelman et al. (2002) found that the occurance of the deepest convection was correlated with the lowest CPT temperatures. They argued that this could be because convection cools the tropopause, or because the lower statical stability in the TTL associated with the colder tropopause causes a higher LNB.

Gettelman et al. (2002) also estimated the convective turnover time, which is the time for convection to replace the air mass at a given altitude (neglecting horizontal transport). For 20°S - 20°N, the convective turnover time was found to be in the order of 2-3 weeks at 12 km, increasing to months at 14-15 km, and more than a year at the tropopause level. Significant regional and seasonal differences were found. The shortest turnover time in the TTL was found in NH winter and in the West and Central Pacific. Here the turnover time was ∼3 months at 15 km, compared to ∼6 months in the tropical average, increasing to ∼9 months at 17 km. Gettelman et al. (2002) concluded that convection is the most important factor for vertical transport in the tropics up to about 15-16 km. Above this altitude, radiative heating will be more efficient. Thus, this should indicate that the contribution of convection overshooting the tropopause to TST is small, and that most air undergoing TST detrains from convection reaching above the LZRH, but not to the tropopause.

Liu and Zipser (2005) studied overshooting convection using 5 years (1998-2003) of precipitation radar (PR) data from the Tropical Rainfall Measurement Mission (TRMM) satellite, using different threshold altitudes. They identified overshooting precipitation features by radar signals stronger than 20 dBZ observed at altitudes above the given threshold. 1.38 % of all the precipitation features reached above 14 km, and 0.11 % above 380 K. Africa was found to give the largest contribution to the overshooting area, and in general the continents contributed more than the oceans (Liu and Zipser, 2005).

In a later paper (Liu et al., 2007), the differences in results between using IR brightness temperature and PR were investigated (both were measured by the TRMM satellite). While the IR brightness temperature detects the temperature of all cloud tops with a sufficient optical thickness, including the non-raining anvil and cirrus clouds, the PR detects how high precipitation particles are present. The difference in height between the IR cloud top and the top of the PR signal (>20 dBZ) is often many kilometers (Liu et al., 2007). They found that the coldest clouds occurred most frequently above the West Pacific, while the highest PR echoes were de-

tected over land, especially above Central Africa (Figure 2.8). The vertical distance between the cloud top height estimated by the two methods was less above the continents. They gave the explanation that above land, particularly in Central Africa, the convective updrafts are more vigorous so that precipitation particles are present higher in the cloud, although the altitude of the cloud tops are not higher than above oceans. In the West Pacific, the LNB (see Section 2.1.3) was found to be in average higher than elsewhere, which permits even weak convective updrafts to create very high, cold clouds (Liu et al., 2007).

To summarize, both tropical continents and oceans occasionally produce convection which reaches high enough to inject air above the LZRH. While the West Pacific contributes most to the highest and coldest convection, the more vigorous updrafts in continental convection, especially in Central Africa, more frequently produces high overshooting events. Convection can penetrate the tropopause, but these events are rare and are not believed to give a major contribution to the air entering the stratosphere. Most TST is accomplished by convective lifting to above the LZRH, followed by slower, radiative ascent.

The regions highlighted in Figures 2.7 and 2.8 can be expected to be important pathways for the transport from the surface to the TTL. The pathways and timescales of transport from the tropical BL to the TTL were studied by Levine et al. (2007), using an Eulerian transport model including a parameterization of vertical transport by convection. Tracer mass was released in the BL. They found that the tropical regions of the Indian Ocean, Maritime Continent and the West Pacific dominated the fast transport from the BL to the TTL. ∼20 % of the air in these regions reached the base of the TTL within 1 week. As the base of the TTL was defined at ∼200 hPa, much of this air must be expected to detrain below the LZRH and stay in the troposphere (Section 2.2.2). However, Levine et al. (2008) used trajectories to study the air entering the stratospheric overworld and found that this air dominantly entered the TTL above the West Pacific and Maritime Continent. Aschmann et al. (2009) implemented a parameterization of convective transport in an Eulerian model to simulate the transport of bromoform (a VSLS) and its degradation products to the stratosphere. They also found that the Maritime Continent and West Pacific were the most important pathways for entry to the TTL on short timescales, as well as the entry to the stratosphere.

2.3.2 Transport from the TTL to the stratosphere

The *Lagrangian* cold point (LCP) is the coldest point that air travelling from the troposphere to the stratosphere encounters during the transfer. The LCP differs from the CPT because the flux across the tropopause is not uniform in space and time. The LCP is an important quantity because its temperature determines how much water vapor can enter the stratosphere (Fueglistaler et al., 2009), and it will also be important for VSLS since their degradation products often are removed by washout (Montzka et al., 2010). Trajectory studies have shown that air preferably enters the stratosphere in the areas and seasons where the CPT is colder than average (Fueglistaler et al., 2005; Krüger et al., 2008), which was originally suggested by Newell and Gould-Stewart (1981) to explain the dryness of the stratosphere.

Fueglistaler et al. (2005) studied the pathways of TST by simulating trajectories released at 400 K backward in time using the reanalysis ERA-40 as input between 1979 and 2001. They detected where the trajectories assumed their minimum saturation mixing ratio, i.e. the Lagrangian cold point, and also where they first crossed the 340 K isentrope (entering the lower TTL, see Figure 2.4). In Figure 2.9 the density of trajectories at these two levels is shown. Most trajectories entrain into the stratosphere above the western Pacific. A second maximum is found further northwest, near the Bay of Bengal and Philippines, in NH summer. The maximum of entrainment is collocated with the lowest tropopause temperatures. Fueglistaler et al. (2005) attributed this to the combined effect of strong convection below the areas of coldest tropopause and that the horizontal winds in the TTL efficiently advect the air through these areas during ascent. The entry to 340 K is in similar locations to the entry to the stratosphere, though shifted slightly more off the equator toward the summer hemisphere.

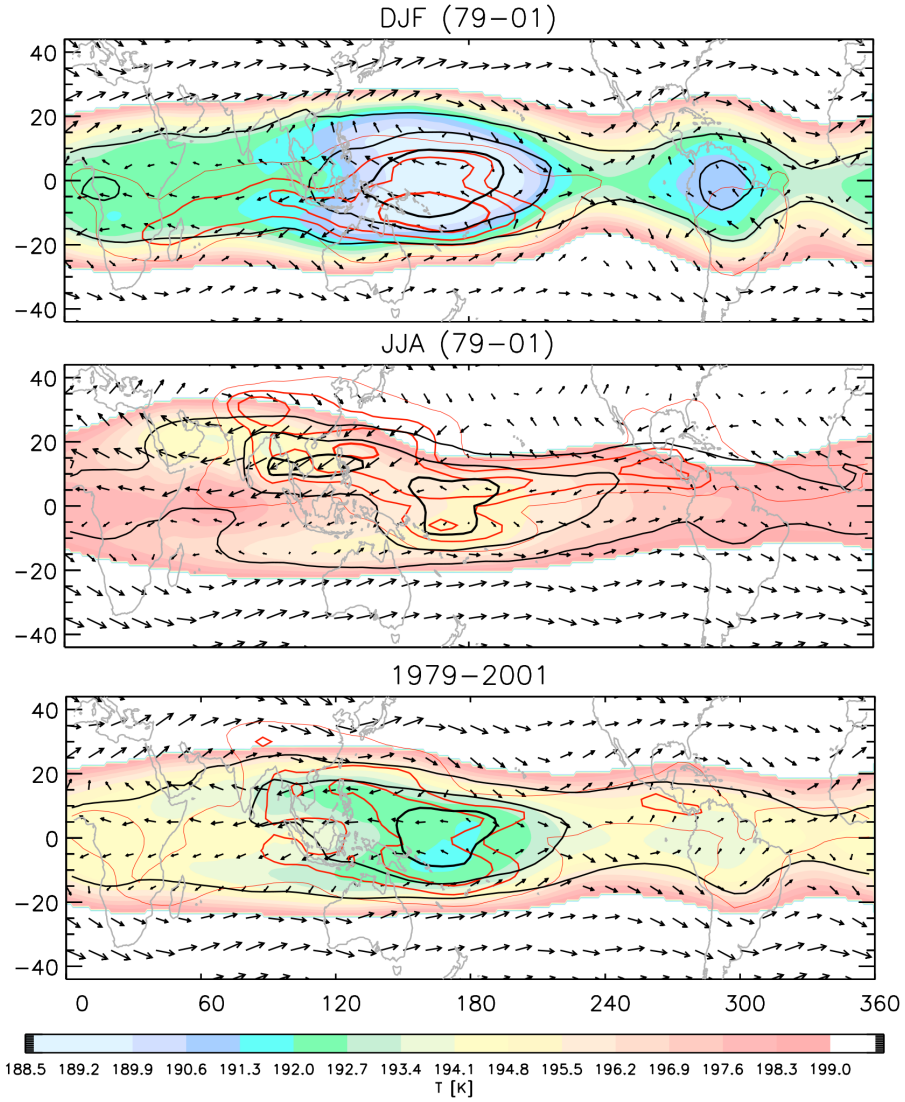

Figure 2.9: For trajectories released at 400 K between 30°S - 30°N: the frequency of the locations of the LCP (black lines) and the irreversible crossing of 340 K (red). The countours show where 0.025 %, 0.1 %, 0.2 % and 0.4 % of the trajectories cross the respective level per 5° longitude and 2° latitude bin. Also shown is climatological wind and temperature at 90 hPa from the ERA-40. Taken from Fueglistaler et al. (2005)

The time for ascending through the upper TTL, from 360 to 380 K, has been estimated to ∼40 days, using radiative heating rates calculated from operational and reanalysis (ERA-40) data from the European Center for Medium-Range Weather Forecasts (ECMWF) (Krüger et al., 2008). Similar timescales have been found using kinematic velocities from the improved reanalysis ERA-Interim (Ploeger et al., 2010).

Chapter 3

Data and method

In this chapter, the model used in this study (Section 3.1) and the input data (Section 3.2) will be presented. Then the experimental setup (Section 3.3) and the analysis of the model output (Section 3.4) are described. The setup is then tested to look for possible issues (Section 3.5) before the analysis setup is further refined (Section 3.6).

3.1 Flexpart model

The Lagrangian model Flexpart (version 9.02) is used to simulate the transport. The first versions of the Flexpart model (Stohl et al., 2011) was relesed in the 1990s and designed for tracking the dispersion of air pollutants from point sources, such as a nuclear accident. Later, it has been further developed and used for other transport modelling purposes, including the transfer of air between the troposphere and the stratosphere. In 2010, the model was used by at least 35 groups in 14 countries (Stohl et al., 2011).

Flexpart is an off-line model driven by global meteorological input fields, in this case the ERA-Interim reanalysis (see Section 3.2.1). The model interpolates the three-dimensional wind to each trajectory's location and uses this wind to advect the trajectory. In addition, modelling of transport by turbulence and mesoscale systems are done with Langevin equations. A scheme for representing vertical transport in deep convection is also implemented, and it is described in more detail in Section 3.1.2. The model allows the trajectories to be tracked both forward and backward in time. For a full model description, see Stohl et al. (2011).

3.1.1 Lagrangian vs Eulerian approach in transport modelling

When simulating transport of tracers in the atmosphere, two fundamentally different approaches can be used. In an Eulerian approach, the spatial domain is divided into grid-boxes, and the development of tracer concentration within each grid-box is modelled. This is done by computing the fluxes of tracer between each box (Jacob, 1999). In a Lagrangian approach, such as Flexpart, the tracer mass is partitioned between a large number of synthetic particles, and the motions of these particles are modelled (Stohl et al., 2011). However, regardless of which of these is used, meteorological data driving the transport must be provided, for example from a reanalysis or a free-running general circulation model. In the Lagrangian approach, the wind and other relevant variables used for parameterizations (such as temperature) must be interpolated to the current location of each trajectory (Stohl et al., 2011).

There are many advantages with the Lagrangian approach, explained by Wohltmann and Rex (2009). Firstly, it involves no numerical diffusion, which is unavoidable in an Eulerian setup due to the use of the mixing ratio gradient to calculate the advection of a tracer. In Lagrangian models, diffusion can be added in a controlled amount to represent physical processes like turbulent mixing. Secondly, there is no stability limit on the timestep in the Lagrangian setup. Other advantages is that the spatial resolution is higher where the concentration is higher (more trajectories), that tracer mixing ratios never get negative from spurious numerical dispersion,

and that each trajectory is modelled independently, which allows for efficient parallelization of the code.

3.1.2 Convection scheme

The representation of convection in the model is of particular interest for this study, since it is likely to have a great impact on the vertical transit times. Rising motions due to large-scale convective areas, such as the ITCZ, is represented partly by the grid-scale (i.e. the $1° \cdot 1°$ horizontal resolution of the input grid) vertical velocities of ERA-Interim (see Figure 3.4). However, this is the residual of small areas of fast ascent and much larger areas of slow descent (see Section 2.1.3), and will therefore not capture the fastest vertical transport (Berthet et al., 2007). A parameterization of subgrid-scale convective motions is therefore needed in order to capture the fastest vertical transport.

In Flexpart, the scheme developed by Emanuel and Živković-Rothman (1999) (hereafter the EZ99 scheme) has been implemented. A full description of the implementation of this scheme in Flexpart can be found in Forster et al. (2007). The EZ99 scheme uses temperature and humidity data to model convective events within each horizontal grid-cell of the ERA-Interim input grid. It uses several parameterizations, involving cloud microphysics, surface fluxes, entrainment and the interplay between rising plumes and downdrafts.

In the scheme, convection is triggered whenever

$$T_{vp}^{LCL+1} \geq T_{v}^{LCL+1} + T_{thres} \tag{3.1}$$

where T_{vp}^{LCL+1} is the virtual temperature[1] of a surface air parcel lifted to the model level[2] above its lifting condensation level, T_{v}^{LCL+1} is the ambient virtual temperature at this level and $T_{thres} = 0.9$ K is a threshold value (Stohl et al., 2011). This is thus an empiric criterion for representing that the ability for the surface air to break through the CIN depends on its temperature and moisture and the static stability of the atmosphere above (see Section 2.1.3).

The EZ99 convection scheme calculates a displacement matrix, where each column describes the convective mass fluxes from one of the model's vertical levels to each of the others. If compared to the total mass of air at each level, these mass fluxes can be used to calculate the probability that an air parcel located at one level will be displaced to each of the other levels during one timestep. An example of such a matrix is plotted in Figure 3.1. At all model levels, the probability is highest for staying at the same level (no convective dispacement). However, the air at the lowest model level has a considerable probability to be moved to model levels throughout the troposphere, and also air at higher levels can be moved either up or down due to entrainment into the convective plumes.

In every timestep, Flexpart calls the convection scheme in each horizontal cell of the input grid, using temperature and humidity data interpolated to the current time. The displacement matrix calculated by the scheme is used to vertically redistribute the trajectories located within that grid-cell in a stochastic way. The displacement matrix only includes up- and downdrafts within the convective cloud systems, which gives a net upward mass transport. To represent the compensating large-scale subsidence in the cloud-free environment, a subsidence velocity is applied to the trajectories that are not convectively displaced.

A technical issue occurs when Flexpart is run in backward mode. The matrix of mass fluxes depends on the cloud base mass flux, whose calculation involves also the cloud base mass flux from the previous timestep (to represent remnants of previously initiated convective cells). However, since the previous time is not yet calculated in backward mode, the Flexpart developers chose to reverse the expression and use the cloud base mass flux of the latter timestep instead (Forster et al., 2007). Although this is unphysical, the difference between convective mass fluxes

[1] The virtual temperature is introduced as a correction for moist air to account for the buoyancy from the water vapor, which have lower density than dry air (Wallace and Hobbs, 2006).

[2] "model level" refers to the the levels of the input data (see Section 3.2.1)

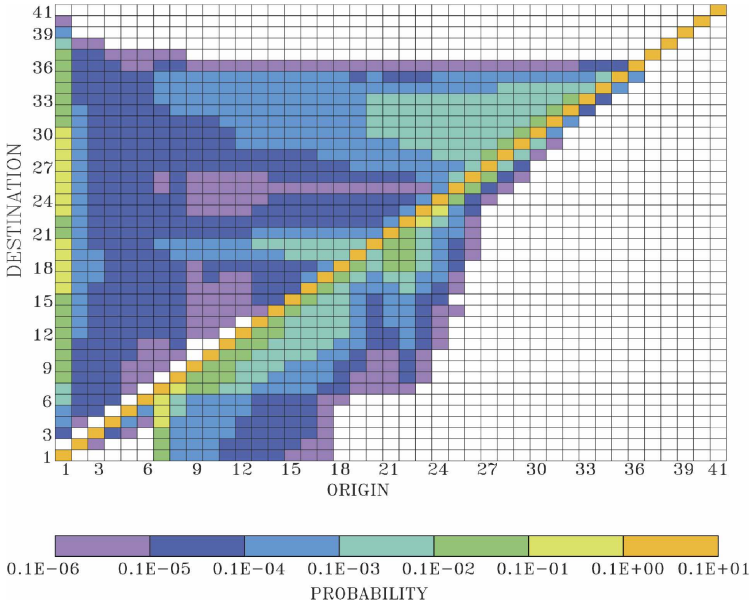

Level	Height (m)	Level	Height (m)	Level	Height (m)
1	8	15	1980	29	9173
2	28	16	2309	30	9890
3	58	17	2667	31	10 654
4	102	18	3054	32	11 445
5	161	19	3470	33	12 296
6	268	20	3915	34	13 200
7	335	21	4389	35	14 151
8	453	22	4893	36	15 143
9	595	23	5427	37	16 172
10	760	24	5989	38	17 247
11	950	25	6578	39	18 375
12	1166	26	7191	40	19 558
13	1409	27	7828	41	20 769
14	1681	28	8488		

Figure 3.1: Left: An example of a mean displacement probability matrix calculated by the convection scheme of Emanuel and Živković-Rothman (1999) for October 1983 along 10° latitude. The colors indicate the probability for air parcels located at a model level (origin) to be convectively displaced to each of the model levels (destination). Right: The approximate height of the model levels in the example (Forster et al., 2007).

in forward and backward runs was found to be less than 3 % when using a timestep of 900 s (Forster et al., 2007), which is also the timestep used in this thesis. They argued that the smaller convective mass fluxes in backward mode can be attributed to the atmospheric column stabilizing during convective events, so that cloud base mass fluxes derived from a later timestep is likely to be smaller than those derived from an earlier timestep.

Forster et al. (2007) evaluated the EZ99 scheme by comparing the computed mass fluxes to those archived in the ERA-40 data. The EZ99 scheme produced 26 % smaller convective mass fluxes in the global average and also less convective precipitation than the ERA-40 scheme. This was interpreted as a positive result, because the total precipitation came closer to that observed in the Global Precipitation Climatology Project (GPCP) when the convective precipitation in ERA-40 was replaced by the convective precipitation calculated in the EZ99 scheme.

3.2 ERA-Interim

The meteorological input fields used to simulate the trajectories with Flexpart in this study is taken from the ECMWF's latest global reanalysis, the ERA-Interim, which covers the period from 1979 and is continuously extended in near real time. A thorough description of this reanalysis is provided by Dee et al. (2011), from which the content of the following paragraph is taken.

A reanalysis is a dataset representing the circulation and properties of the global atmosphere and its underlying surface over a given period, usually many years. It is created by running a numerical weather forecast model assimilated by various observations, including both in situ measurements from weather stations, ships, aircrafts and balloons, and remote sensing from surface or satellite instruments. The observations go through rigorous quality checks before they are assimilated in the model. There is a very important difference between a reanalysis and the operational weather forecasts. In the operational weather forecasts, models and assimilation routines are frequently changed to improve the performance, and several models are run to get an ensemble of predictions. However, reanalyses are made to be able to look for long-term

trends and variability in the climate system, and must therefore follow a consistent method for the whole period. Therefore, a reanalysis is run using the one and same model with the same settings for all the years. However, the amount of observations used is not constant due to the rapid increase in available observations in the last decades.

3.2.1 Flexpart input data

In this study, Flexpart uses 3-hourly input fields from ERA-Interim. Data at 00, 06, 12 and 18 UTC are provided from the 4-dimensional analysis, while the 03 and 15 UTC data come from 3h forecasts and the 09 and 21 UTC data from 9h forcasts. The data is given on 60 hybrid (sigma-pressure) levels extending from the surface to 0.1 hPa (≈65 km). These are the same vertical levels as in the original model grid. In the horizontal, the data has been transformed from spectral coefficients (T255) to $1° \cdot 1°$ latitude/longitude grid points. See the ECMWF webpage for a further explanation of these data (`http://old.ecmwf.int/products/data/archive/descriptions/ei/oper.html`). The Flexpart pre-processor calculates the vertical wind in hybrid coordinates using the spectral data to get better mass-consistency (Stohl et al., 2011).

In order to document the input data, climatological fields for the period of this study (2002-2013) are displayed for ERA-Interim variables that I consider to be especially important for the transport. The figures described below show the average of monthly means of daily means of the variables. The monthly mean data were downloaded from the ERA-Interim website (ECMWF: `http://apps.ecmwf.int/datasets/data/interim-full-moda/`).

Figure 3.2 shows the mean SST in each season. As described in Section 2.1.3, the SST is important for the occurrence of deep convection and a threshold value of 26°C has been found from observations (Zhang, 1993). The SST exceeds 26°C in most of the inner tropics and is particularly high (above 29°C) in the equatorial West Pacific, the so-called warm pool (Marshall and Plumb, 2008). The warm pool extends north and west during NH spring and summer to include also the Indian Ocean and South China sea. The SST is also generally higher in the Indian Ocean than in the Atlantic, except for the warm waters near Mexico in NH summer. The SH East Pacific is cold in all seasons, which is due to upwelling of water along the coast of South America (Hartmann, 1994).

Figures 3.3 and 3.4 display the horizontal and vertical velocities, respectively, at 200 hPa. This level, at ∼12-13 km, is approximately the level of main convective outflow in the tropics (Fueglistaler et al., 2009). The flow at this level can therefore be important for where the air can ascend into the TTL (see Section 2.2.2). The subtropical jets are clearly visible in Figure 3.3 as strong westerly velocities to the north and south of the tropics in all seasons. There is also westerly flow above the equatorial Pacific; this is the upper branch of the Walker circulation. A pronounced divergence can be seen in the West Pacific, consistent with outflow from the abundant deep convection in this region. In Figure 3.4 three main areas of upward motion can be found. The strongest and largest of them is located in the West Pacific and Maritime Continent in NH winter. In NH summer it shifts north to also include South-East Asia, in particular the Bay of Bengal. The second area is above equatorial Africa, and the third is located in Central and South America. In addition, there is a thinner line of ascent along the ITCZ which is not visible in all seasons. These features are collocated wtih the areas of the coldest convective clouds found by Gettelman et al. (2002) (see Section 2.3.1) and indicate that there is an upward mass flux into the TTL in these areas, in agreement with the theory.

Climatological vertical winds for 125 hPa (∼15 km) and 100 hPa (∼17 km) are shown in Figure A.3 and A.4 in the Appendix. The upward velocities decrease by an order of magnitude from 200 hPa to 100 hPa, but the area of ascent can also be seen to widen significantly with altitude, from the rather restricted areas of ascent at 200 hPa to covering most of the tropics at 100 hPa. However, there are also areas in the tropics where the ERA-Interim vertical winds are downward, especially above the East Pacific.

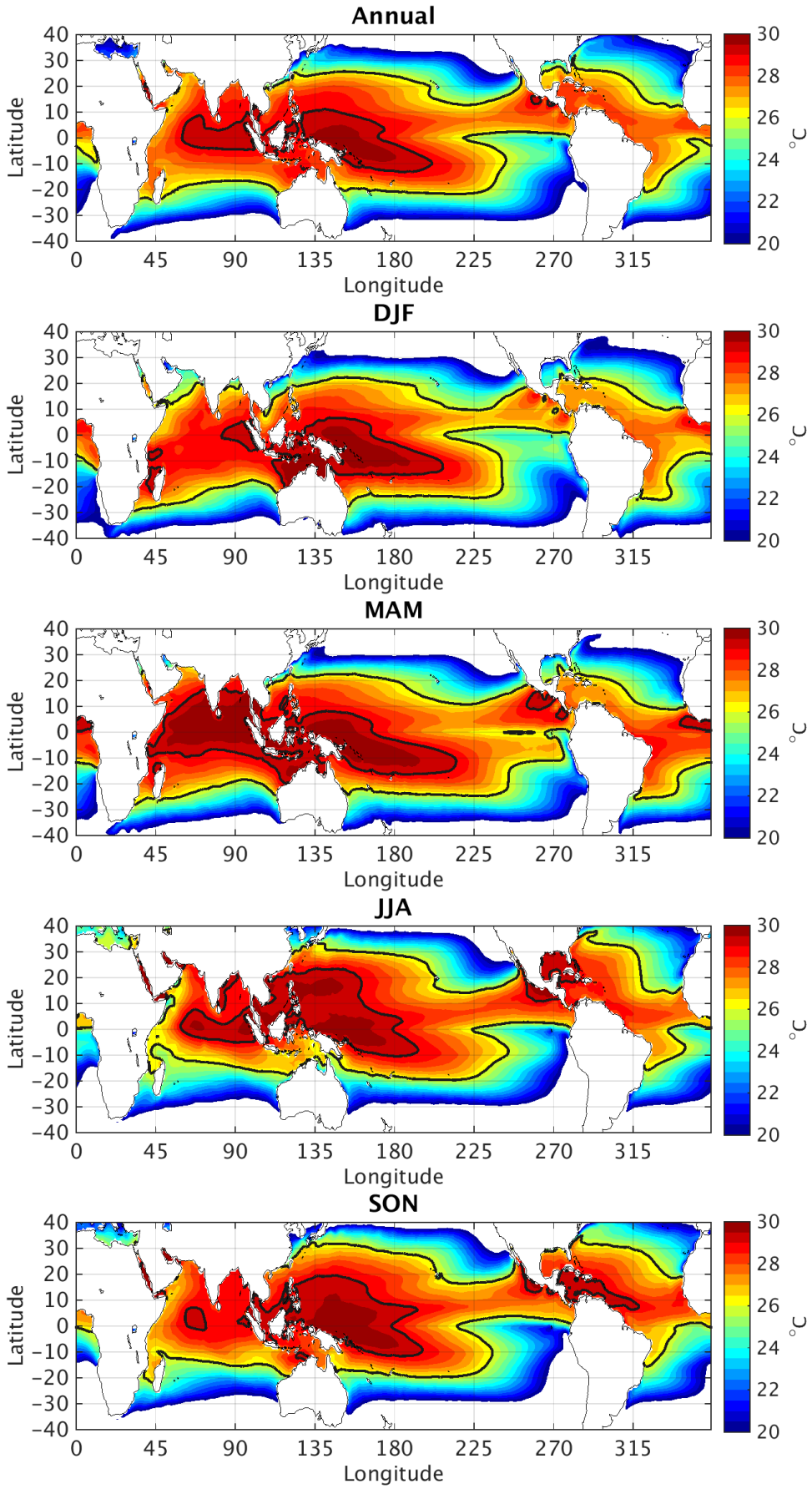

Figure 3.2: Sea surface temperature (°C) from ERA-Interim: Mean for the period May 2002 - April 2013. Top: All months. Below: For each season. The black contours mark the 26 and 29°C isotherms.

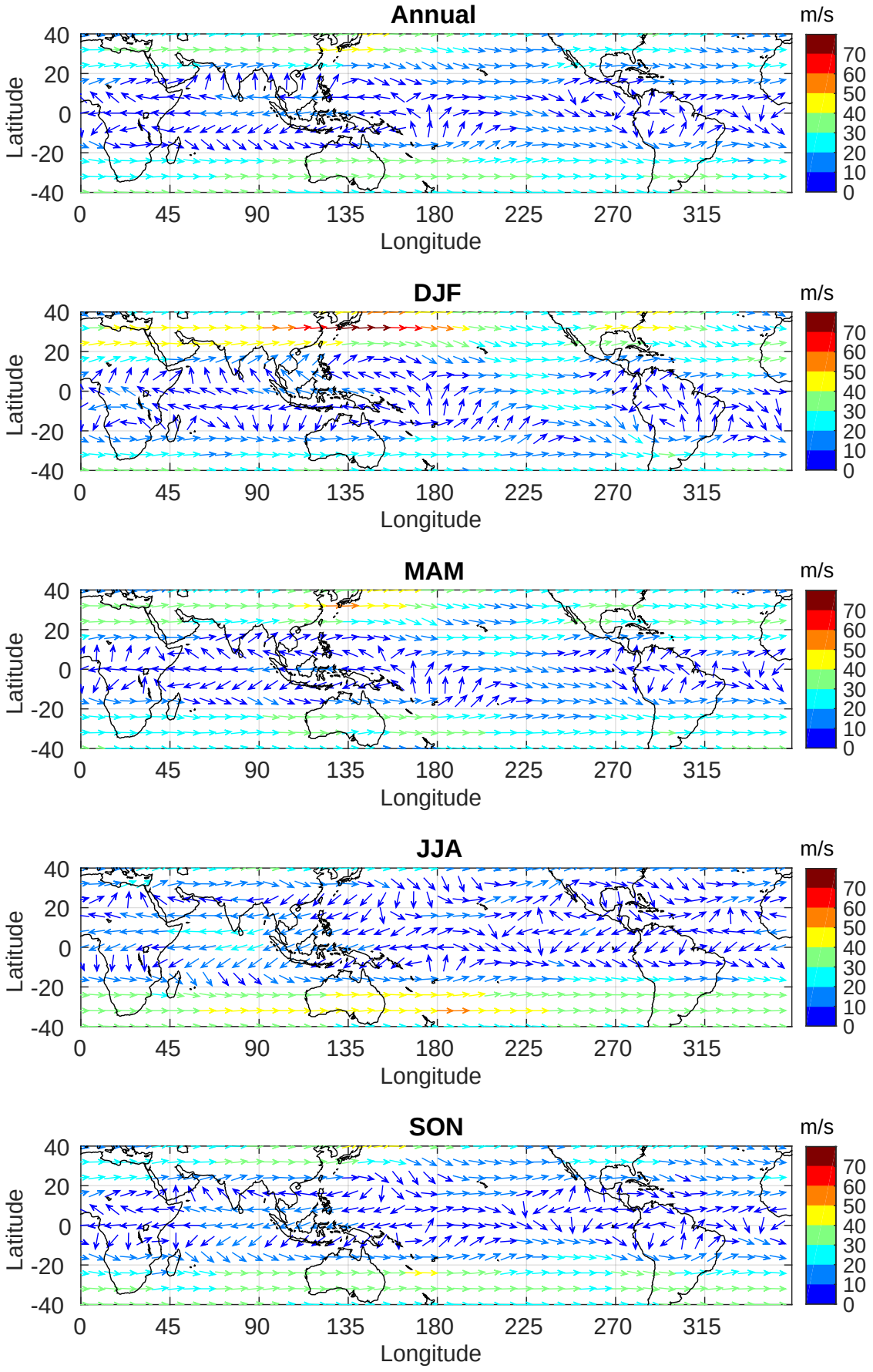

Figure 3.3: Horizontal velocity (m/s) at 200 hPa from ERA-Interim: Mean for the period May 2002 - April 2013. Top: All months. Below: For each season. Wind-speed is indicated by the color of the arrow. The velocity is valid for the location at the mid-point of the arrow.

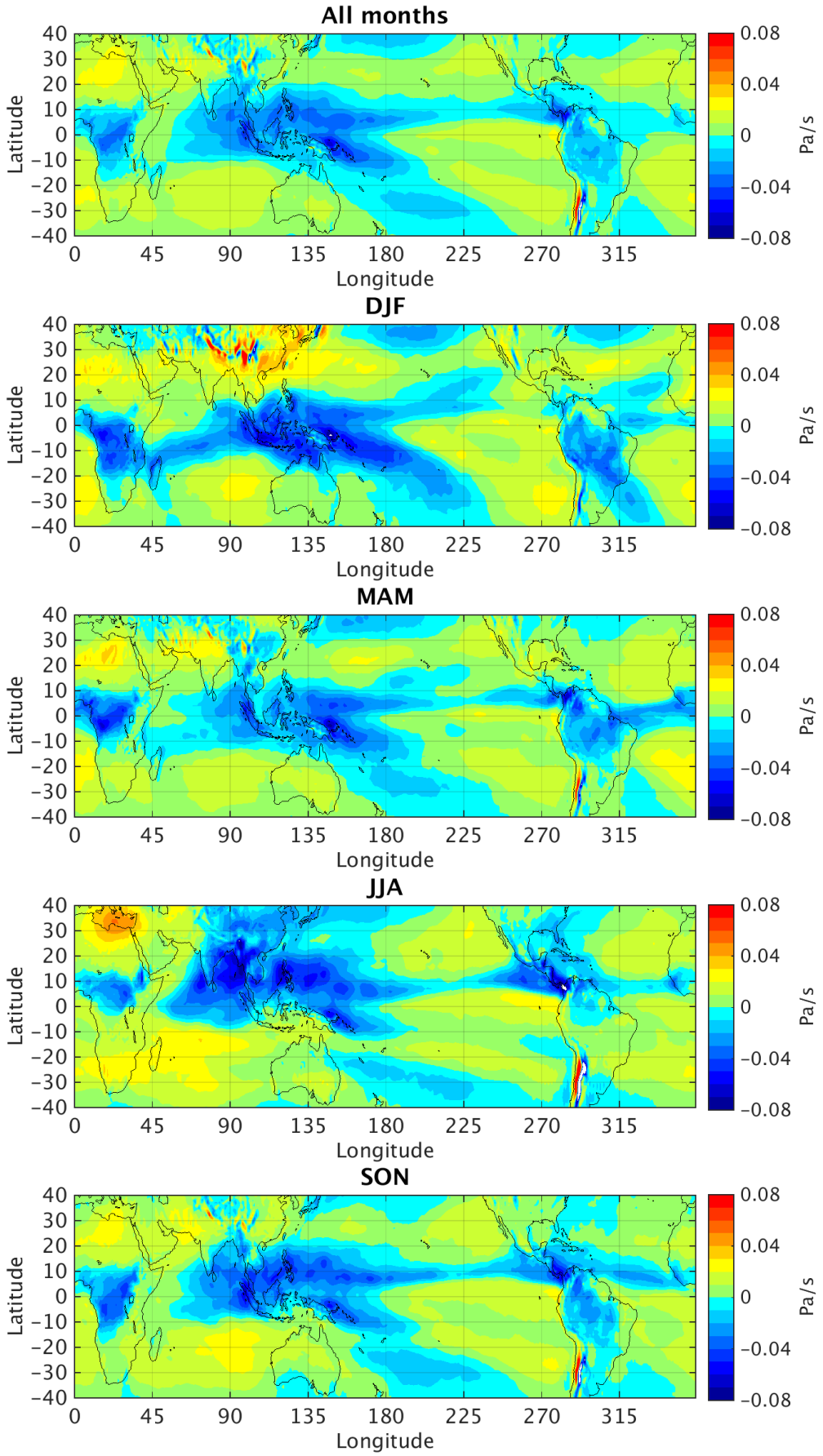

Figure 3.4: Vertical velocity (Pa/s) at 200 hPa from ERA-Interim: Mean for the period May 2002 - April 2013. Top: All months. Below: For each season. Note that the velocity is in pressure coordinates, so negative values indicate ascent.

3.2.2 Quality of the vertical winds

It is important to remember that a reanalysis is not a perfect representation of the atmosphere. The Flexpart results can never be better than the meteorological input data, so it is important to be aware of uncertainties in ERA-Interim. In this study it is in particular uncertainties in the vertical velocities that is an issue, as these will be the main factor determining the modelled transit times in the TTL above the detrainment from convection.

To represent the weak, large-scale vertical velicites, transport studies can use the kinematic vertical velocity, which is calculated from the pressure tendency (using the divergence of the horizontal wind and the continuity equation), or they can use the diabatic heating rate in isentropic (potential temperature) coordinates (Ploeger et al., 2010). The diabatic approach has been shown to give less vertical dispersion of tracers in the upper TTL than the kinematic approach (Ploeger et al., 2010). Diabatic velocities have also been shown to give a slower and more realistic stratospheric circulation (Monge-Sanz et al., 2007). However, the diabatic method is not as well suited for the troposphere (Aschmann et al., 2009). As the main focus of this study is the troposphere, kinematic velocities are used.

In the previous reanalysis of ECMWF, the ERA-40, the stratospheric circulation was much too fast, but substantial improvements have been made in ERA-Interim (Dee et al., 2011). Using backward trajectories released at 40 hPa at the equator, Monge-Sanz et al. (2007) found that the kinematic velocities in ERA-Interim was considerably less vertically dispersive in the lower tropical stratosphere than those of ERA-40. Using an Eulerian CTM, they also found that the ERA-Interim gave a much more realistic stratospheric circulation than ERA-40. This should indicate that the vertical transport in the upper TTL (15-17 km), which is largely stratospherically controlled (see Section 2.2.2), can be modelled with a reasonable precision using the kinematic velocities of ERA-Interim.

3.3 Model setup

In order to catch the TTL in all seasons, trajectories are released between 40°S - 40°N. They are released from two altitudes, 15 km and 17 km above sea level. In the tropics the lower level represents roughly the LZRH and the upper level the CPT. These levels mark important borders in the TTL for trajectories undergoing TST (see Section 2.2.2). Trajectories are released with 1° spacing in longitude and latitude at 00 UTC at the first day in the month. Thus, each month a total of $360 \cdot 81 = 29,160$ trajectories are released at 15 km and at 17 km. The trajectories are simulated for 90 days backward in time from their release. A timestep of 900 seconds is used internally in the model, while particle output, including the current longitude, latitude and altitude of each trajectory, as well as ambient temperature, density and below-trajectory topography, is saved every 6 hours, at 00, 06, 12 and 18 UTC.

The Flexpart convection scheme (see Section 3.1.2) is switched on in all the runs, except when testing the sensitivity to not using it.

Flexpart can use a shortened timestep to more precisely model the turbulent motions in the BL (Stohl et al., 2011). However, in this study the details of the motions in the BL are not in focus, and it is assumed that a trajectory having reached sufficiently low will mix with the surface air on timescales much shorter than those of the transfer from the lower troposphere to the CPT. As recommended by Stohl et al. (2011) for large-scale studies, this option is therefore not used.

3.4 Trajectory analysis

The analysis of the trajectories is based on the 6-hourly model output described above. Figure 3.5 shows the time series of the altitude above sea level of an example trajectory to illustate the different quantities that are computed for each trajectory.

The numerical experiments aim to locate the surface origins for air in the TTL, i.e. the last

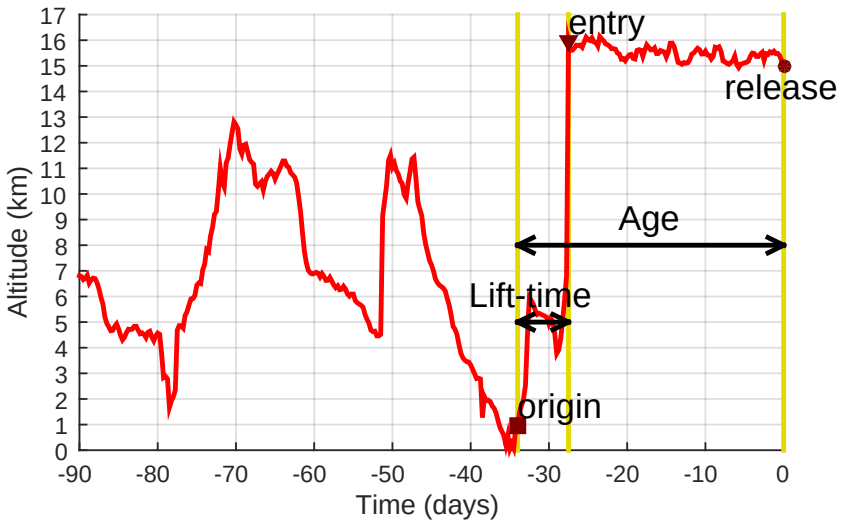

Figure 3.5: Example trajectory: The trajectory's altitude above sea level is plotted against the time elapsed since its release. Note that the time is negative because the trajectory is simulated backwards in time. The statistics used in this study are illustrated; see text for details.

time it mixed with surface air, and the age of the air relative to these origins. In this study the focus is on free tropospheric processes in the tropics, mainly convection, and I have therefore chosen to analyse the transport starting from 1 km altitude, corresponding roughly to the top of the BL. Moreover, since the main motivation of the study is to investigate surface-to-tropopause transport relevant for surface trace gas sources such as the ocean, the origins are not allowed to be above too high terrain. The (BL) origin of a trajectory is defined as the last time in the model output when the trajectory's altitude above sea level was less than 1 km. As 1 km is a typical height for the BL and vertical mixing throughout the BL normally happens on timescales of hours or less (see Section 2.1.2), it is reasonable to assume that for a trajectory located below 1 km the timescale for mixing with surface air is short compared to the transit times to 15 or 17 km.

Once the BL origin has been detected, the age of the trajectory is determined as the time from origin to release. The age defined in this way describes how long it is since air located at 15 or 17 km was last below 1 km, hence in surface contact according to the assumption above.

However, to describe the duration of the trajectory's ascent to 15 or 17 km, it can be useful to use another measure than the age. This is because the trajectories usually have not ascended gradually through the upper troposphere shortly before the release. They have often lingered for weeks near or above their release altitude, after a rather fast lift from the BL, as is the case for the example trajectory shown in Figure 3.5. Another time-statistic, the lift-time, has therefore been defined. Once the origin has been located, the first time the trajectory was above 15 km after the origin can be found; this is called its entry to 15 km. For trajectories released at 17 km, the entry to 17 km can also be defined in the same manner. The time from origin to entry is called the lift-time (to 15 or 17 km), and it represents the time it took for the trajectory to rise from the BL to the respective altitude. If a trajectory released at 15 km does not reach above 15 km between origin and release, the lift-time to 15 km is identical to the age of the trajectory. However, normally the lift-time is much shorter than the age.

To summarize, from the computed statistics described above, the ensemble of trajectories can be characterized by an age distribution, a distribution of lift-times and a geographical distribution of BL-origins. These are the three basic statistics in this study. However, not all the trajectories will reach below 1 km during the simulation. For those who do not, none of the statistics can be computed; these trajectories are called the 'non-transferred' trajectories. The statistics are available only for the trajectories that *do* reach below 1 km during the 90 days.

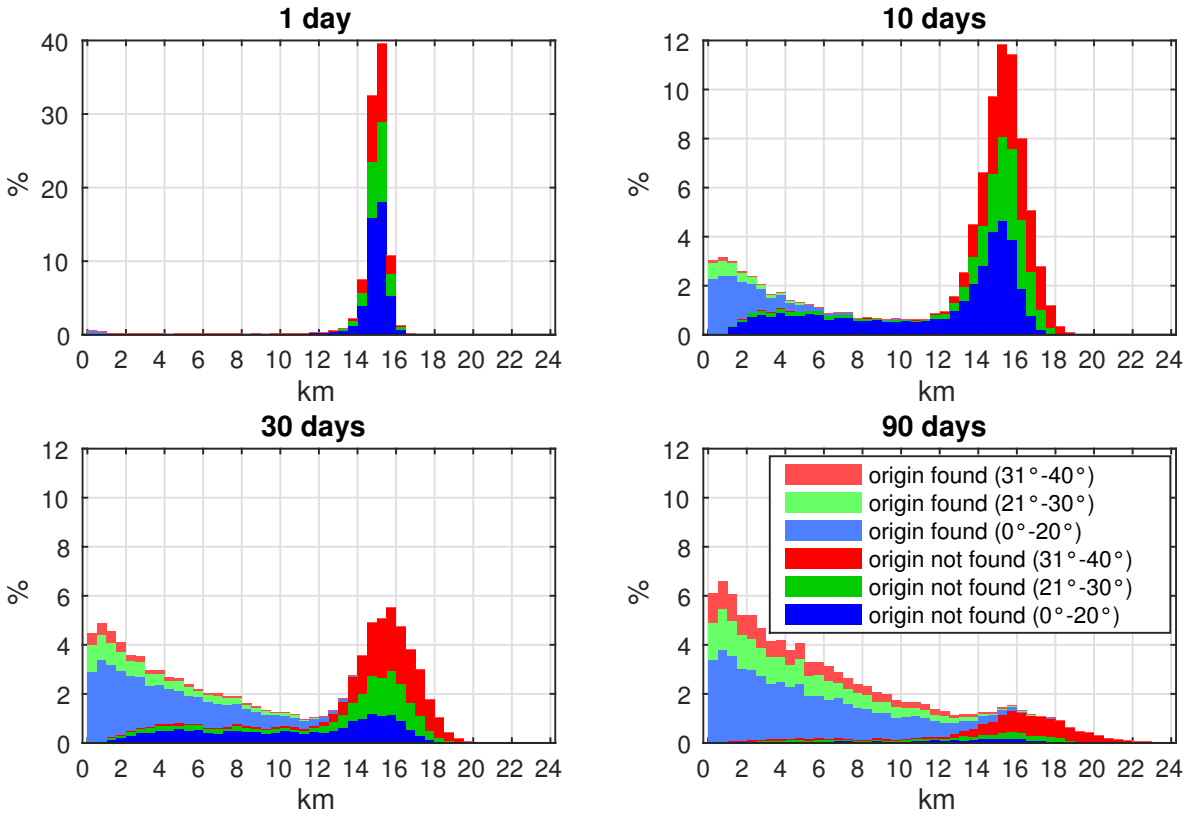

Figure 3.6: Distribution (in %) of altitude above sea level for the trajectories released at 15 km on 1. March 2013, after 1 day, 10 days, 30 days and 90 days of backward simulation. The distribution is subdivided into the trajectories released between 20°S - 20°N (blue), those released in 21°-30° S/N (green) and 31°-40° S/N (red). It is further subdivided to distinguish the trajectories for which the origin has been found (i.e. have been below 1 km) so far in the simulation – these are shown with paler colors. The bin width is 0.5 km.

These are called the 'transferred' trajectories.

Note that when the origin is located, no interpolation is done to estimate when the trajectory crossed 1 km; it is simply the latest output time it was below 1 km that is used. This means that both the age and the lift-time as recorded by the analysis is an upper estimate. Therefore, whenever descriptions like 'trajectories younger than 30 days' or 'trajectories lifted in less than 1 day' are given, it also includes the trajectories for which the computed age or lift-time was exactly that value.

3.5 Test results

The setup described in Sections 3.3-3.4 was tested using trajectories releases on 1. March 2013 at 15 km. The winter season was chosen because that is when the tropical upwelling to the stratosphere (across 100 hPa) is strongest (Holton et al., 1995), and the 2012-13 winter season was relatively unperturbed by ENSO (see Figure 5.18). Here some test results are presented, and some issues regarding the analysis are discussed.

Figure 3.6 shows the distribution of altitudes for the trajectories at different stages in the 90 day simulation. During the first 10 days of backward simulation, the trajectories initially located at 15 km disperse in the vertical down to 12 km and up to 18 km. The distribution also has a left-wing tail of trajectories that have reached down through the troposphere, and many (16.2 %) have already been below 1 km. This tail is mainly trajectories released within 20°S - 20°N.

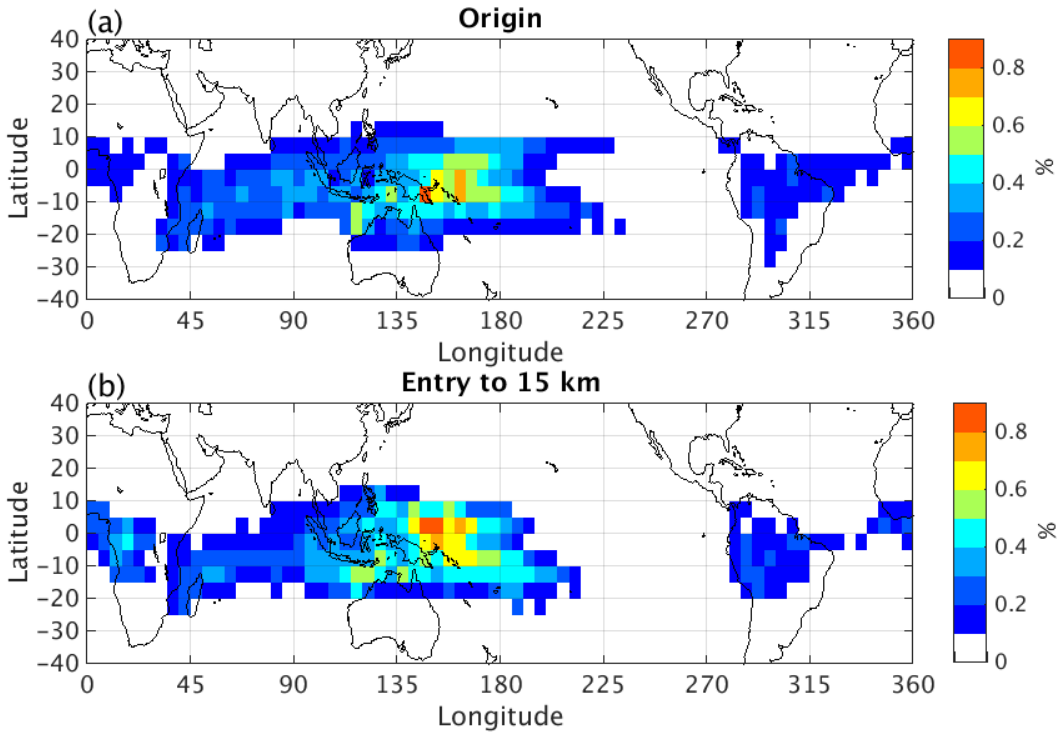

Figure 3.7: Geographical distribution of origins (a) and entry to 15 km (b) locations for the trajectories released at 15 km on 1. March 2013. The colors indicate the percentage of the trajectories that have origin/entry within each bin of 5° x 5°.

As time goes by, the majority of the trajectories move from the TTL to the troposphere, and an increasing number has been below 1 km. After 30 days, there is still a considerable number of trajectories located in the troposphere below 12 km but not having been below 1 km (14.2 % of the total number in the simulation). However, after 90 days this amount is very small (1.5 %). After 90 days, still 17.2 % of the trajectories have not found an origin, but these mainly consist of trajectories released outside 30°S - 30°N that has stayed above 12 km in the whole simulation[3]. To sum up, the majority of the releases at 15 km fulfill the transport criteron in 90 days. 94.4 % of those released in 20°S - 20°N are transferred, while it is 84.4 % for those released in 21°-30° and 57.3 % for those released in 31°-40°.

Figure 3.7 shows the geographical distribution of origin (a) and entry to 15 km (b) for the transferred trajectories. The trajectories originate mainly in the West Pacific and Indian Ocean, with smaller contributions from Africa and South America. This is as expected as it is in these areas the deepest convection occurs in NH winter (Gettelman et al., 2002). Entry to 15 km is roughly in the same areas, which is likely due to the domination of short lift-times (not shown). More than 25 % of the transferred trajectories have a lift-time to 15 km of less than 1 day, and most of these (19.3 %) were lifted betweeen two neighboring output-times (i.e. in less than 6 hours). Moreover, it turns out that as much as 87.9 % of the transferred trajectories at some point between origin and release were lifted more than 5 km during 6 hours, and 56.0 % were lifted 10 km in 6 hours. As it is improbable that the grid-scale vertical velocities are able to produce these very fast lifts, the convection scheme must play an important role here (see Section 3.1.2).

Figure 3.8 shows the percentage of trajectories that are younger than 90, 30 and 10 days as function of release location at 15 km. The air is youngest above the West Pacific and the Indian

[3]That they have not been below 12 km during the simulation cannot be deduced from the figure; this was found by considering the whole altitude time series of the non-transferred trajectories.

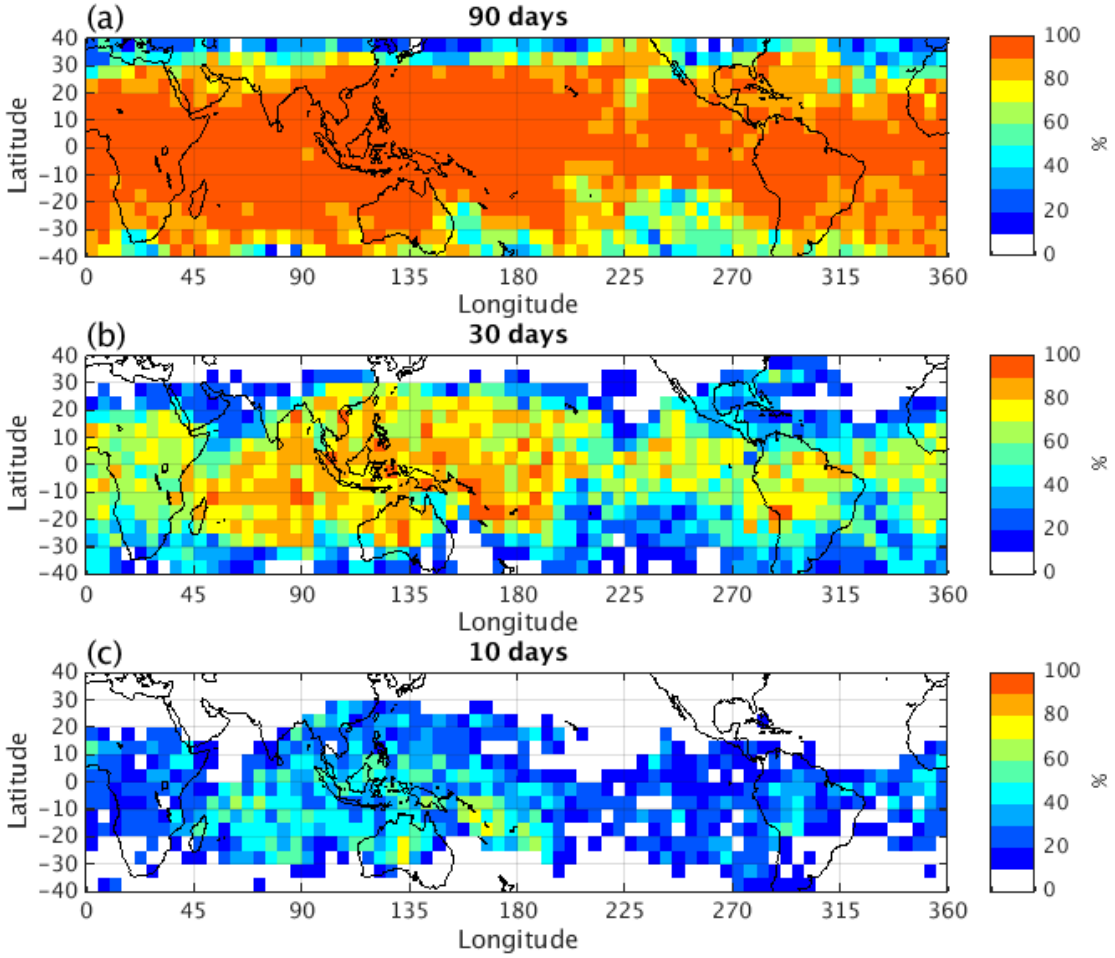

Figure 3.8: Percentage of the trajectories released at 15 km on 1. March 2013 that are younger than 90 days (a), 30 days (b) and 10 days (c). Trajectories are binned at their release locations. The bin size is 5° x 5°.

Ocean (here ∼80 % are younger than 30 days and ∼40 % are younger than 10 days), and is in general younger near the equator and older toward higher latitudes. There is a sharp decrease in the fraction of young trajectories around 30°S/N, and near 40° the relatively few trajectories that are transferred are old.

An important question is whether the trajectory pathways are consistent with *tropical* transport. Could it be that a large portion of the trajectories are rising via the extratropical troposphere? In particular, the releases furthest away from the equator should be carefully examined. It could be that many of these releases have not been transferred in the tropics if they are located on the extratropical side of the subtropical jets. To check this issue, the latitudes of the trajectories in different stages of the transport were investigated. Figure 3.9 shows, for the transferred trajectories, the latitude (north or south) of origin and for entry to 15 km, as well as the highest latitude visited during the initial lift to 15 km and in the time after entry to 15 km. Hardly any trajectories have origin or entry to 15 km outside the tropics (>23.5°). During the lift, they frequently move into the subtropics, but few go poleward of 40°. On the other hand, there is a considerable number that travel into the extratropics in the time after they enter the TTL (Fig. 3.9d). However, as virtually all of them have origin and entry to 15 km within or near the tropics, I find that the excursions into the extratropics after being lifted to 15 km can be tolerated.

Another issue to be considered is the use of constant altitude surfaces for releasing trajectories. In the inner tropics (about 23°S - 23°N) both the tropopause and the isentropes near it

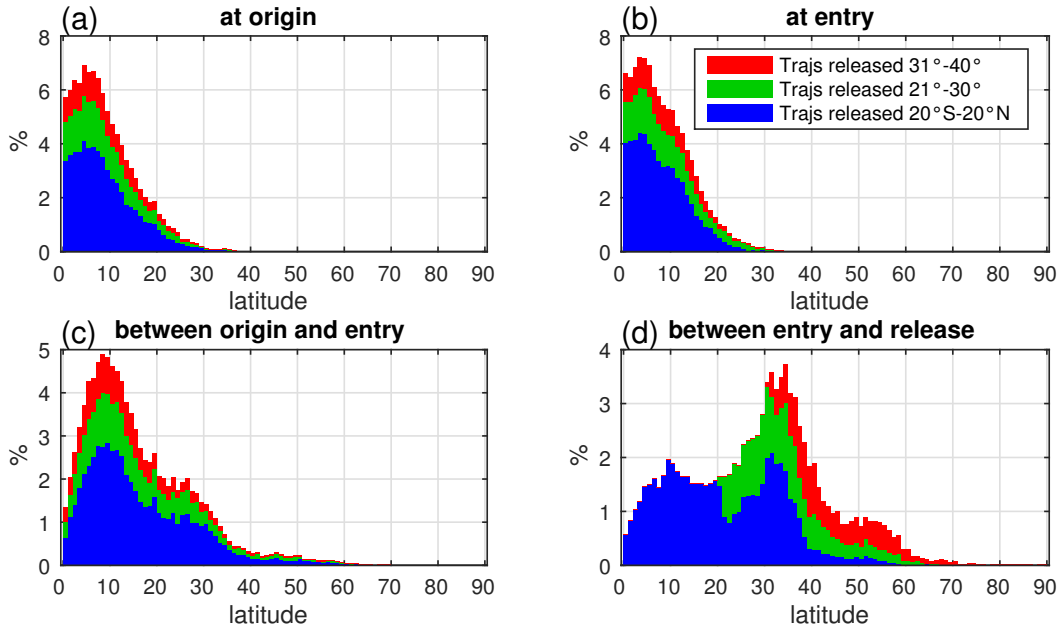

Figure 3.9: The distribution of latitude (north or south) of the transferred trajectories: (a) latitude at origin, (b) latitude at entry to 15 km, (c) highest latitude during lift from origin to entry to 15 km, (d) highest latitude between entry to 15 km and release. The PDF is separated into contribution from trajectories released at different latitudes in the same way as in Figure 3.6. The bin width is 1 degree of (absolute) latitude.

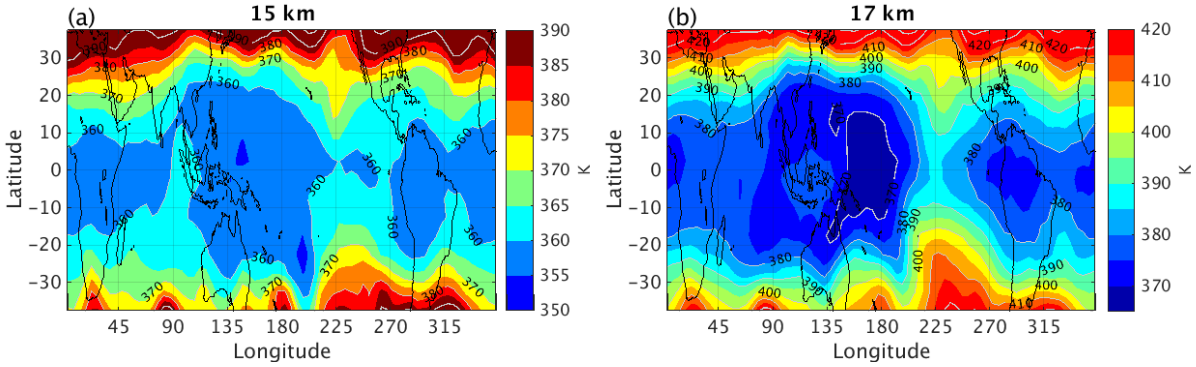

Figure 3.10: Potential temperature (K) at 15 km (a) and 17 km (b) on 1. March 2013 00 UTC.

are close to horizontal, but in the subtropics these surfaces slope downward with higher latitude (Holton et al., 1995). Because of the tropopause sloping downward away from the tropics, the releases at the higher latitudes (30°-40°S/N) will be more stratospheric than releases close to the equator, and they will be at a higher potential temperature. This difference in regime is illustrated in Figure 3.10a, which shows the potential temperature at 15 km on 1. March 2013. Due to the slope of the isentropic surfaces, the trajectories released at 15 km at 30°-40°, especially in the winter hemisphere, have a higher potential temperature (380-390 K) than those released at the same altitude closer to the equator (∼360 K). In a thermodynamic context, they are therefore 'higher'. If a trajectory at 40°N and a trajectory at 10°N both are at 15 km and have travelled adiabatically from the equator, the former will have left the equator at a higher altitude than the latter. Nevertheless, Figure 3.10a indicates that the potential temperature does not vary very much at 15 km within the inner tropics, in agreement with Holton et al. (1995), so that this issue mainly concerns the releases in the sub- and extratropics. In Figure 3.10b, the potential temperature at 17 km has been plotted. The same issue is found at this

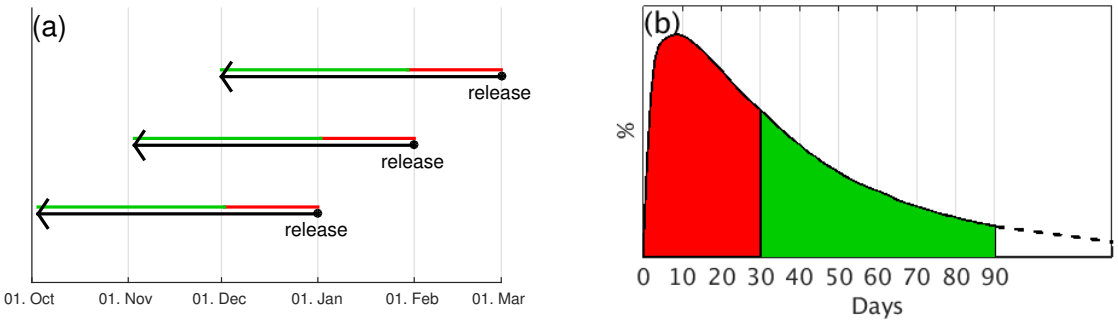

Figure 3.11: (a) Timeline of the three backward simulations of 90 days used to study a DJF season. Trajectories originating in the red part of the simulations are younger than 30 days. (b) Illustration of the age distribution plot. It displays the relative number of trajectories having different ages. Trajectories younger than 30 days are shown in red. The dotted line represents the trajectories older than 90 days, whose origin is not known.

altitude; here the difference in potential temperature is even larger and it begins at a lower latitude. The sloping isentropes should therefore particularly be kept in mind when studying trajectories released at 17 km.

Because the large differences in potential temperature is most pronounced poleward of 30°, and also because the trajectories released here to a larger extent move into the extratropics (Fig. 3.9) and are not transferred (Fig. 3.8), I have chosen to exclude the releases poleward of 30° for most of the analyses (see Section 3.6).

3.6 Conventions

The statistics defined for each trajectory have now been described (Section 3.4) and studied in a test run (Section 3.5). In this section, the conventions for analysing results from the ensembles of trajectories will be described.

3.6.1 Sampling of trajectories

In the results, the 15 and 17 km releases will always be shown in separate plots. Due to the issues discussed in Section 3.5, the analysis will be limited to the trajectories released within 30°S - 30°N. The releases in 30°-40° will only appear in maps binning the trajectories at their release locations, such as in Figure 3.8. In some cases, the ensemble of trajectories used will be further limited by looking at the subset of the releases in 30°S - 30°N that either have origin or release within specified regions.

The trajectories are always released at the interface between two months, i.e. at 00 UTC on the first day in each month. Results for each season will often be presented in this thesis, referred to as DJF (December-February), MAM (March-May), JJA (June-August) and SON (September-November). Whenever considering results from a season, the releases at the end of each of the 3 months of the season are used (e.g. for DJF, the releases on 1. January, 1. February and 1. March, see Fig. 3.11a).

3.6.2 Diagnostics

To study the age of air, probability distribution functions (PDF), showing how many percent of the trajectories have different values of age, are plotted. The idea is illustrated in Figure 3.11b, and is in anology to the age spectrum used in the stratosphere (Waugh and Hall, 2002). The age of the non-transferred trajectories is unknown, but it *is* known to be above 90 days. These trajectories therefore constitute a continuation of the tail of the age distribution, as illustrated

in Figure 3.11b. Therefore, for all statistics of the age, 100 % will mean the total number of trajectories simulated, including also the non-transferred trajectories. In addition to displaying the whole distribution, the age will be analysed using the median age[4] and the percentage of trajectories that are younger than 30 days (or sometimes another threshold).

The transferred trajectories will further be used for studying locations of origin and entry, and the lift-times. Nothing is known about the origins, entries and lift-times of the non-transferred trajectories; even though they are older than 90 days, their lift-times could be short, and they are likely to originate from the same important areas in the tropics as the transferred trajectories. It is therefore most meaningful to exclude the non-transferred trajectories when studying origin, entry and lift-time, so 100 % will in these cases mean the total number of transferred trajectories. Furthermore, when studying origins and entries (to 15 or 17 km), only trajectories younger than 30 days are considered. There are two reasons for this. Firstly, as the fastest transit times are most important for the transport of short-lived species, the sources of the air younger than 30 days is more interesting that the sources of air with age of 30-90 days. Secondly, locating origins 30 days back only ensures that all trajectories originate in the same season as they are released, which avoids confusing the seasons together (i.e. the trajectories aged 30-90 days will in some cases originate in the previous season, as illustrated by the green lines in Fig. 3.11a). When studying the distribution of lift-times, however, trajectories originating in all the 90 days will be considered.

To sum up, the following diagnostics will be used:

- **Age:** Using all trajectories released between 30°S - 30°N, or from specified region, or in 5° x 5° cells. Separate study of 15 km and 17 km releases.
  - distribution of age (PDF or cumulative PDF)
  - median age
  - percentage that are younger than 30 days
- **Lift-time:** Using all *transferred* trajectories released between 30°S - 30°N, or from specified region. Separate study of 15 km and 17 km releases. For 15 km, the lift-times to 15 km are studied. For 17 km, lift-times to 15 km and to 17 km are studied separately.
  - distribution of lift-time (PDF or cumulative PDF)
  - median lift-time
  - percentage that are lifted in less than 1 day / 10 days
- **Origin:** Using trajectories younger than 30 days released between 30°S - 30°N. Separate study of 15 km and 17 km releases.
  - display of the percentages that originate from 5° x 5° cells (map), or from larger, specified regions (visualized with bars)
- **Entry:** to 15 km or (for 17 km release only) 17 km. Studied in the same way as the origins[5]

[4]The median age is the age which half the trajectories (including also the non-transferred) are younger than. Although it is the *mean* age of air that is often used in the literature on transport (e.g. Waugh and Hall (2002), Park et al. (2007)), I prefer to use the median in this study. This is simply because it is always possible to calculate the median age as long as more than half of the trajectories considered are transferred. I order to calculate the mean, the age of the non-transferred trajectories must either be neglected or extrapolated from the distribution. I found this problematic, since the mean is sensitive to the tail of the distribution. If the median age found here is to be compared with the mean age calculated in another study, it should be kept in mind that median age will always be lower than the mean due to the right-skewed form of the age distribution.

[5]The entry will not be much used as a diagnostic in this study. Its main purpuse is to calculate the lift-time.

Chapter 4

Sensitivity studies

In this chapter, several sensitivity tests to changes in the experimental setup are performed. The tests are described in Section 4.1, and the results are presented in Section 4.2 and discussed in Section 4.3. A summary of the main findings are given in Section 4.4.

4.1 Experimental setup

To investigate how sensitive the results are to changes in various factors in the setup, several more runs with releases on 1. March 2013 were performed, varying model or analysis parameters. The sensitivity tests are summarized in Table 4.1 and are described in the following.

The definition of the origin is rather arbitrary. Analyses using 0.5 km and 2 km as origin height, as well as using 1 km above the local topography (instead of above sea level) were performed to test the sensitivity to this definition. A run with more frequent output was also carried out, which in some cases allows detection of low trajectory altitude that is missed with less frequent output. This run was analysed using origin height of 1 km and 0.5 km.

A run with more trajectories (0.5° distance between releases) and one with fewer (2° distance)

Setup name	Difference from baseline	Nr of trajs
Baseline	DJF, backward from 15 km above sea level, 1. Mar 2013, every 1°, 30°S - 30°N, conv. scheme on, BL-scheme off, output every 6h origin: 1 km above sea level (a.s.l.)	21960
BL 500m	origin: 0.5 km a.s.l.	21960
BL 2km	origin: 2 km a.s.l.	21960
BL-topo	origin: 1 km above topography	21960
dt=1h	hourly output	21960
dt=1h + BL 500m	hourly output, origin: 0.5 km a.s.l.	21960
0.5°	release every 0.5° lon/lat	87120
2°	release every 2° lon/lat	5580
rel 40-40	include releases 30°-40°	29160
rel 20-20	releases 20°S - 20°N only	14760
BL-scheme on	turbulence in BL modelled more accurately	21960
3 releases	releases also 1. Feb, 1. Jan	65880
17km	release: 17 km a.s.l.	21960
Conv off	convection scheme off	21960
Conv off + 17km	conv. scheme off *and* releases: 17 km a.s.l.	21960
Forward	Forward in time, release at topography $<$ 1 km a.s.l. 1. Dec 2012	20976

Table 4.1: Sensitivity studies: The table describes the setup used in each sensitivity test and gives the number of trajectories used in the analyses.

were also carried out to see whether the number of trajectories is sufficient.

Following the conventions given in Section 3.6, the baseline setup only uses the trajectories released in 30°S - 30°N for the analysis. To study how the results change by the width of the latitude-band considered, analyses using releases in 40°S - 40°N and 20°S - 20°N were performed.

Although the BL-turbulence parameterization in Flexpart should not make much difference in large-scale studies (see Section 3.3), a run with this scheme switched on was cunducted just to check.

The trajectories are released on 1. March and run for 90 days in order to capture the NH winter season (DJF). However, as the age distribution is relatively dominated by trajectories younger than 30 days, especially in the most important convective areas (see Figure 3.8), the run will represent February more than the two other months. A run where trajectories were released also 1. February and 1. January was therefore carried out, to see if the results are different when the three months are more equally represented (this is also the way the seasons will be represented in the later results, see Figure 3.11a).

A run was also performed where trajectories were released at 17 km instead of 15 km, to see how the trajectory behavior changes when they are released at the higher level. Both for releases at 15 and 17 km, a run without the convection scheme (see Section 3.1.2) was carried out to see how significant this scheme is for the results.

Finally, a run was performed using Flexpart in forward mode to test how a forward trajectory run differs from the backward runs. In the forward run, trajectories were released at the same latitudes and longitudes as in the baseline run, but from the surface (topography), on 1. December 2012, and simulated 90 days forward in time. Only trajectories that were released from topography lower than 1 km are considered in the analysis. Entry both to 15 and 17 km can be found for a trajectory in the forward run by locating the first time it was above the respective altitude. The origin is defined as the last time the trajectory was below 1 km above sea level before this, and is thus defined separately for 15 and 17 km. Having found both an origin and an entry, the lift-time can be computed in the same way as in the backward runs. However, the age cannot be calculated in an equivalent way. It could be defined as the time from release to first reaching 15 or 17 km, but then it would not be the time since the last BL-contact because the trajectory is below 1 km at the origin (and possibly also several times between the release and the origin). Age is therefore not defined in the forward run.

For all the backward setups, the geographical locations of origins will be studied using all 90 days as well as only the first 30 days, to see how large the difference by limiting to the first 30 days is.

4.2 Results

Figure 4.1 (left panel) shows the percentage of the trajectories that are transferred during the simulation, and the percentage having age below certain values. In most of the runs, the majority of the trajectories are transferred, around half of them are younger than 30 days and around 20 % is younger than 10 days. In the runs releasing at 17 km and/or without the convection scheme, these numbers are lower. The most striking outlier is the forward run, which have very few transferred trajectories. Note that the forward run is not present in the age statistics because age is not defined in the forward run. The right panel in Figure 4.1 shows the percentage of transferred trajectories lifted in less than 1 and 10 days to 15 and 17 km. A considerable percentage of the trajectories are lifted in less than 1 day in all the runs except for the ones without convection scheme. Figure 4.2 shows the locations of origin of the trajectories, using a region classification for the tropics. Indonesia and West Pacific are the regions from which most trajectories originate in all the runs, but most of the regions contribute significantly. The most important features appearing in these two figures for each run will now be pointed out.

Using more or less trajectories (setups 0.5°, 2°) give results very similar to the baseline. This is true also for the run with the BL-scheme on. The run with releases in all three months ('3

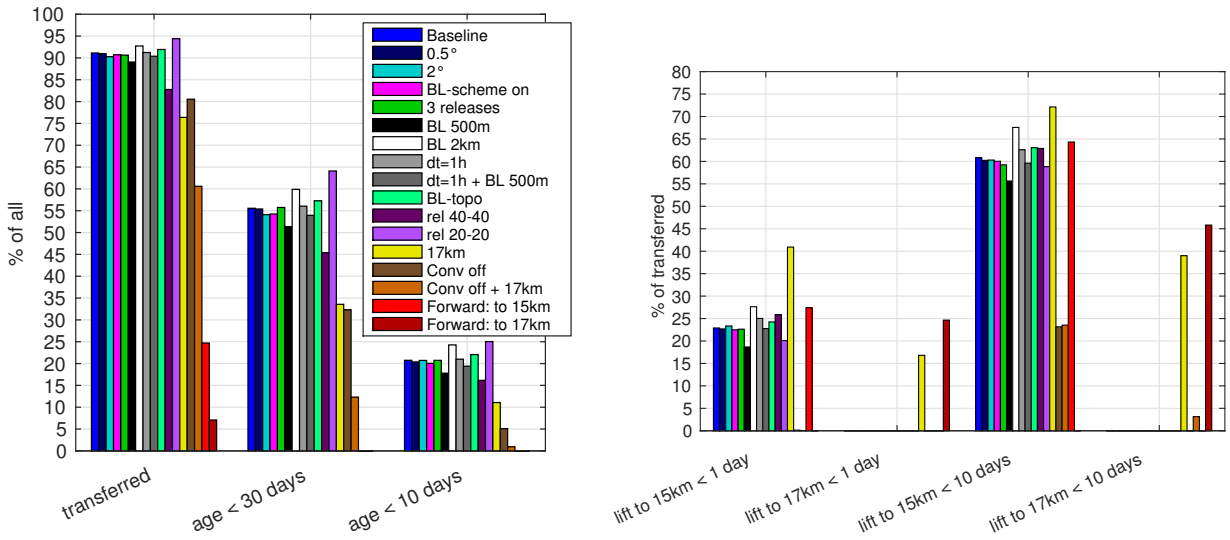

Figure 4.1: Left: The percentage of the trajectories in each sensitivity study (Table 4.1) that (from left) are transferred between 1 km and 15 km (17 km for '17 km', 'Conv Off + 17 km' and 'Forward: to 17 km') during the 90 days, and are younger than 30 and 10 days. Right: The percentage of the *transferred* trajectories in each study that have lift-time to 15 km and 17 km less than 1 day and 10 days. Note that the lift-time to 17 km is only defined for the runs with releases at 17 km and for the forward run.

releases') does not give noticably different results either, except that slightly more trajectories originate from the South America region, especially when considering origins from all 90 days.

On the other hand, changing the origin height causes some difference. The trajectories are slightly older (fewer have age less than 10 or 30 days), and with longer lift-times to 15 km (fewer have lift-time less than 1 or 10 days), if 500 m is used, compared to 'Baseline'. Conversely, they are younger, with shorter lift-times, if 2 km is used. In 'BL 500m', 51.3 % and 17.8 % of the trajectories are younger than 30 and 10 days, respectively, against 55.6 % and 20.8 % in the baseline and 59.9 % and 24.3 % in 'BL 2km'. Thus, an increase in the origin height from 500 m to 2 km results in a relative increase in the trajectories younger than 30 days at 15 km of 16.8 %, and 36.4 % for the number younger than 10 days. The median age (not shown) is about 3 days higher in 'BL 500m' than in 'Baseline' and 3 days higher in 'Baseline' than in 'BL 2km'. The percentage with lift-time to 15 km of less than 1 day is 48.0 % higher in 'BL 2km' relative to 'BL 500m', and for lift-time of less than 10 days the relative difference is 21.4 %.

Furthermore, there is a westward shift in the origins in the Pacific in the 'BL 2km' setup (more origins in West Pacific and less in Central and East Pacific) and a corresponding eastward shift in the 'BL 500m' setup. This shift is more pronounced when the origins of trajectories older than 30 days are also included. There is also a decrease in the origins from Africa of ∼30 % in 'BL 500m' relative to 'Baseline'.

There are slightly more trajectories younger than 30 days and with short lift-times in the run using hourly output ('dt=1h') compared to 'Baseline' (which uses 6-hourly output). This effect is small compared to the effect of changing the origin height (described above). However, the difference between using 1 km and 0.5 km as origin altitude is weaker in the run with hourly output. For example, in the "age $<$ 30 days" bars in Figure 4.1 the 'dt=1h' and 'dt=1h + BL 500m' are closer together than the 'Baseline' and 'BL 500m'. The difference in median age (not shown) between 'dt=1h' and 'dt=1h + BL 500m' is only 1.7 days, while this difference is found to be 3 days between 'Baseline' and 'BL 500m'.

Using 1 km *above topography* as origin definition ('BL-topo') does not have a large impact, but is noticable by slightly younger trajectories and an increase of the origins above continent

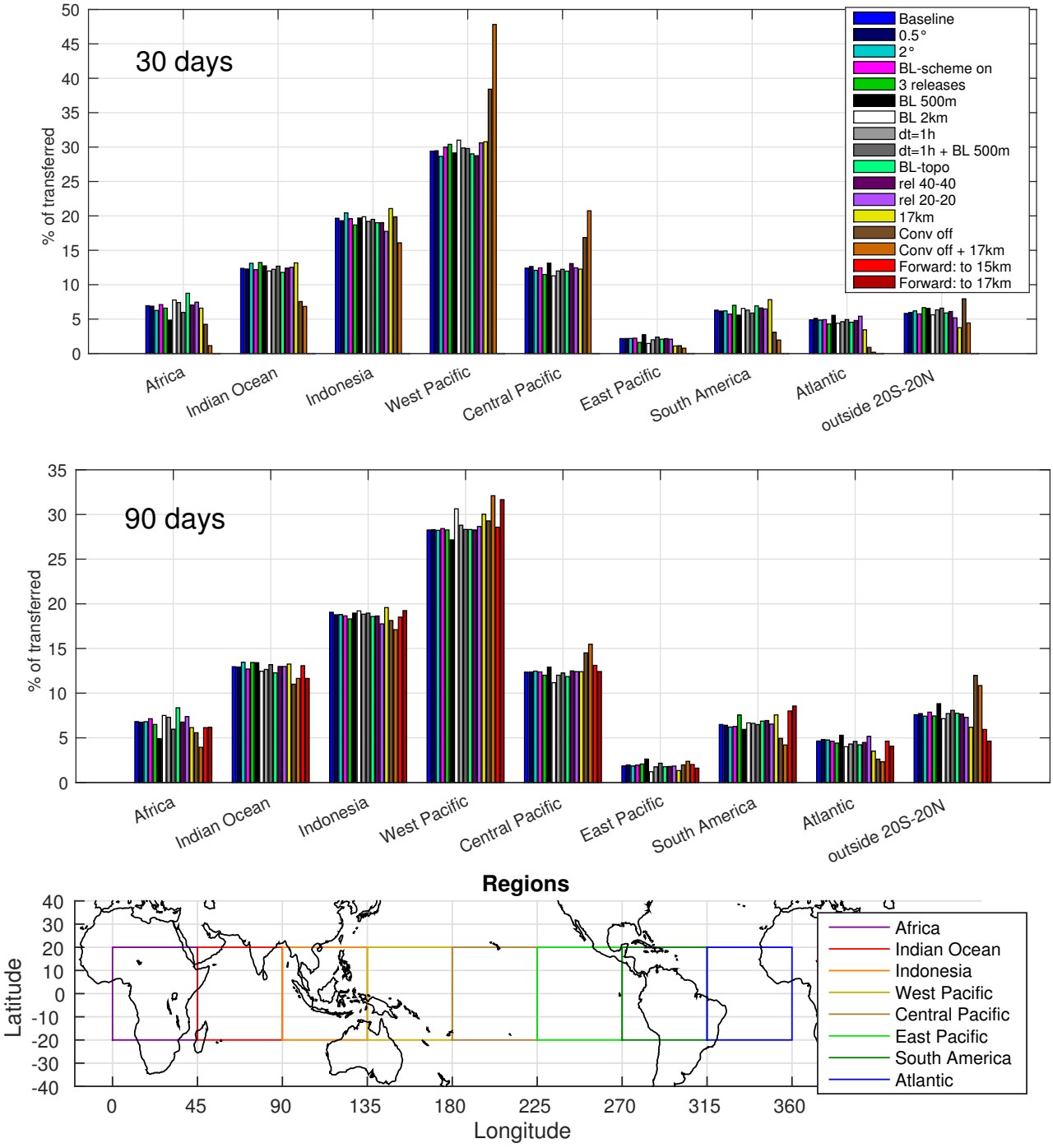

Figure 4.2: The percentage of the transferred trajectories in each sensitivity study (Table 4.1) that have origin in each region; top: origins of trajectories younger than 30 days only; middle: origins of all transferred trajectories; bottom: the definition of the regions. Because age is not defined in the forward run, the origins in this run is only shown in the 90 days plot, where origins found in the entire simulation are included.

regions relative to 'Baseline' (Africa experiences a 26.0 % increase, and South America 9.8 %, using 30 days).

The width of the latitude band has a large impact on the percentage of young trajectories; the 'rel 40-40' has 18.4 % fewer trajectories younger than 30 days, and the 'rel 20-20' has 15.4 % more, relative to 'Baseline'. The lift-time shows an opposite tendency to that of the age: there are *more* fast lifts to 15 km in 'rel 40-40' than in 'rel 20-20', although the difference is

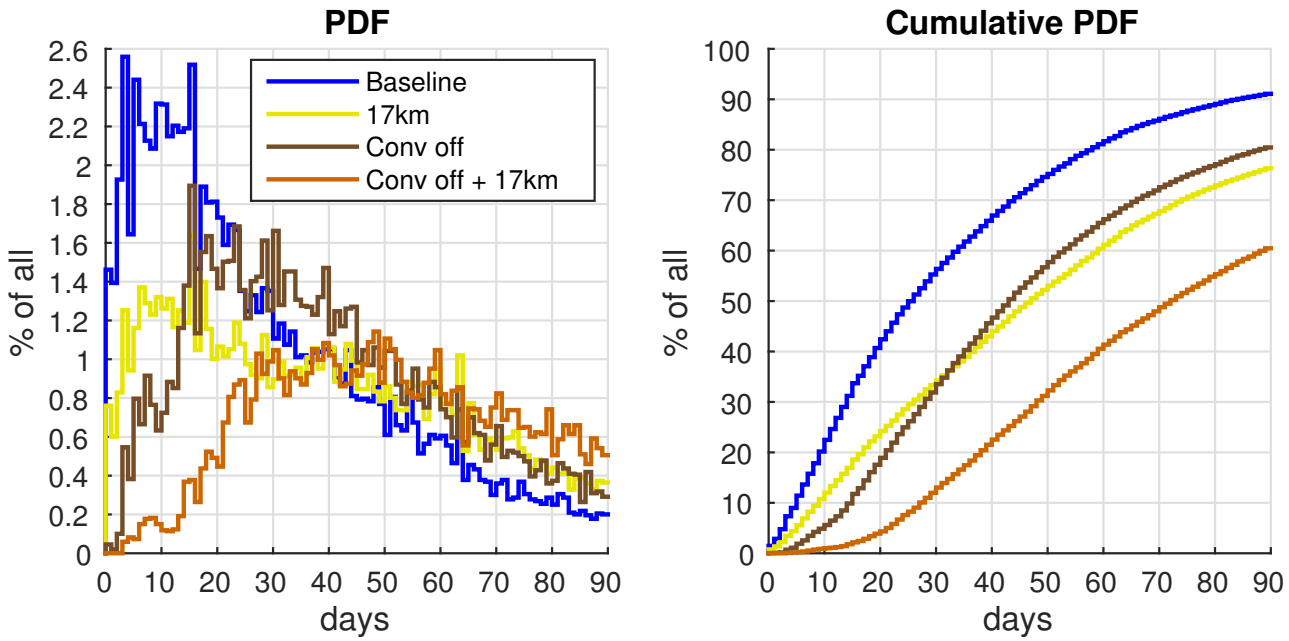

Figure 4.3: Distributions of age for the trajectories in the sensitivity runs (described in Table 4.1) with releases at 15 and 17 km with and without the convection scheme. Left: Probability distribution functions of age. Right: The same distributions are plotted cumulatively. The bin width is 1 day.

not as large as for the age. The origin locations, on the other hand, do not appear sensitive to including trajectories released at 20°-40° latitude.

There are fewer young trajectories in the '17 km' run than in 'Baseline'. Only 33.6 % are younger than 30 days, and 24.6 % are not transferred in 90 days, compared to 8.9 % in 'Baseline'. The origins, however, are largely in the same areas in '17 km' and 'Baseline', although there is a small increase in the importance of South America, Indonesia and the West Pacific for the releases at 17 km.

Switching off the convection scheme leads to older trajectories. The percentage of trajectories younger than 30 days is 32.3 % at 15 km and 12.3 % at 17 km without the convection scheme, compared to 55.6 % and 33.6 % when the scheme is used. The lift-times below 1 day disappear almost completely, while the lift-times of less than 10 days become much more rare, especially for lift-times to 17 km. While 39.0 % of the lifts to 17 km are faster than 10 days in '17 km', this is only 3.1 % in 'Conv off + 17 km'. The patterns of origins change too. For trajectories younger than 30 days, there are much less origins from South America, Africa, the Indian Ocean and the Atlantic, while a larger portion comes from the West and Central Pacific, when the convection scheme is not used. In both 'Baseline' and '17 km', ∼42 % of the trajectories originate from these two regions, while this is 55.3 % in 'Conv off' and 68.6 % in 'Conv off + 17km'. The differences are still present, though not nearly as pronounced, when also the transferred trajectories older than 30 days are included.

In the forward run, very few of the released trajectories complete the transfer. While 91.1 % of the trajectories in 'Baseline' and 76.4 % in '17 km' are below 1 km during the 90 days, only 24.7 % of the trajectories in the forward run reach 15 km, and only 7.1 % reach 17 km. However, the origin locations are similar in the backward and forward setups.

4.2.1 Age distribution

To further study how the age of air differs between 15 km and 17 km and in runs with and without the convection scheme, the distributions of age in these runs are plotted together in Figure 4.3. Both releasing higher and switching off the convection scheme cause a shift in the

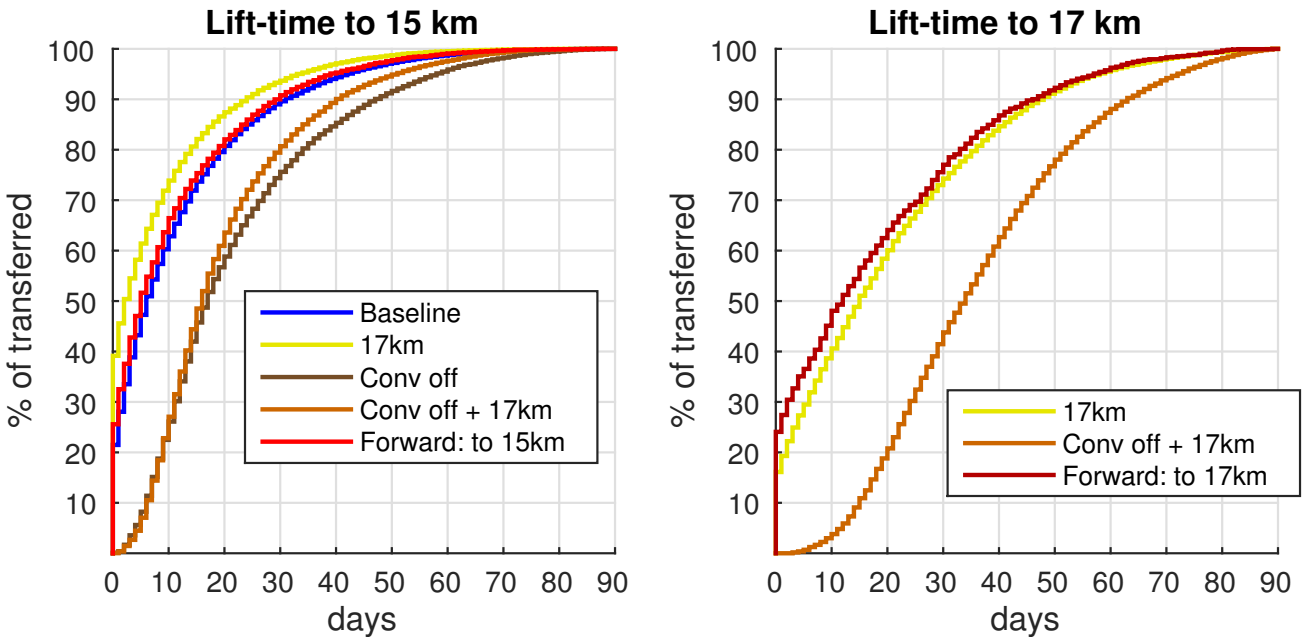

Figure 4.4: Cumulative PDFs of lift-time for the transferred trajectories released between 30°S - 30°N in some of the sensitivity runs. The bin width is 1 day. Thus, the value of the first bar is the percentage lifted in less than 1 day. Note that these distributions reach 100 % because the non-transferred trajectories are excluded from the analysis of lift-times, unlike in the analysis of age (see Section 3.6.2).

age distribution to higher ages, and the distribution gets a broader, less prominent peak. The median age is a simple quantification of the transit times and can be read directly off the CDF (where it crosses 50 %). The median age at 15 km is 26 days with the convection scheme and 43.5 days without. At 17 km it is 47.25 and 72.5 days, respectively. Another striking difference is that there are much fewer trajectories at the lowest ages in the runs without convection scheme. This is particularly the case at 17 km, where only 0.9 % of the air is younger than 10 days without the scheme, compared to 11.1 % when the scheme is used. It is important to remember that these numbers are averages for 30°S - 30°N. The age distribution will vary from area to area.

4.2.2 Lift-time distribution

Figure 4.4 compares the distribution of lift-times in the baseline run, the forward run and the runs with releases at 17 km and/or without convection scheme. This figure supplements the results on lift-time shown in the right panel of Figure 4.1.

The lift-time distribution is dominated by short lift-times when the convection scheme is switched on. In the baseline run, 22.9 % of the transferred trajectories are lifted in less than 1 day, and 60.8 % in less than 10 days. In the '17 km' run, the lift-times to 15 km are even lower; as much as 40.9 % of the transferred trajectories are lifted to 15 km within 1 day. The lift-times to 17 km get a larger contribution from longer times, but is still dominated by fast lifts. 16.8 % of the trajectories are lifted to 17 km within 1 day in the '17 km' run, and 39 % within 10 days. The lift-times are similar in the forward run, but slightly faster, in particular to 17 km.

When the convection scheme is not used, the very large peak at lift-times of less than 1 day disappears, and the majority of the trajectories have lift-time to 15 km between 5-35 days, and to 17 km between 15-60 days.

4.3 Discussion

In several of the sensitivity studies, smaller or larger differences compared to the baseline run has been detected. Now a discussion of what can be learned from these is given.

The results are found not to be sensitive to increasing the number of trajectories by a factor 4 relative to 'Baseline' ('0.5°'). This is taken to imply that the baseline setup uses a sufficient number of trajectories to capture the important features of the transport. The absence of changes from switching on the BL-scheme is as expected, and it confirms that the more detailed modelling of BL-turbulence is not central for this study, as proposed in Section 3.3. Of course, this insensitivity is also due to starting at 1 km, which means that the trajectories in many cases will not be in the BL at the origin, and the use of the BL-scheme is therefore irrelevant for these trajectories.

The small differences obtained by releasing trajectories also 1. January and 1. February indicate that the features of the transport is similar in the three months. It is therefore reasonable to assume that these features vary on timescales longer than a month, so that releasing once a month will be sufficient to represent the temporal variability of the transport features. The increase in origins South America when using all 90 days is probably due to the inclusion of origins in October and November. As can be seen in Figure 5.11, there are more trajectories originating in Central America in NH automn than in NH winter.

The number of young trajectories (age $<$ 30 days) as well as the lift-time show a notable sensitivity to the critical height of origin. This can indicate that the 1 km level is not always rapidly mixed with the surface air; this is reasonable, as the BL top can be lower than 1 km (see Section 2.1.2). However, since the sensitivity to reducing the origin height is less when using hourly output, some of this sensitivity is due to the trajectories staying for a shorter time below 500 m than below 1 km, so that the rather infrequent output fails more often to capture the lower criterion. The off-line way of detecting the BL-origin is thus not suited for defining an origin too close to the surface. It is therefore better to use 1 km than a lower altitude.

A westward shift in the origins in the Pacific is found with increasing origin height. This is probably due to the lower branch of the Walker circulation (see Section 2.2.4) transporting ascending air westward, so that for trajectories rising relatively slowly out of the BL, the origin will be located further west the higher the origin is defined.

More trajectories originate from Africa in the 'BL-topo' run. This could indicate that there are some trajectories being advected past elevated terrain in Africa at altitudes of 1-2 km above sea level, so that they are registered as originating from Africa when the topography definition is used, but not otherwise. The decrease of importance of Africa with a lower critical height can also be related to this: above continents, trajectories are less likely to be registred to be located below 500 m than above oceans, due to the topography. This effect will also be part of the cause for the decrease in young trajectories in 'BL 500m' compared to 'Baseline'. As the origin above continents should not be ruled out in this study, this is another argument for not choosing a too low origin height.

In NH summer, the difference between the topography and sea level definitions of the origin is found to be more important (figure not shown). Releasing trajectories at 15 km on 1. September 2012, a considerable number of trajectories originate from the high elevation of Himalaya and Tibet when using the topography definition. With the sea-level definition, these areas are ruled out and there are instead more origins in India and the Bay of Bengal. This result was a main motivation for choosing the sea level definition.

The increase in age when a wider release belt is used is as expected from the preliminary analysis in Section 3.5. The trajectories released at 20°-40° are older than those released closer to the equator, which can be due to both that they have traveled further from their entry to the TTL and their higher values of potential temperature, which was discussed in Section 3.5. The same argument can be used to explain the slightly more domination of fast lifts for the releases at 20°-40° than for those at lower latitudes. Fewer of the trajectories released further away

from the equator are transferred (Section 3.5), and the probability of being transferred should presumably be higher if the lift to 15 km is faster. This will increase the chance of completing the longer transfer distance in the TTL in 90 days, and to experience the required amount of diabatic heating to reach the higher potential temperature. On the other hand, the fact that the origin locations hardly change when varying the width of the release band indicates that the young air at 15 km has been lifted to the TTL from the same BL-sources regardless of their current latitude.

Both age and lift-time is longer when the trajectories are released at 17 km, compared to 15 km. This is as expected because, according to the theory, most air that reaches the CPT has detrained from convection several kilometers lower and risen on to 17 km more slowly by radiative heating (Section 2.2.2). The large amount lifted to 17 km in less than 10 days, and particularly in less than 1 day, is therefore surprising. This result obviously depends on the convection scheme, since there are hardly any trajectories lifted in less than 10 days to 17 km in the run without convection scheme. Thus, it appears that the scheme produces a large amount of convection penetrating the tropopause. This issue will be further discussed in Section 5.2.5, using data from more years and seasons.

The lift-times to 15 km are markedly shorter for the releases at 17 km compared to releases at 15 km. This indicates that the trajectories lifted more slowly to 15 km have a smaller chance to continue the ascent to 17 km. This result will be discussed further in Section 5.2.5, using results from more years.

There are fewer trajectories younger than 30 days at 17 km without the convection scheme, and in particular much fewer fast lifts and very young trajectories. This is in accordance with the study of Pisso et al. (2010), who also used Flexpart and found a reduction of an order of magnitude in the fraction of a 20 day lifetime tracer entering the stratosphere when not using the convection scheme. This confirms that the results of studies looking at the transport from the surface to the stratosphere on short timescales will be sensitive to how the convection is handled. On the other hand, the majority of the trajectories, both at 15 and 17 km, are transferred even when the convection scheme is not used. This indicates that the convective transport in the tropical troposphere is captured in the ERA-Interim vertical velocities, although the timescales are longer.

The West and Central Pacific was found to give a larger relative contribution to the origins when the convection scheme is switched off, especially for the trajectories younger than 30 days. This is probably due to the higher vertical velocities in this area relative to other areas in the DJF season (see Figure 3.4), enabling trajectories following this pathway to be transferred in a shorter time. Other source regions, such as Africa and South America, seem to depend more strongly on the convection scheme to be captured on short timescales.

Fewer trajectories are transferred from 1 km to 15 km, and much fewer to 17 km, in the forward run compared to the backward runs. This may reflect the fact that most air rising in the tropics does not reach higher than the main convective outflow at 12-13 km and stays in the troposphere (Gettelman et al., 2004); see Section 2.3.1. Therefore, it is reasonable that most of the forward trajectories will not enter the TTL. This is also in accordance with the study of Fueglistaler et al. (2004), who compared the preference for ascent vs. descent between forward and backward trajectories at levels from 340 K ($\sim$main convetive outflow altitude) to 400 K (in the lower stratosphere). In both cases, ascent dominated above $\sim$360 K, but lower down the majority of forward trajectories descended while the opposite was the case for the backward trajectories. On the other hand, that the origin locations and lift-times are similar in the backward and forward mode indicates that the transport does not behave very differently, so that results using the two approaches are comparable. However, the backward approach is most convenient to use because a much larger percentage of the trajectories actually fulfill the transport criterion. The slight decrease in lift-times in the forward runs relative to the backward runs is possibly related to the difference in algorithm in the convection scheme between backward and forward runs (see Section 3.1.2).

4.4 Summary

From the sensitivity studies it has been found that the number of trajectories and model output frequency in the baseline setup is sufficient to capture the main features of the transport from 1 km (∼BL) to the TTL. The relatively infrequent output makes it impractical to start at a lower altitude than 1 km. The width of the release-belt (how high latitudes the trajectories are released from) needs to be chosen carefully, as the age increases strongly with latitude. The use of the convection scheme makes the air younger both at 15 km and at 17 km, increases the importance of source regions outside the western Pacific (at least in the DJF season) and produces a remarkable amount of very fast lifts to 17 km. Except for the runs without the convection scheme, the origin locations of the trajectories younger than 30 days are similar to those of the older ones. Forward trajectories are lifted slightly faster, but otherwise give similar results as the backward trajectories. However, the much smaller amount of the trajectories that fulfills the transfer in forward mode makes this approach less practical.

Chapter 5

Results and discussions

This chapter has three parts. In Section 5.1, three DJF seasons with different ENSO phase are studied. Thereafter, a climatology for the transport in the period 2002-2013 is presented (Section 5.2), and finally the interannual variability in this time period is considered (Section 5.3).

5.1 ENSO case study

5.1.1 Experimental setup

For the ENSO case study, the DJF-seasons of the El Niño event 2009-10, the La Niña event 2010-11 and the neutral event 2012-13 are considered. Trajectories were released 1. January, 1. February and 1. March at 15 km and 17 km altitude in each of the three seasons and simulated 90 days backward in time (Table 5.1). Model setup and analysis follow the description provided in Chapter 3. Table 5.1 gives the SOI for each of the three seasons. The El Niño in 2009-10 was an El Niño Modoki event (see Section 2.2.4), which had record-breaking high SSTs in the Central Pacific, and during 2010 it rapidly decayed into a strong La Niña (Kim et al., 2011).

DJF season	ENSO phase	SOI	Trajectories released
2009-10	El Niño	-10.5	1. Jan, 1. Feb, 1. Mar at 15 & 17 km
2010-11	La Niña	23.1	1. Jan, 1. Feb, 1. Mar at 15 & 17 km
2012-13	Neutral	-3.6	1. Jan, 1. Feb, 1. Mar at 15 & 17 km

Table 5.1: Short description of the three DJF seasons studied in Section 5.1. The SOI (see Section 2.2.4) is a mean of December-February, taken from Australian Government: Bureau of Meteorology.

5.1.2 Age in the TTL

Figure 5.1 shows the percentage of the trajectories that are younger than 30 days (referred to as 'young air') at 15 and 17 km in each event. Figure 5.2 shows the regional averages. In all three cases, there is a belt extending approximately from 20°S to 20°N at most longitudes where more than half of the air at 15 km is younger than 30 days. Within this belt, the air is youngest above the Indian Ocean, Maritime Continent and the western Pacific (>70 % is younger than 30 days), and there is less young air above the eastern Pacific and Atlantic. A similar pattern is found at 17 km, but with an overall lower percentage, and more domination of the Pacific and Indian Oceans.

During the El Niño, there is more young air above the West and Central Pacific than in the La Niña case, both at 15 and 17 km. There is a large area at 15 km in the equatorial Pacific, and even an area at 17 km, where more than 80 % of the air is younger than 30 days. The area

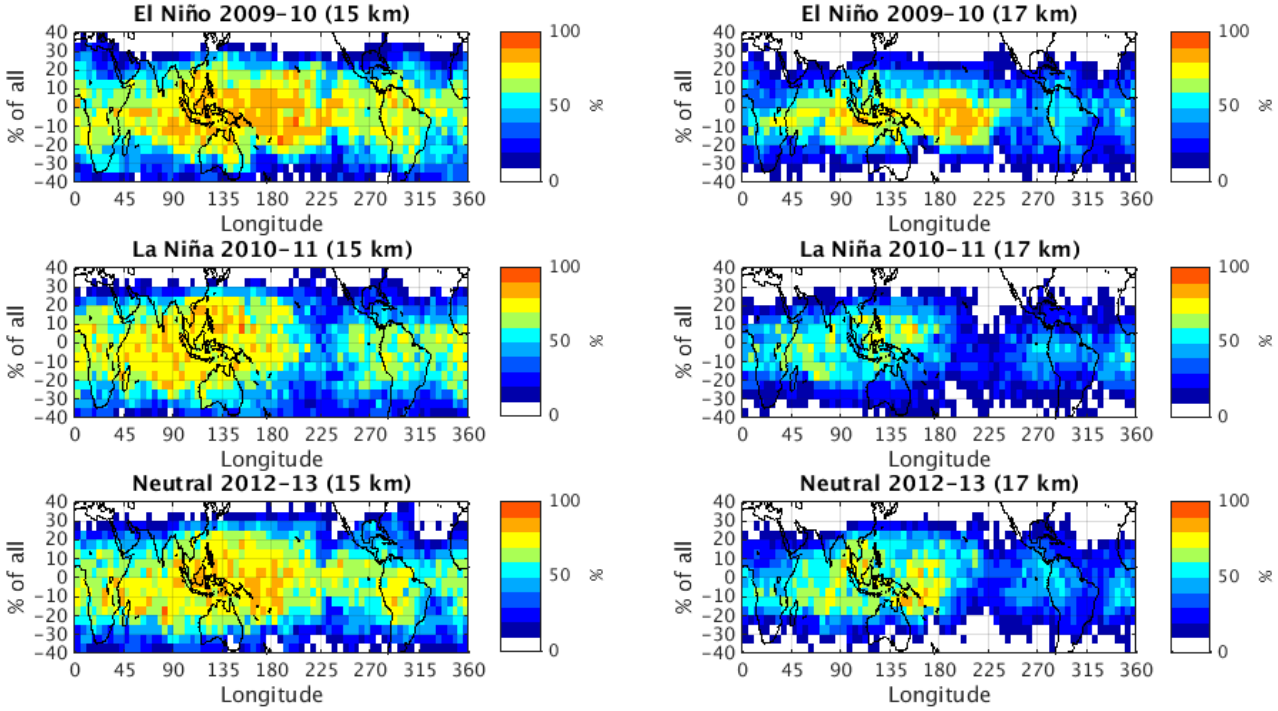

Figure 5.1: Percentage of trajectories that are younger than 30 days, binned at their release locations, for the El Niño DJF season (top), the La Niña season (middle) and the neutral season (bottom). Left: Releases at 15 km. Right: Releases at 17 km. The bin size is 5° x 5°.

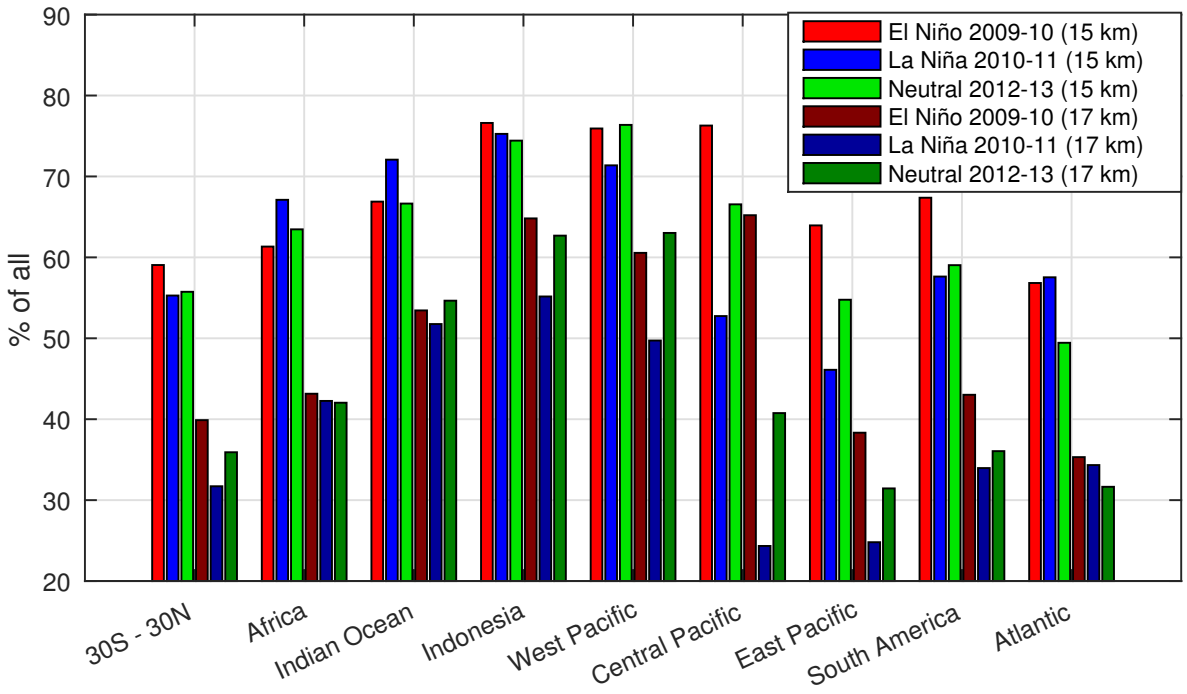

Figure 5.2: Percentage of the trajectories released in each DJF season in each region at 15 km (left) and 17 km (right) that are younger than 30 days. Also shown is the percentage for all releases in 30°S - 30°N that are younger than 30 days. The geographical extent of the regions are defined in Figure 4.2.

of youngest air also extends further toward the East Pacific compared to the ENSO neutral case. Conversely, the young air extends less eastward in the La Niña event than in the neutral case, although the difference is not as large.

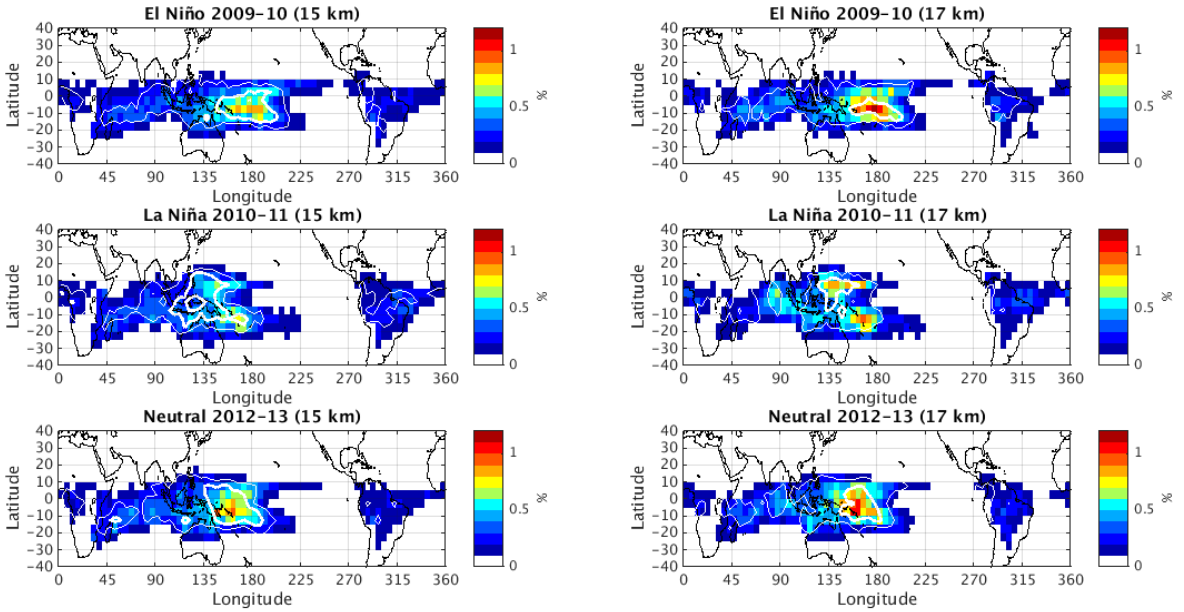

Figure 5.3: Geographical distribution of origins of trajectories younger than 30 days, released at 15 km (left) and 17 km (right) between 30°S - 30°N in the three DJF-seasons. Colors show the percentage of these trajectories having origin within each bin of 5° x 5°. Contours enclose bins where more than 0.25 % (thin) and 0.5 % (thick) of the trajectories are located at the entry to their release altitude.

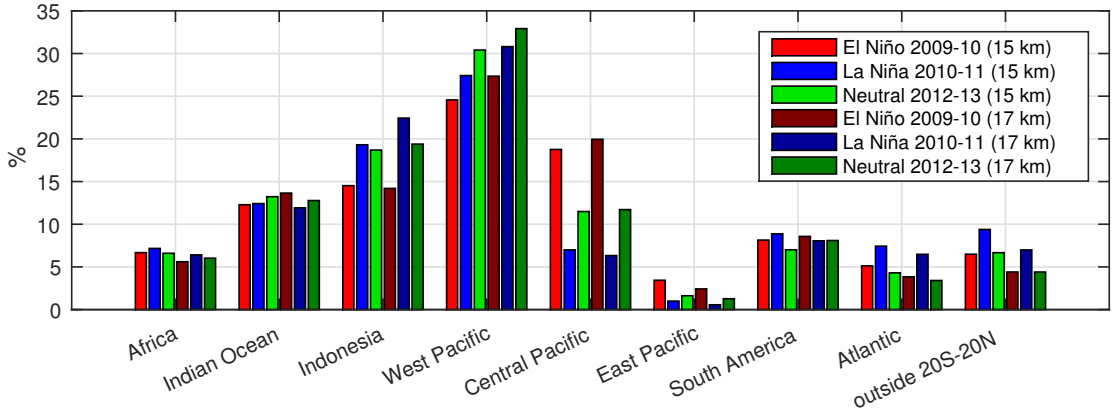

Figure 5.4: Percentage of the trajectories described in Figure 5.3 that originate within each region defined in Figure 4.2.

The most striking differences occur in the Central and East Pacific. In the Central Pacific there is 45 % more young air at 15 km and 168 % more at 17 km in El Niño relative to La Niña. The La Niña event has fewer young trajectories than both of the other two ENSO cases in all three Pacific regions. While there is more young air at 15 km above the Indian Ocean in the La Niña event than in the El Niño event, the opposite is the case at 17 km. Inspecting the 30°S - 30°N as a whole, there are less young trajectories in La Niña compared to El Niño. The difference is more pronounced for the 17 km than for the 15 km releases.

5.1.3 BL-origins

Figure 5.3 shows the location of origin and entry (to the altitude of release) for the trajectories younger than 30 days in each of the three seasons. The origins are quantified by regions in Figure 5.4. In all three seasons the West Pacific region gives the largest contribution to the origins, although ∼70 % of the the trajectories originate from other regions. The areas of largest

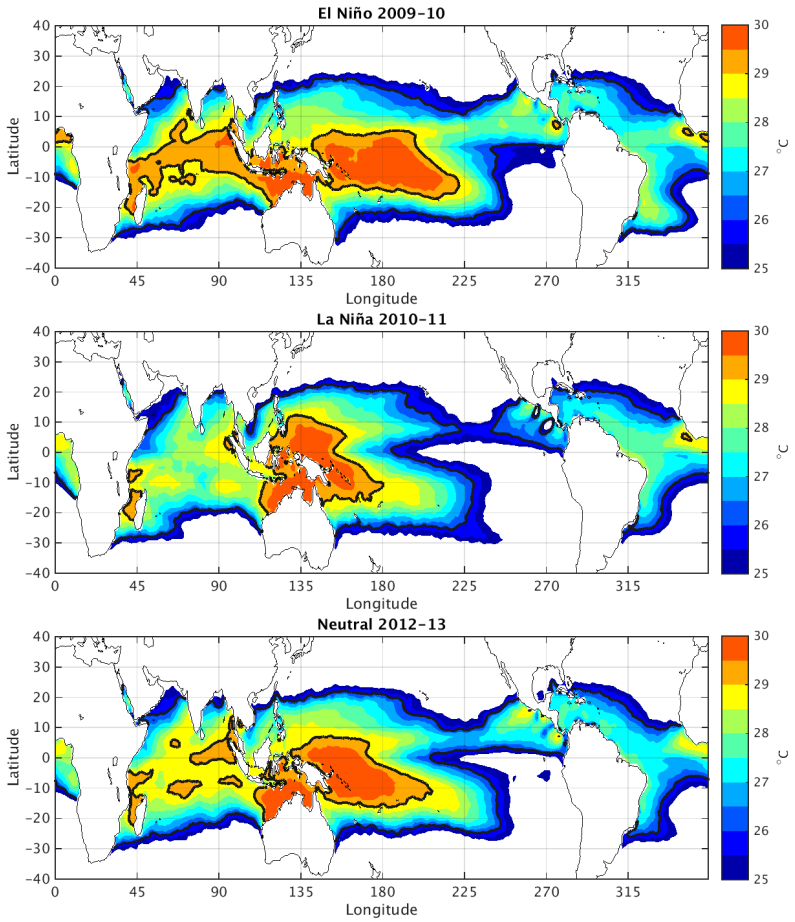

Figure 5.5: Mean sea surface temperature (from ERA-Interim) during each of the DJF-seasons studied in Section 5.1. Contours of 26 and 29°C are shown in black.

percentage of young air in Figure 5.1 are located close to the maximums of origins in Figure 5.3, but the origins are more spatially concentrated than the areas of most young air.

Relative to the neutral case, an eastward shift in the area of most origins is found in the El Niño event, while there is a westward shift in the La Niña event. The areas of entry are closely collocated with the origins, except for a westward shift at 15 km in the La Niña event. In the La Niña event, there are two maxima in origins above the West Pacific, at either side of the equator. This dual pattern was also found in other DJF seasons, but not as strongly as in this La Niña event (not shown).

It is again the Central Pacific which shows the most striking difference between the ENSO cases. In the El Niño event almost as much air originate from the Central Pacific as from the West Pacific, due to the eastward shift. In the other cases the Central Pacific has less than half the contribution of the West Pacific.

5.1.4 Discussion

The pattern of origins (Figure 5.3) can be explained by the main convection associated with the ITCZ and the West Pacific warm pool (Sections 2.2.1, 2.2.4). The vertical motions transport air rapidly upward from the BL into the TTL. Since the lift-times are very short, the collocation between origins and the high percentage of young trajectories can be due to the shorter horizontal distance trajectories released close to the convective activity have traveled from the place they entered the TTL. Trajectories released further away from the convective areas will typically have stayed in the TTL longer.

The eastward shift of the origins in the El Niño case is as expected since the convection moves

eastward in an El Niño, following the shift in the warmest water (see Section 2.2.4). Figure 5.5 shows the mean SST for each of the three DJF-seasons. The shifts in the origin maximum in Figure 5.3 resemble the shifts in the warm pool. During the El Niño, SSTs exceeding 29°C extend further east, and they extend further north toward the Philippines and less east during the La Niña event.

The air within 30°S - 30°N both at 15 km and 17 km was found to be younger in the El Niño event than in the La Niña event. Part of this difference can be explained by the zonally wider area of young air during the El Niño event. However, also when comparing just the West Pacific, more young air is found in El Niño, especially at 17 km. This could indicate that the flux of air into the TTL and the stratosphere was stronger in the El Niño event than in the La Niña event. However, one cannot say if this may be a general feature of the ENSO phase without looking at more ENSO events. In Section 5.3.3, the releationship between ENSO phase and the amount of young trajectories above the Pacific will be studied further using all 11 DJF seasons.

5.2 Transport climatology

5.2.1 Experimental setup

Trajectory calculations for the period 2002-2013 are analysed to create a climatology for surface-to-TTL transport. The period is long enough to study year-to-year variations within a decade (Section 5.3), and to make the results more robust compared to using only single years.

Trajectories were released the first day in each month at 15 km and 17 km altitude in the period 1. June 2002 to 1. May 2013 ($11 \cdot 12 = 132$ different release dates) and simulated 90 days backward in time, following the setup described in Chapter 3. To calculate the all-month climatological statistics, the trajectories released on all the 132 dates were included in the computations. For the climatology of a season, the trajectories released at the end of each of the three months of that season in each year were put together in one sample for which the statistics were calculated. A summary of which trajectories are used for the climatological statistics is given in Table 5.2.

Sample	Release dates used
All months	1st of every month 1. June 2002 - 1. May 2013
DJF	1. Jan, 1. Feb, 1. Mar 2002-2013
MAM	1. Apr, 1. May 2003-2013 and 1. Jun 2002-2012
JJA	1. Jul, 1. Aug, 1. Sep 2002-2012
SON	1. Oct, 1. Nov, 1. Dec 2002-2012

Table 5.2: The release dates used for all-month and seasonal samples in the climatology.

5.2.2 All-month climatology

The age distribution for all releases at 15 km and at 17 km in the 11 years is shown in Figure 5.6. At 15 km, 89.3 % of the trajectories are transferred (i.e. younger than 90 days), and 55.7 % are younger than 30 days. At 17 km, these numbers are 70.6 % and 32.3 %, respectively. At 15 km there is a clear peak in the age distribution at ages 3-10 days, and the distribution falls off quite rapidly so that there are much fewer trajectories with ages 60-90 days. At 17 km, the distribution falls off less markedly. The peak is broader: ages in the whole interval 0-30 days are almost equally common. The median age is 26 days at 15 km and 50 days at 17 km.

The climatological distributions of lift-times are shown in Figure 5.7. As already noted in Chapter 4, the lift-times both to 15 km and 17 km are dominated by fast uplifts. $\sim$25 % of the trajectories released at 15 km have been lifted from 1 km to 15 km in less than 1 day, and the majority has been lifted in less than 10 days. For the releases at 17 km, the percentage lifted

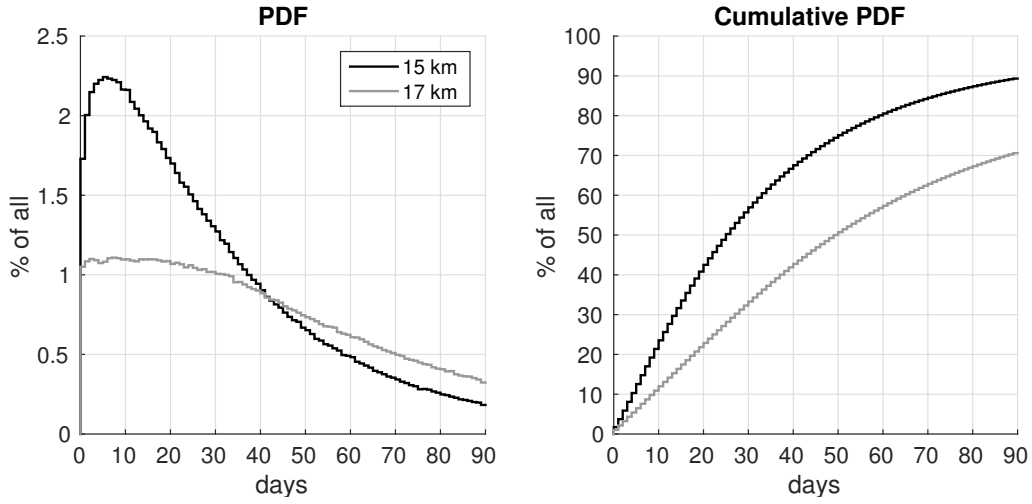

Figure 5.6: Age distribution for trajectories released at 15 km and 17 km between 30°S - 30°N in the period 1. June 2002 - 1. May 2013. Bin width is 1 day.

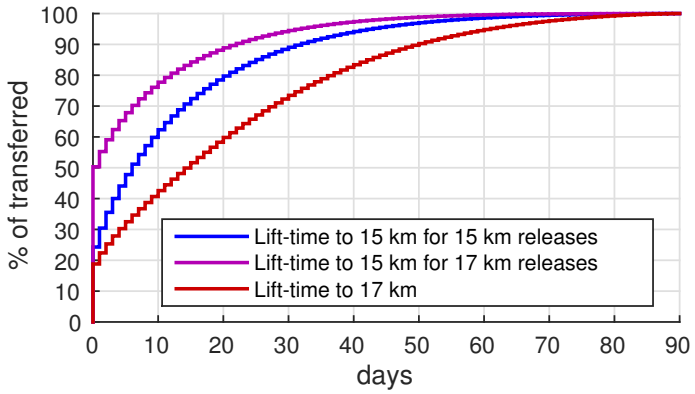

Figure 5.7: Cumulative PDF of lift-times for trajectories, released between 30°S - 30°N in the period 1. June 2002 - 1. May 2013. Bin width is 1 day.

to 15 km in less than 1 day is twice as large as for the releases at 15 km, comprising half of the transferred trajectories. The lift-times to 17 km are longer: half of the lifts last longer than 15 days and nearly 30 % last more than 30 days. Still, there is no doubt that there is a large amount of very fast lifts to 17 km: 18.8 % of the trajectories released at 17 km were lifted from the BL to 17 km in less than 1 day, and 14.7 % in less than 6 hours (not shown).

5.2.3 Seasonal cycle

The age distributions at 15 and 17 km for each season are displayed in Figure 5.8. The seasons are very similar at 15 km, while there are larger differences at 17 km. At 17 km, the SON season and especially the JJA season have fewer transferred trajectories than the other seasons, and there is most air younger than 30 days in the MAM season. While no clear seasonal cycle in the median age is found at 15 km, at 17 km it is lowest in MAM (45 days) and highest in JJA (58.75 days).

Figure 5.9 shows the geographical distribution of the young air percentage. In all seasons, there are much more young trajectories in the tropical belt than outside. This "band" of young air experiences a seasonal shift in latitude, but is more or less centered at the equator in all seasons except for JJA, when it is considerably shifted off the equator. In particular at 17 km there are very few trajectories younger than 30 days south of 20°S in JJA, and relatively more young air north of 30°N. As the analysis uses releases within 30°S - 30°N, this can partly explain

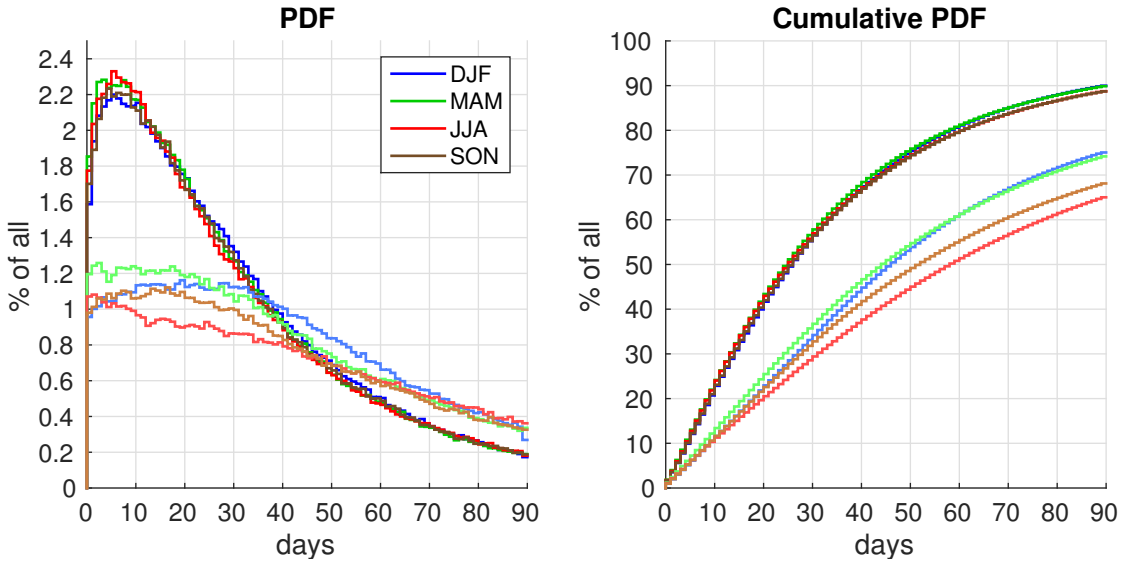

Figure 5.8: Age distribution for trajectories released at 15 km and 17 km (more transparent colors) between 30°S - 30°N in the period 1. June 2002 - 1. May 2013, showing the releases in each season separately. Bin width is 1 day.

the low amount of young trajectories at 17 km in the JJA season in Figure 5.8. Nevertheless, Figure 5.9 reveals that also if comparing only the areas of most young air in each season, the JJA season clearly has less young air at 17 km than the other seasons (by about 10 %-points), and the band of young air is narrower.

At 15 km there is a large region in the tropics above the Indian Ocean, Maritime Continent and West Pacific where more than 70 % of the air is younger than 30 days in all seasons. In JJA there is an increase in young trajectories above India and Africa, and the air is younger above South and Central America in MAM and JJA than in DJF. The regions with the youngest air are located similarly at 17 km. 50-60 % of the air at 17 km above the Indian Ocean, Maritime Continent and West Pacific is younger than 30 days in all seasons except JJA.

Figure 5.10 shows the mean potential temperature at 15 and 17 km. At 15 km the potential temperature in most of the release domain (30°S - 30°N) is close to 360 K in all seasons, though rising to higher values toward the winter subtropics. Due to the small variability of the potential temperature, the trajectories released at 15 km are more thermodynamically comparable than those released at 17 km, where the potential temperature varies much more within the release domain and between seasons. At 17 km there is a minimum in potential temperature above the West Pacific, and also above Africa and South America in all seasons except JJA. In JJA there is a minimum above the Indian monsoon region, but in most other areas of the tropics the potential temperature is considerably higher (about 5-10 K) in JJA compared to the other seasons.

Figure 5.11 shows the origins of the trajectories younger than 30 days in each season. The areas in white comprise only ∼5 % of the origins. In Table 5.3, the contributions from 5 major source regions are quantified by numbers. The most important origin area is the western Pacific in all seasons both at 15 and 17 km. About half the trajectories originate within the West/Central Pacific region defined in Table 5.3. In DJF the western Pacific maximum is shifted to the SH, and in JJA and SON to the NH. In MAM it is centered at the equator. This maximum extends slightly past the dateline. A weaker band of origins stretches east across the equatorial Pacific, and there is another extension into the southern Central Pacific. These patterns fit to the locations of the ITCZ and SPCZ, respectively (Waliser and Gautier, 1993). In JJA there is a prominent maximum in the Indian monsoon region (India and Bay of Bengal). Many trajectories also originate in the Caribean Sea both in JJA and SON, especially at 17 km.

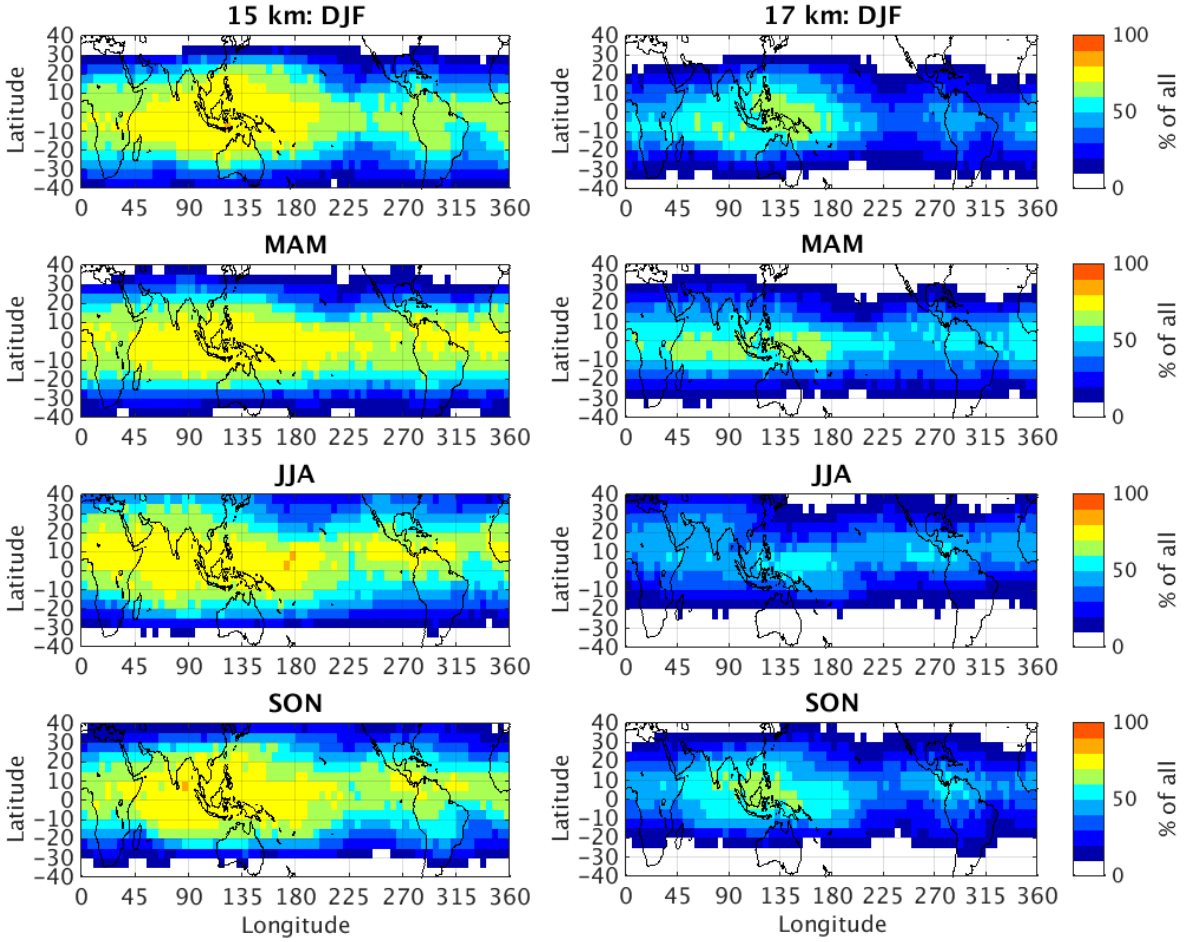

Figure 5.9: The percentage of all trajectories released at 15 km (left) and 17 km (right) within 5° x 5° bins that are younger than 30 days. This is shown for the seasonal subsets of trajectories released in the period 1. June 2002 - 1. May 2013.

The tropical parts of South America, Africa and the Atlantic Ocean give stable, but less strong, contributions throughout the year. The SH Indian Ocean gives an important contribution in DJF, when there are much less origins close to India. In general, the origin locations are similar at 15 and 17 km, but the 17 km origins are slightly more concentrated: less trajectories come from the edges and more from the central parts of the areas with most origins.

Figure 5.12 shows the lift-time distributions for each season. The trajectories released at 15 km show little seasonal variability in lift-times, as also was the case for the age (Fig. 5.8). For the 17 km releases, lift-time both to 15 km and 17 km is less in JJA than DJF. While 41.3 % is lifted to 15 km and 14.2 % to 17 km in less than 1 day in DJF, these numbers are 58.7 % and 24.2 % in JJA.

5.2.4 The western Pacific

So far the analysis has considered all releases within 30°S - 30°N as a whole. As discussed in Section 3.5, this causes challenges due to the difference in potential temperature with latitude, particularly at 17 km. Moreover, transport studies in the TTL, such as Fueglistaler et al. (2005), have shown that the majority of the air crosses the cold-point tropopause above the western Pacific (see Section 2.3.2). Motivated by this, a separate study of this area was carried out. Based on the study by Fueglistaler et al. (2005), the region within 15°S - 15°N, 120°E - 150°W (see Figure 5.13) was chosen. This region is termed “western Pacific”.

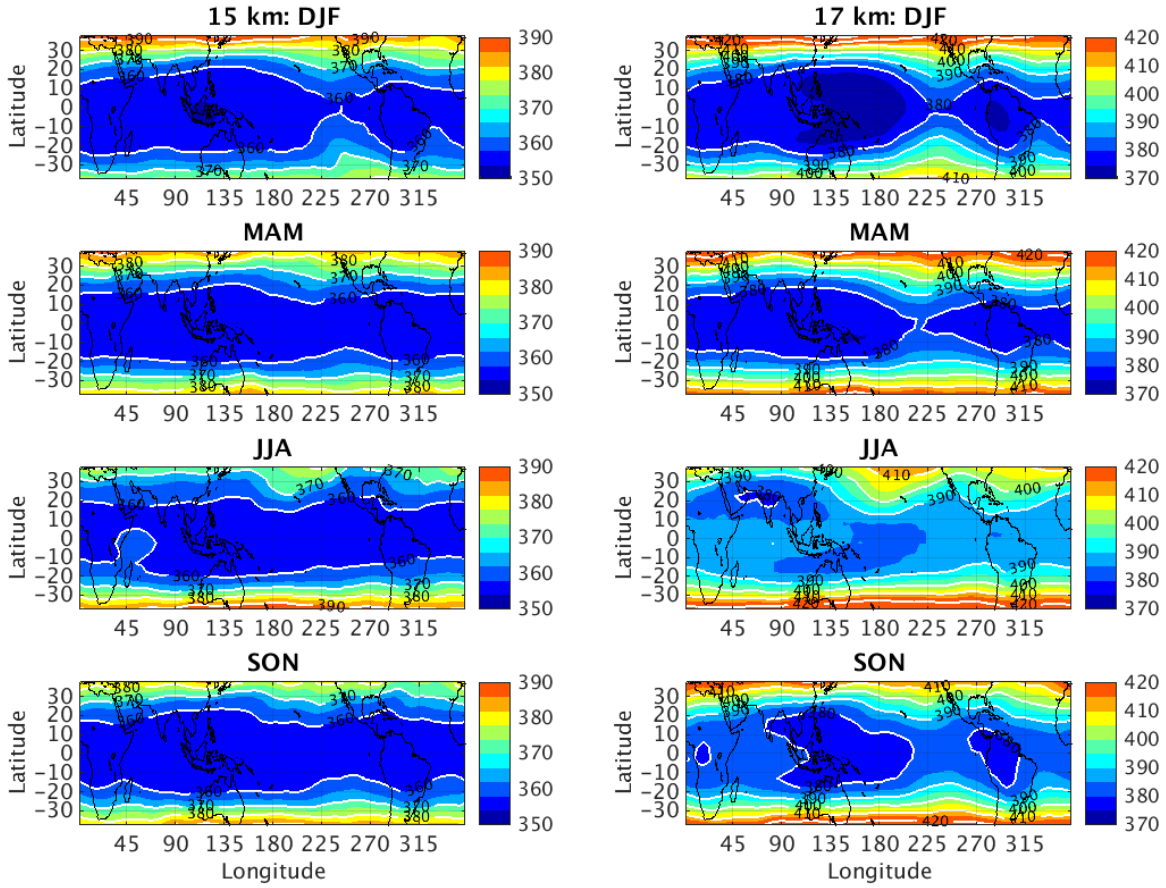

Figure 5.10: Seasonal mean potential temperature (K) at 15 km (left) and 17 km (right) for the period 1. June 2002 - 1. May 2013. The displayed values are calculated by averaging the potential temperature at release of all trajectories released (in the respecitve season and at the respective altitude) within 5° x 5° bins and then drawing contours.

Figure 5.14 shows the age distribution of the trajectories released above the western Pacific for all-month climatology and for each season. Considering all months, 96.4 % of the trajectories released at 15 km is younger than 90 days, and 72.2 % are younger than 30 days. At 17 km 84.4 % are younger than 90 days and 49.6 % are younger than 30 days. This is markedly more than in 30°S - 30°N as a whole (Section 5.2.2). The age distributions, both at 15 km and 17 km, peak at the lowest ages, making the amount of trajectories younger than 10 days large (35.0 % at 15 km, 21.8 % at 17 km). The seasonal variation in age is weak at 15 km, but there are slightly more trajectories younger than 5 days in JJA than in DJF. At 17 km, the number of trajectories younger than 10 days varies little with season, while there are considerably more trajectories with ages 10-40 days in DJF than in JJA. In total, more trajectories are transferred to 17 km in the DJF season (88.9 %) than in the JJA season (78.9 %). The median age is close to 16 days in all seasons at 15 km. At 17 km it varies between 27.25 days in DJF and 37.25 days in JJA.

Figure 5.15 shows the origins for the releases above the western Pacific region. They are mainly located in the western Pacific Ocean, indicating little horizontal transport, with some contributions from the eastern Indian Ocean and the eastern equatorial Pacific. In JJA, Central America also appears as an origin region of some importance.

The lift-time distributions for air released in the western Pacific region are very similar to those for the whole 30°S - 30°N, shown in Figure 5.12. The largest difference is a slight decrease in fast lifts in the DJF season (not shown here).

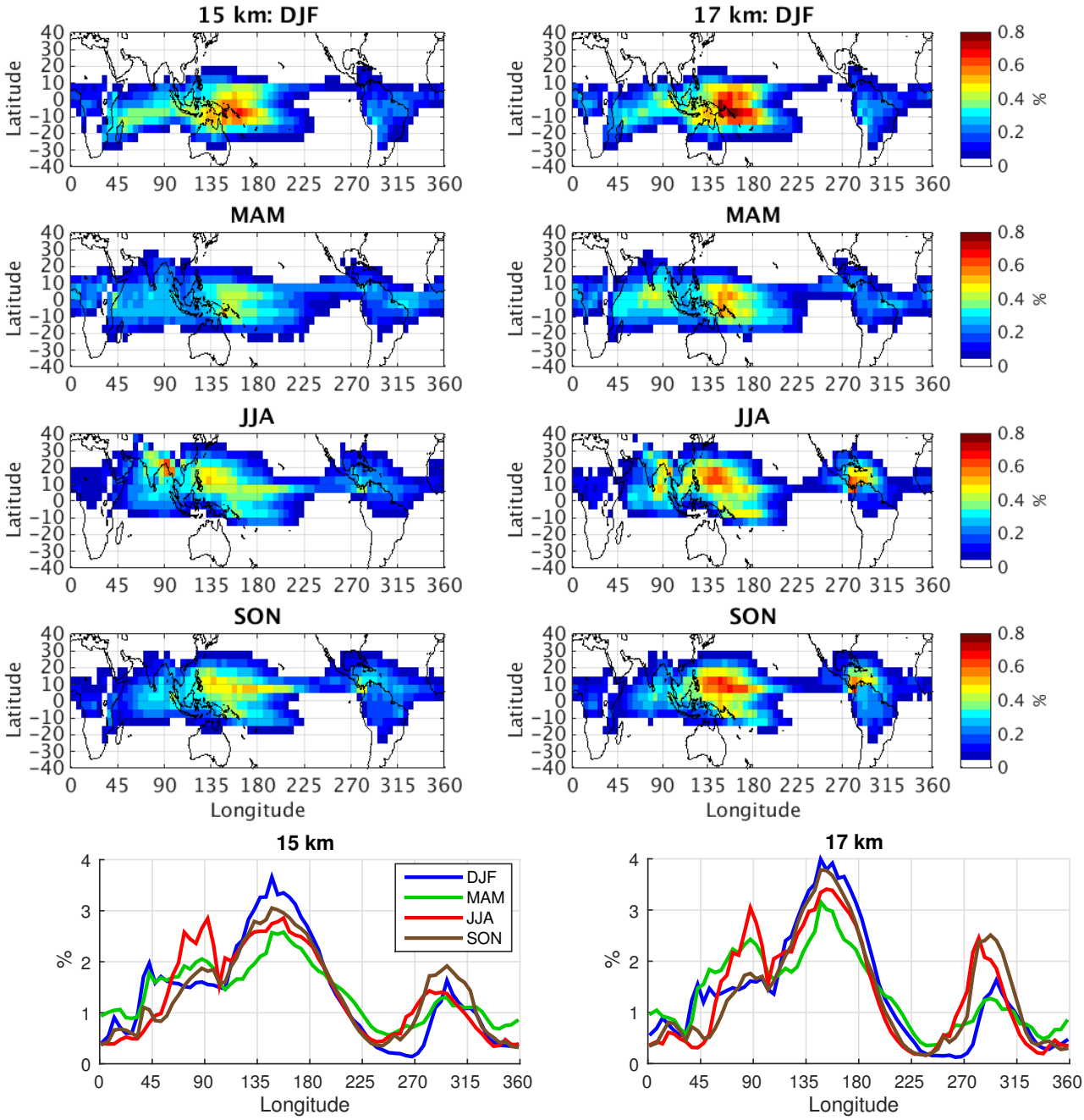

Figure 5.11: The origins at 1 km of the trajectories younger than 30 days released at 15 km (left) and 17 km (right) within 30°S - 30°N in each season in the period 1. June 2002 - 1. May 2013. Above: Percentage of origins within bins of 5° x 5°. Below: Zonal distribution of origins, using a bin width of 5°. The percentages are relative to the total number of trajectories younger than 30 days at the respective altitude in the respective season.

5.2.5 Discussion

The age of air at 17 km

The age distribution at 17 km is an estimate of the transit times from the surface to the stratosphere. This is calculated for 30°S - 30°N as a whole (Figures 5.6 and 5.8) and for the western Pacific only (Figure 5.14). Since the western Pacific is the region where the air is youngest at 17 km, the latter approach results in considerably shorter transit times; the median age is ∼50 days in 30°S - 30°N as a whole and ∼30 days above the western Pacific. The western Pacific

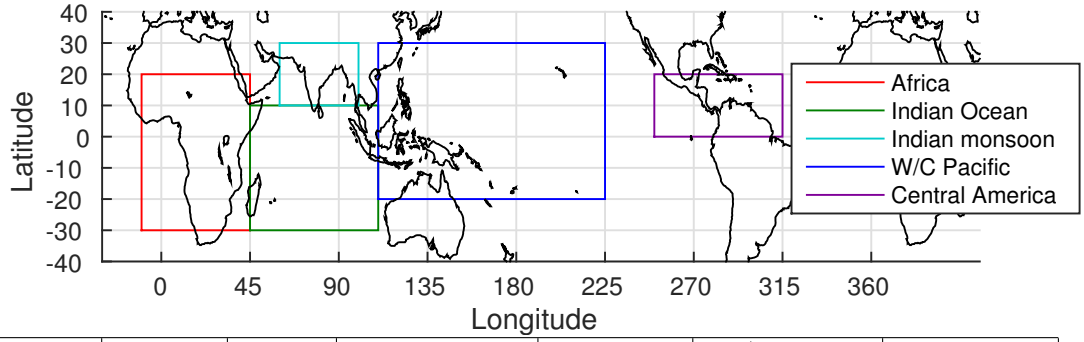

Season	Release	Africa	Indian Ocean	Indian m.	W/C Pacific	C. America
DJF	15 km	9.0	19.8	0.3	51.3	3.6
	17 km	8.3	18.4	0.4	55.8	3.9
MAM	15 km	11.1	17.3	4.2	42.3	7.7
	17 km	9.6	20.5	4.3	44.7	7.5
JJA	15 km	4.1	10.4	10.7	47.0	10.1
	17 km	4.1	12.2	8.9	48.3	13.2
SON	15 km	6.5	13.2	4.0	49.7	10.6
	17 km	5.8	11.8	3.6	52.5	12.8

Table 5.3: Lower panel: The relative contribution (in %) of 5 major regions (displayed in the upper panel) to the origins of trajectories younger than 30 days in each season: Africa (10°W-45°E, 30°S-20°N), Indian Ocean (45°E-110°E, 30°S-10°N), Indian monsoon region (60°E-100°E, 10°N-30°N), West/Central Pacific (110°E-135°W, 20°S-30°N) and Central America (110°W-45°W, 0°N-20°N). The percentages are relative to the total number of trajectories younger than 30 days at the respective altitude in the respective season.

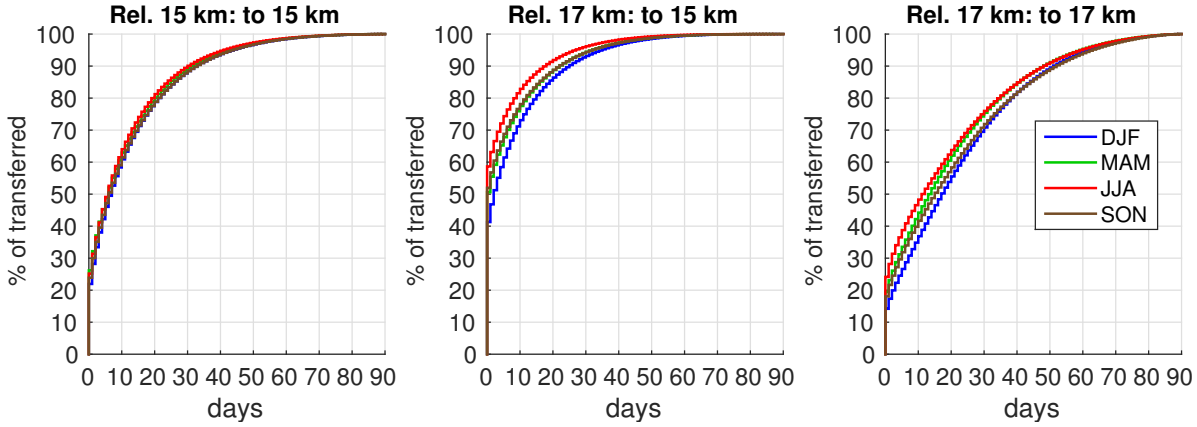

Figure 5.12: Cumulative lift-time distributions for each season for trajectories released between 30°S - 30°N in the period 1. June 2002 - 1. May 2013. For trajectories released at 15 km, lift-times to 15 km are shown (left). For trajectories released at 17 km, lift-times to 15 km (middle) and 17 km (right) are shown. The bin width is 1 day.

is also the region where most air enter the stratosphere (Fueglistaler et al., 2005). These two approaches give an estimate of the range of the age of air reaching the stratosphere; while air does not enter the stratosphere uniformly between 30°S - 30°N, it is neither exclusively entering above the western Pacific.

Previous studies have also estimated the tropospheric age of air entering the stratosphere. In particular, it can be interesting to compare with Rex et al. (2014), because they also calculated a distribution of transit times and used ERA-Interim, as in this study. They used the Lagrangian model ATLAS (Wohltmann and Rex, 2009). They studied the residence time between 800 hPa

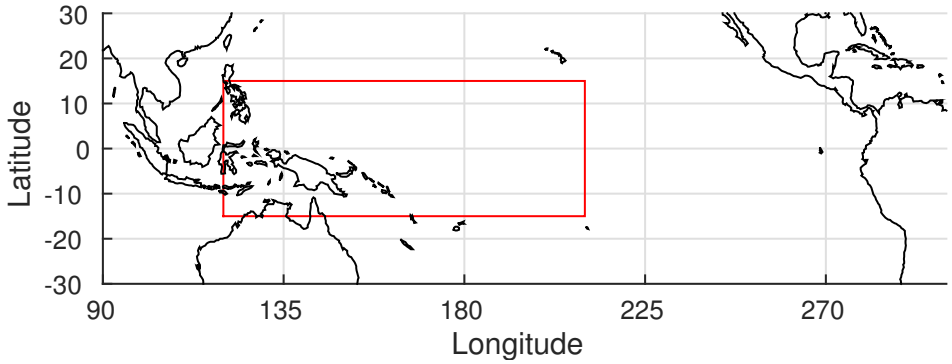

Figure 5.13: The region 'western Pacific' in which the trajectories studied in Section 5.2.4 are released. Its extent is 120°E-210°E(150°W), 15°S-15°N.

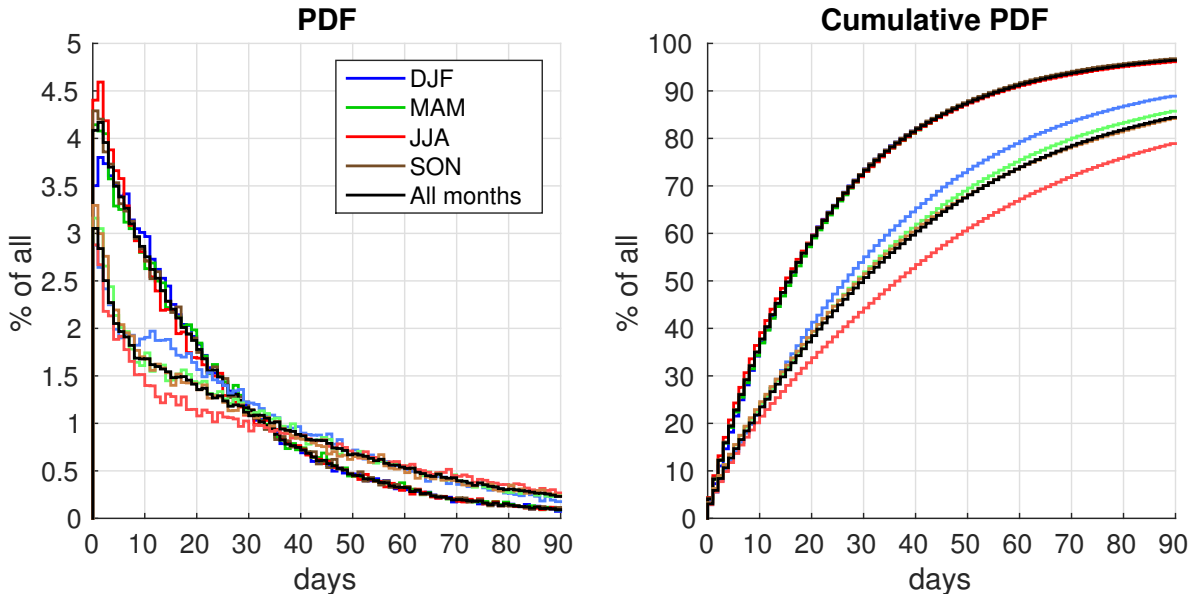

Figure 5.14: Age distribution for trajectories released at 15 km and 17 km (more transparent colors) above western Pacific (see Fig. 5.13) in the period 1. June 2002 - 1. May 2013: all trajectories (black), and each season (colored). Bin width is 1 day.

(∼2 km) and the LCP, using backward trajectories released between 30°S - 30°N at 400 K at the end of each January and simulated for 120 days, for the years 2002-2011. By releasing at 400 K, the tropospheric transit times can be calculated using the locations where the trajectories actually cross the CPT, which might be a more accurate representation of the transport than sampling the whole 30°S - 30°N at a constant altitude. However, the approach of Rex et al. (2014) has the disadvantage that no parameterization of convection was used in the ATLAS model.

In Figure 5.16, the age distribution of Rex et al. (2014) is compared to the ones found in this study for the DJF season using 30°S - 30°N and only western Pacific releases, respectively. The distribution of Rex et al. (2014) is quite similar to the age distribution for 30°S - 30°N found here. Both are right-skewed and have a peak at ∼30 days. However, there are also significant differences. The distribution of Rex et al. (2014) falls off rapidly with decreasing age below the peak, so that very few trajectories are younger than 10 days. In the 30°S - 30°N distribution from this study, there are almost as many trajectories aged 1 day as 30 days. This discrepancy is most probably explained by the lack of a convection scheme in the simulation by Rex et al. (2014). The age distribution in the sensitivity run without convection ('Conv off + 17km' in Figure 4.3) looks more similar to the distribution of Rex et al. (2014), although with the peak at a slightly higher age. The higher age could be due to the inclusion of trajectories released at subtropical latitudes, which are released at a higher potential temperature (Figure 5.10) than

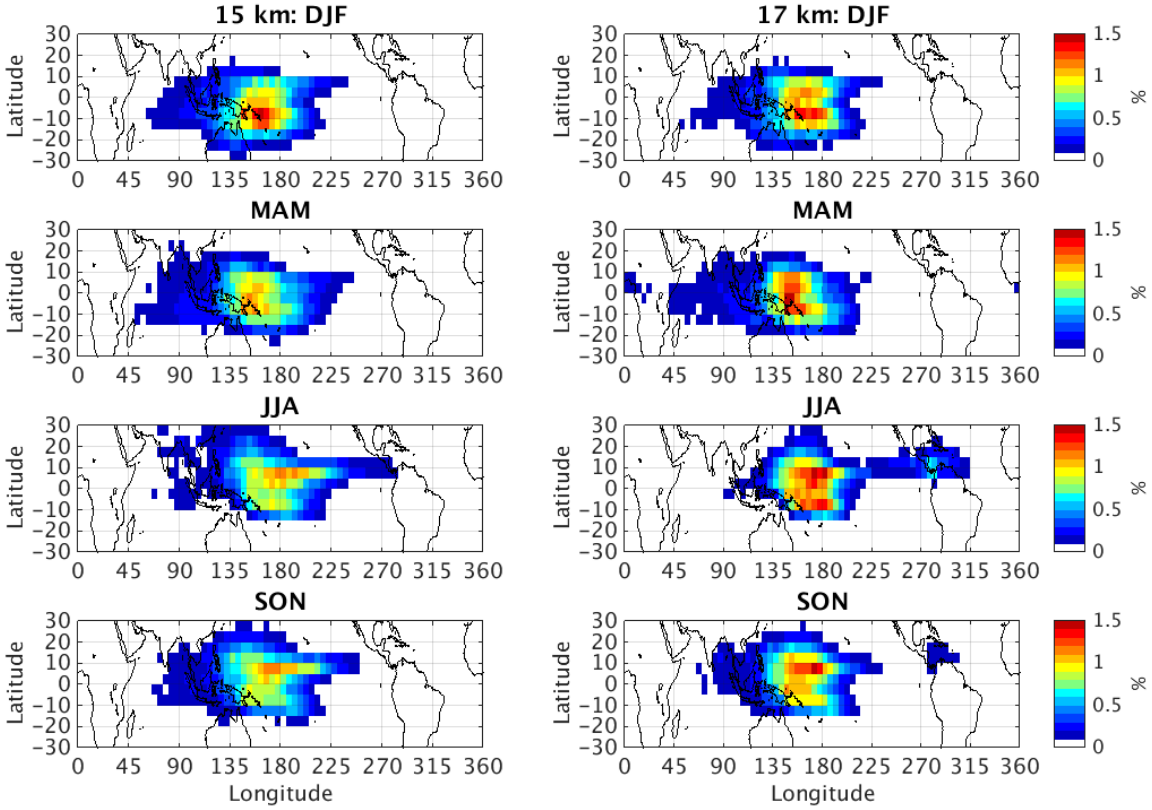

Figure 5.15: Origins of trajectories younger than 30 days released at 15 km (left) and 17 km (right) above the western Pacific (see Fig. 5.13). Shown is the percentage of origins within bins of 5° x 5°.

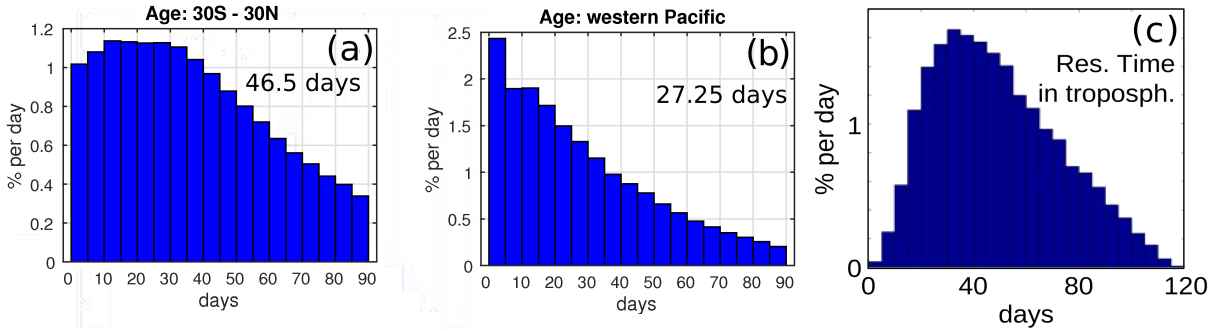

Figure 5.16: (a) The age distribution at 17 km calculated in this study for the DJF seasons of 2002-2013, using releases within 30°S - 30°N, and (b) using releases in western Pacific only (the region in Fig. 5.13). The median age in each case is indicated. (c) The residence time in the troposphere in NH winter (in the years 2002-2011) estimated by Rex et al. (2014) (their Fig. 4h). Note that in (c), the percentages are relative to all transferred trajectories, while in the other two, the percentages are relative to all trajectories released, including the non-transferred ones. This will make the values higher in (c).

those near the equator and at latitudes which are probably overrepresented relative to their actual contribution to the LCP crossing (see Section 2.3.2). The age distribution in the western Pacific (Figure 5.16b) has clearly more young trajectories than the one for 30°S - 30°N. This is probably due to the pronounced convective activity in this region in NH winter (Gettelman et al., 2002). To summarize, the age distributions at 17 km in NH winter found in this study reveal younger air at the tropopause than in Rex et al. (2014). The differences can plausibly be

explained by the convection scheme, which gives a more realistic representation of the tropical troposphere. The inclusion of the convection scheme causes an important difference since the existence of very short transit times is of importance for the transport of VSLS.

Lift-times to 15 km

For the trajectories released at 15 km, the lift-time to 15 km is found to be generally low (Figure 5.7). ∼25 % of the trajectories are lifted to 15 km in less than 1 day, and ∼60 % in less than 10 days. The age of the trajectories at 15 km is considerably higher, with a median of 26 days (Figure 5.6). This can be interpreted in the following way: The convection is necessary for lifting air rapidly upward, but once the air has detrained from convection near the altitude of the LZRH and no longer has a latent heating source, the vertical motions will become weaker. Since the LZRH is located close to 15 km, but also varies by a few hundred meters in time and space, the air around 15 km can be expected both to ascend and descend (Gettelman et al., 2004). Either upward or downward motions can be expected to be relatively slow compared to trajectories having reached higher in the TTL (Fueglistaler et al., 2004). It is therefore not surprising that the trajectories released at 15 km have stayed around this altitude for several weeks. Although the time to rise from the BL to 15 km is short, the air located at this level can be much older than this.

One can even argue that there maybe are too few fast lift-times to 15 km, since according to Gettelman et al. (2004) convection has to transfer the air all the way up to the LZRH. The tail of the lift-time distribution at 15 km (Figure 5.7) can be explained by air that has previously detrained from convection lower than 15 km and then becomes entrained into another convective cell. It can also be explained by cases when the LZRH is slightly lower than 15 km, so that air detraining from convection below this level can continue to rise to 15 km by slower, radiative heating. Finally, some of it may be spuriously caused by the model. The ERA-Interim vertical winds are upward in the main convective areas in the tropics (Figure 3.4), so that trajectories will rise when not being displaced by the convection scheme, contrary to the descent that is known to take place outside convective cells (see Section 2.1.3). This is because the grid-scale vertical winds from ERA-Interim incorporate the convective transport, and they are therefore able to produce the transfer to 15 km without the convection scheme, as was demonstrated in the runs without the convecton scheme in Chapter 4. Thus, the lifting from 1 km to 15 km of the trajectories will be represented (at least partly) by the slower grid-scale vertical winds, which give too long lift-times.

The lift-times of less than 1 day to 15 km is found to occur more often for trajectories released at 17 km than for those released at 15 km (Figures 5.7, 5.12). This indicates that the trajectories have a higher chance of reaching 17 km if lifted faster to 15 km. Fueglistaler et al. (2004) found a stagnation zone around 360 K (corresponding to 15 km) where their trajectories rose more slowly than below and above. They also found that many trajectories were transported to the extratropics after entering the TTL, which is also a major result of Levine et al. (2008). Both these factors could contribute to make a faster lift to (and past) 15 km favorable for a trajectory to reach 17 km.

Lift-times to 17 km

A large number of trajectories are lifted rapidly to 17 km (Figures 5.7, 5.12). ∼19 % of the trajectories released at 17 km are lifted from 1 km to 17 km in less than 1 day, and ∼15 % in less than 6 hours. This indicates that 15 % of surface-to-stratosphere transport is from convection overshooting the tropopause, and that an additional ∼4 % detrains high enough to be able to reach the tropopause within 24 hours. Gettelman et al. (2002) estimated that the convective turnover time (see Section 2.3.1) at 17 km is less than 1 year in the western Pacific, which is only 3-4 times longer than the ∼3 month turnover time found at 15 km. A small, but still significant, contribution from convection penetrating the tropopause is therefore plausible. However, studies

of the vertical profile of the convective mass flux in the TTL give varying results, and the relative importance of convection overshooting the tropoause is not well understood (Fueglistaler et al., 2009). In this study, these events can also be expected to be slightly overrepresented in the results since the trajectories with low lift-time will have a higher probability to be transferred in the 90 days of simulation than trajectories lifted more slowly.

The convection scheme in Flexpart, described in Section 3.1.2, is obviously important for the fast lifts to 17 km. In addition, the dispersivity of the vertical winds in the upper TTL (see Section 3.2.2) might also contribute to creating some of the fast lifts. If a trajectory is lifted close to, but below, 17 km by the convection scheme, an anomalously high vertical velocity from ERA-Interim could bring it above 17 km shortly afterward. However, as the model output from Flexpart is only every 6 hours, it has not been possible to find out how high the convection scheme lifts the trajectories, and how much of the fast lifts to 17 km can be attributed to the ERA-Interim vertical winds. A separation of the contribution to the vertical transport of the convection scheme and the ERA-Interim winds could be done online in Flexpart, but is beyond the scope of this study.

At 17 km the air is expected to rise gradually from radiative heating (Section 2.2.2). However, since the lift-times to 17 km are shorter than the age at 17 km (compare Figures 5.6 and 5.7), the trajectories appear to rise and sink past this level repeatedly. A possible explanation could be noise the vertical winds in ERA-Interim, but it could also partly be due to the difference in potential temperature (Figure 5.10), which allows air traveling poleward from the equator above 17 km to sink even if it is radiatively heated.

Locations of BL-origin

The origin locations at 1 km for trajectories younger than 30 days (Figure 5.11) are similar for releases at 15 km and 17 km, and they are in good agreement with the regions of high convection observed by Gettelman et al. (2002) in each season. Thus, our results reveal that deep convection is the most important process for the transport from the BL to the TTL. The BL-origin locations are more concentrated for releases from 17 km than for releases from 15 km. A speculation for expaining this can be that the trajectories reaching 17 km in 30 days require deeper convection than those reaching 15 km, and that this is less likely to occur in the peripheries than in the central parts of the convective regions.

Seasonal cycle in the age at 17 km

Considerably less young trajectories are found at 17 km in JJA than in the other seasons, and the median age in JJA is higher by ∼9 days than in the climatological period as a whole (Figure 5.8). This seasonal cycle at 17 km could represent a variability of the transit times to the CPT. The upward flux across 100 hPa in the tropics is only about half as large in JJA as in DJF (Holton et al., 1995), and the air near this level can therefore be expected to be older in JJA. Levine et al. (2008) also found that a larger fraction of the trajectories released at the base of the TTL reached the stratospheric overworld in 4 weeks in DJF than in JJA. However, there are also other factors that could contribute to a higher age at 17 km in the JJA season. The tropopause is lowered by about 0.5 km in the JJA season relative to the DJF season, from ∼17 km to ∼16.5 km (Seidel et al., 2001). The trajectories at 17 km are therefore more stratospheric at the release in this season. The potential temperature at 17 km is found to be ∼10 K higher in JJA than DJF in all of the tropics except above the Asian monsoon regions (Figure 5.10). Thus, the 17 km surface is higher in terms of thermodynamics in JJA, so that the ascent to 17 km by radiative heating can be expected to require more time. Finally, since the shift in the tropical belt toward the summer hemisphere is larger in JJA than in DJF, due to the Asian monsoon, more extratropical air will be sampled in 30°S - 30°N in this season, which also increases the age.

5.3 Interannual variability

5.3.1 Experimental setup

In this section the interannual variability of the age at 15 km and 17 km is investigated. The analysis is based on trajectories released each month from 1. June 2002 - 1. May 2013 (the same trajectories as in Section 5.2). Monthly values of median age are calculated using the trajectories released at the end of the respective month[1] to create a time series of monthly mean age. Annual and seasonal time series were also created by combining the monthly samples belonging to each year or season. Table 5.4 explains how this sampling is done. The main analysis of the variability uses releases between 30°S - 30°N, but analyses using only the releases between 20°S - 20°N and 10°S - 10°N were also carried out.

Sample	Releases used in the sample of a year	time series covers the years
Annual	1. Feb, 1. Mar, ... , 1. Jan (next year)	2003-2012
DJF	1. Jan, 1. Feb, 1. Mar	2003-2013
MAM	1. Apr, 1. May, 1. Jun	2003-2012
JJA	1. Jul, 1. Aug, 1. Sep	2002-2012
SON	1. Oct, 1. Nov, 1. Dec	2002-2012

Table 5.4: The release dates used for the annual and seasonal samples for each year, and the years for which these samples are created.

5.3.2 Variability in the median age

The time series of the median age at 15 km and 17 km is shown in Figure 5.17. The mean and standard deviation of each time series are given in Table 5.5. The median age decreases over the period, especially at 17 km. There seems to be a shift around 2009 for both altitudes, with a lower age in the years after this than in the years before. In addition, there are considerable month-to-month variations (∼2-5 days at 15 km, ∼5-15 days at 17 km); the variations within a year are larger than the decrease over the whole period at both altitudes. There is a seasonal cycle at 15 km, but it is of smaller magnitude than at 17 km and less consistent throughout the period. This may explain why the seasonal differences in the age distribution at 15 km are small (Figure 5.8). At 17 km, a seasonal cycle is clear. The air is oldest in JJA and youngest during DJF and MAM, and the seasonal difference in median age in more than 10 days. This was already noted in Section 5.2.3, but in Figure 5.17 it can be seen that this seasonal difference is relatively similar each year during the period. The exception is the DJF season in 2010-11, when the air is almost as old as in the previous JJA season. The annual peak in median age at 17 km occurs most frequently in August (trajectories releases on 1. September) and the lowest median age is most frequently in April (released 1. May).

Changes of the median age over the period were calculated using linear regression for each time series. Table 5.6 displays the calculated changes using different widths of the latitude band where trajectories were released[2]. There is a decrease in all seasons, and it is present also when restricting the latitude band of releases to the innermost part of the tropics. The absolute decrease is considerably larger at 17 km than at 15 km in all cases. Using the monthly time series, the median age in 30°S - 30°N decreases by 1.6 days per decade at 15 km, and by 9.5 days per decade at 17 km. At 17 km the decrease is largest in JJA and smallest in DJF.

The interannual variability of the percentage of trajectories that are younger than 30 days was also considered. This quantity is closely related to the median age, to which it is anti-correlated:

[1]For example, the monthly values for May 2004 is based on the releases 1. June 2004. Since the age distributions have an overweight on trajectories younger than 30 days (Figure 5.6), most of the transport will be in May, although trajectories also will also originate in March and April.

[2]The plots equivalent to Figure 5.17 for release bands of 20°S - 20°N and 10°S - 10°N can be found in Figure A.1 in the Appendix.

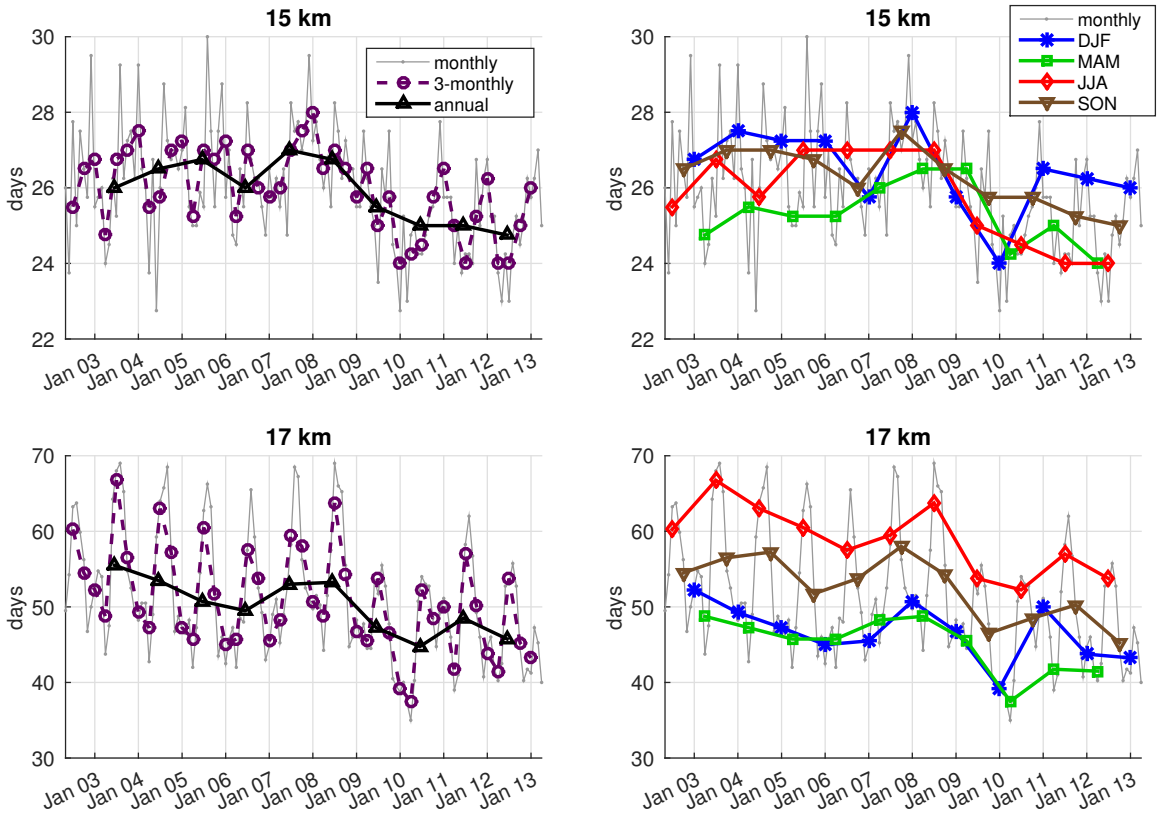

Figure 5.17: Time series of median age of trajectories released between 30°S - 30°N at 15 km (above) and 17 km (below). Left: Time series of median age for each (monthly) release (thin, grey line). The position on the x-axis indicates the month at the end of which the trajectories were released. Also shown is the time series of seasonal (thick, dashed line) and annual (thick, solid line) samples (see Table 5.4). Right: Time series of each season are shown separately.

Sample	15 km		17 km	
	mean	std	mean	std
monthly	26.0	1.5	51.0	7.9
annual	25.9	0.8	50.2	3.6
DJF	26.5	1.1	46.6	3.8
MAM	25.3	0.9	45.1	3.7
JJA	25.8	1.2	58.9	4.6
SON	26.3	0.8	52.4	4.3

Table 5.5: Mean and standard deviation of the monthly, annual and seasonal time series of median age at 15 km and 17 km between 30°S - 30°N for the period 1. June 2002 - 1. May 2013. See Section 5.3.1 for a description of the monthly, seasonal and annual samples.

The lower the median age, the more trajectories are younger than 30 days. This quantity therefore shows largely the same features as the median age (Figure A.2 in the Appendix).

5.3.3 ENSO analysis

In the case study (Section 5.1), the phase of ENSO appeared to have an effect on the age. Now the effect of ENSO on the age is investigated using all 11 years. The SOI is used as a proxy for the phase of ENSO. The monthly SOI for the experimental period is shown in Figure 5.18.

Sample	30°S-30°N		20°S-20°N		10°S-10°N	
	15 km	17 km	15 km	17 km	15 km	17 km
monthly	-1.6	-9.5	-1.5	-8.9	-1.7	-8.4
annual	-2.0	-9.7	-1.7	-8.7	-1.8	-7.8
DJF	-1.6	-6.3	-1.1	-5.8	-0.9	-5.3
MAM	-0.7	-8.8	-0.1	-6.9	-0.1	-5.4
JJA	-2.4	-10.1	-2.5	-10.3	-2.8	-9.9
SON	-1.8	-9.8	-2.1	-8.7	-2.6	-8.4

Table 5.6: Changes of the median age at 15 km and 17 km over the period 1. June 2002 - 1. May 2013 (in days per decade) calculated using linear regression on trajectories released within different latitude bands. See Section 5.3.1 for a description of the monthly, seasonal and annual samples.

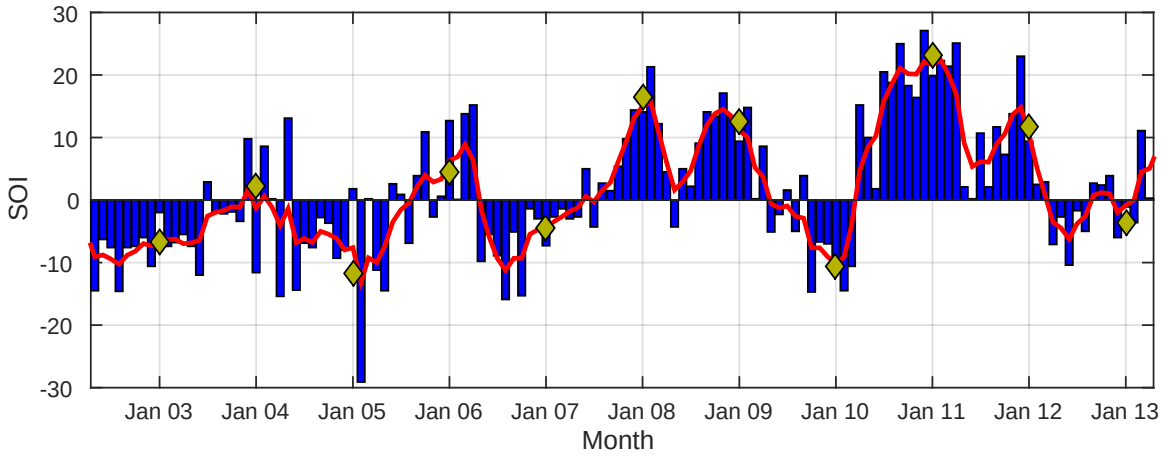

Figure 5.18: Monthly mean Southern Oscillation Index May 2002 - April 2013 (blue bars). The red line is a 5-month weighted average. Yellow diamonds mark the DJF mean. Sustained SOI of less than -8 indicates El Niño conditions, while values above +8 indicates La Niña. The data are taken from Australian Government: Bureau of Meteorology.

During the 11 year period, El Niño conditions prevailed in the DJF seasons of 2004-05 and 2009-10. Both these were of the type El Niño Modoki (Zhang et al., 2011) (see Section 2.2.4). La Niña conditions were present in the DJF seasons 2007-08, 2008-09, 2010-11 and 2011-12. ENSO signals closer to normal were present in the rest of the DJF seasons.

To investigate if some of the interannual variability in the median age can be explained by ENSO, the time series of SOI was compared to that of the median age in 30°S - 30°N. A distinct relationship was only found in DJF. In Figure 5.19, the mean SOI for each DJF season is plotted together with the median age in that season. In the first years of the period, there is not a clear relationship, but from around 2008 they seem more related, with a higher median age in La Niñas than in El Niños. At both altitudes, the El Niño in 2009-10 is accompanied by the lowest median age in DJF in the period, while in the La Niña in the following year the DJF median age is notably higher (by about 2.5 days at 15 km and 10 days at 17 km).

Tropical Pacific

Finally, to investigate if the changing patterns found above the tropical Pacific Ocean in DJF in Section 5.1 can be related to the phase of ENSO, the regions above the tropical Pacific are investigated in more detail using all 11 DJF seasons.

Figure 5.20 shows the relationship between the median age and the SOI for trajectories

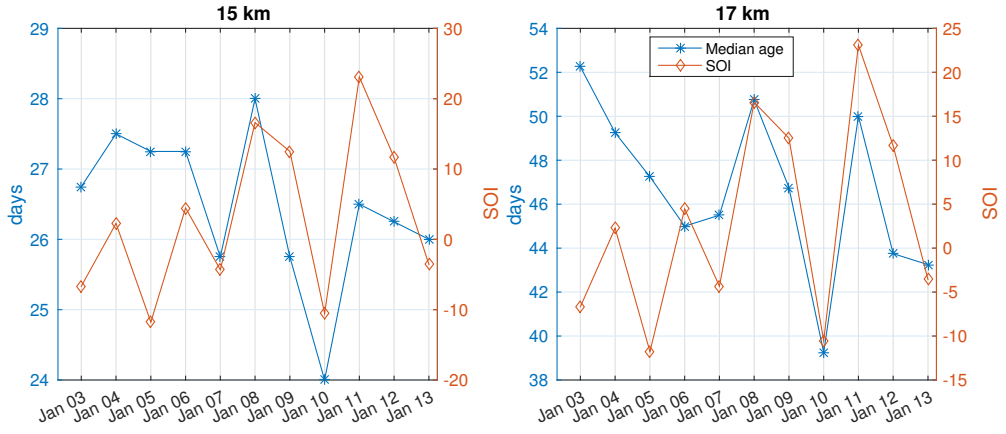

Figure 5.19: Median age for trajectories released at 15 km (left) and 17 km (right) between 30°S - 30°N in each DJF season plotted together with the mean SOI of that season.

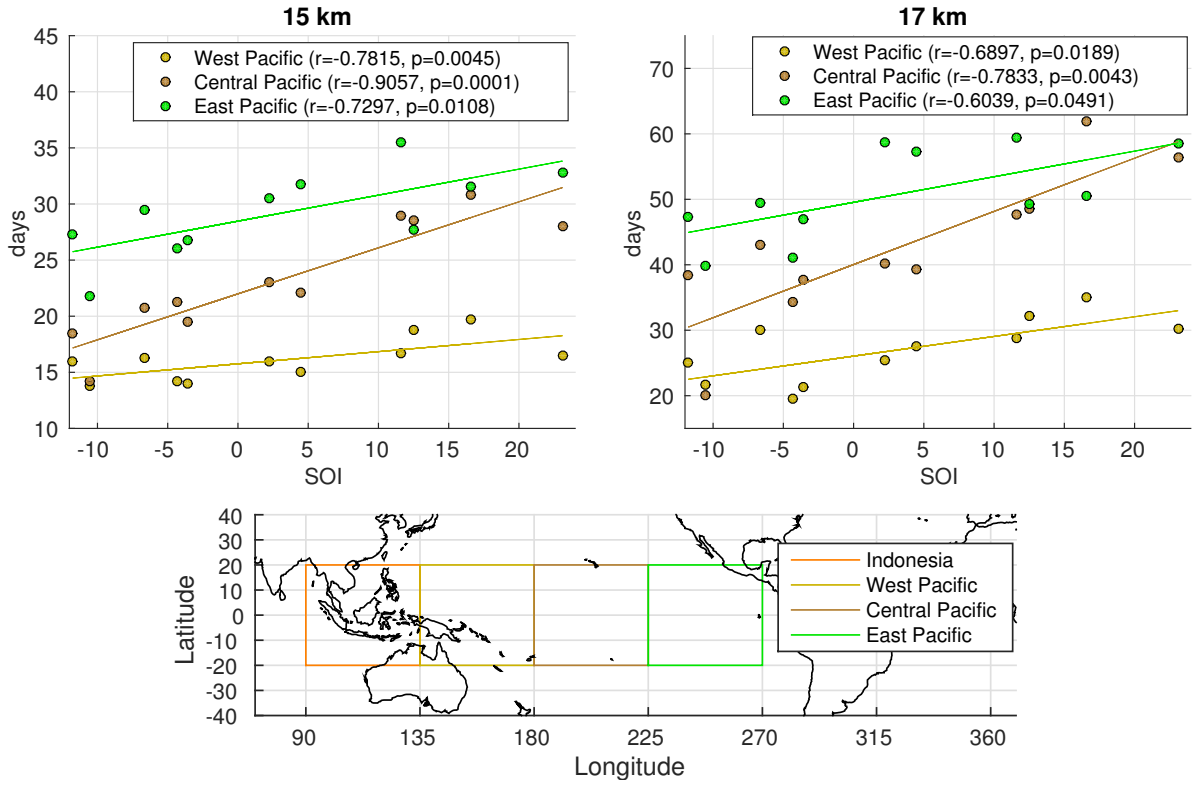

Figure 5.20: For each DJF season from 2002-03 to 2012-13: The percentage of the trajectories released at 15 km (left) and 17 km (right) above each of the regions (see the map below), that are younger than 30 days, plotted against the SOI. Linear regression lines are added, and statistical R- and p-values are written in the legend. The geographical extent of the regions are shown below.

released above different parts of the tropical Pacific. A strong, positive correlation is found for the Central Pacific (brown line). At 15 km the median age above this region is ∼20 days for El Niños and ∼30 days for La Niñas. At 17 km the correlation is weaker, but the median age is clearly higher in the four La Niña events than in the other DJF seasons. Also above the West and East Pacific the median age is lower in El Niños than in La Niñas, both at 15 km and 17 km, although the correlations are not as strong as for the Central Pacific. The median age above Indonesia was uncorrelated with SOI at both altitudes (not shown).

In Figure 5.21 the relative contributions of each region to the origins of trajectories younger

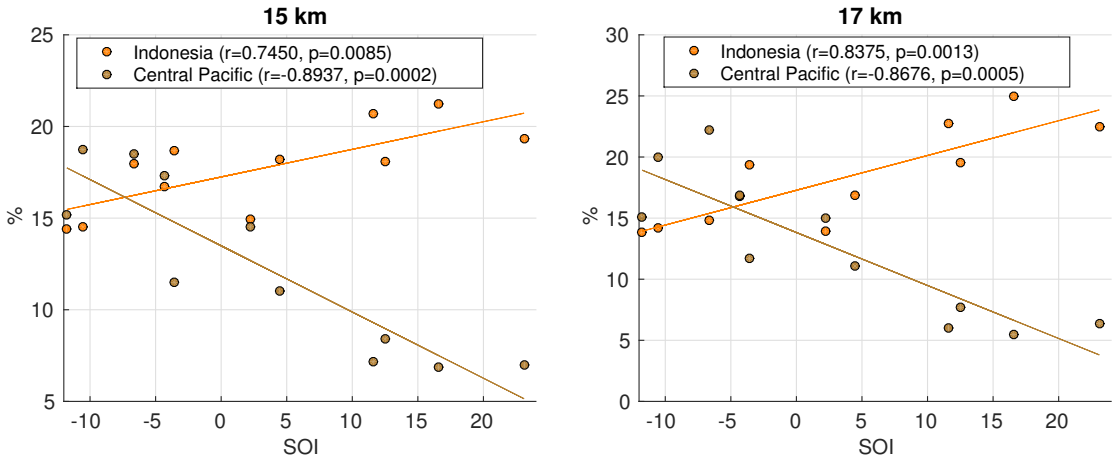

Figure 5.21: For each DJF season from 2002-03 to 2012-13: The percentage of the trajectories released at 15 km (left) and 17 km (right) that have origin within each of the regions (see Fig. 5.20), plotted against the SOI. Only trajectories that are released between 30°S - 30°N and are younger than 30 days are considered, and the percentages are relative to the total number of trajectories younger than 30 days on the respective altitude in each DJF season. Linear regression lines are added, and statistical R- and p-values are written in the legend.

than 30 days are plotted against SOI. The interannual variability is largest in the Central Pacific, where the correlation with SOI is strong: the contribution of this region to the origins for 15 km releases is about twice as large in the El Niños compared to the La Niñas. For 17 km releases, the difference is even larger. The correlation is opposite for Indonesia; during La Niñas, more of the air originate from there (20-25 %) than during El Niños (∼15 %). The relation is similar at 15 km and 17 km. Very few trajectories (<4 %) originate from the East Pacific in all DJF seasons, but there is still a negative correlation with SOI (not shown). For all years, the West Pacific is the region with most origins (25-35 %), and its interannual variability has a weak correlation with the SOI (not shown).

To summarize, the results found in Section 5.1 generalizes to the whole 11 year period. There are more young trajectories above West, Central and East Pacific in El Niño than in La Niña DJF seasons during the period, both at 15 km and 17 km. There is also a shift in the origin locations toward Indinesia during La Niña and a shift toward the Central Pacific during El Niño.

5.3.4 Discussion

The median age in the TTL decreases during the 2002-2013 period (Figure 5.17), the decrease being particularly large at 17 km (∼10 days in 10 years). This could indicate that the transport from the surface to the stratosphere is increasing. However, to conclude that there is a significant trend, a longer time period must be considered. A compicating factor is the increase in the height of the tropical tropopause which has been observed in the last decades, and is believed to be related to global warming (Santer et al., 2003). The age of the air at the tropopause could therefore be decreasing less than the age at 17 km, because the 17 km level becomes more tropospheric with time.

The age above the tropical Pacific in DJF is lower during El Niño events and higher during La Niña events, at both 15 km and 17 km (Figure 5.20). The same relationship was also found when considering the whole 30°S - 30°N (Figure 5.19). The relationship is not clear in the beginning of the period, but this could be because the ENSO events in the first years were less strong than those in the later years (Figure 5.18). These results indicate that the transport from the surface to the stratosphere is faster during El Niño than La Niña. However, longer time series with more pronounced ENSO variability are needed to verify this hypothesis.

During the period 2007-2011 a similar signal as that of DJF is visible also for the annual mean

time series at 17 km, and to some degree also at 15 km (Figure 5.17). The annual mean median ages increase during the 2007-08 La Niña, followed by a strong decrease near the 2009-10 El Niño event, and then a slight increase again during the strong La Niña of 2010-11. Thus it may be interpreted that there is a long-term decrease in the age at 17 km, and that ENSO-related variability is superimposed on this. These two effects could then together cause the apparent step in the median age around 2009 for both altitudes.

Chapter 6

Summary and conclusions

The timescales transport from the surface to the tropical tropopause layer (TTL) were investigated for the period 2002-2013. Backward trajectories driven by ERA-Interim data in the Lagrangian transport model Flexpart were released at 15 km and 17 km and simulated backward in time for 90 days. The transit times from 1 km above sea level, representing the boundary layer (BL) top, to 15 km, close to the level of zero radiative heating (LZRH), and to 17 km, close to the cold point tropopause (CPT), were calculated.

Various sensitivity studies were carried out, and the results from the most important ones are now summarized. The age of air in the TTL was found to be sensitive to the width of the latitude band where trajectories are released because the age increased toward the subtropics. Forward and backward trajectories were compared and found to give similar BL-origins and lift-times to the TTL, although a much smaller percentage of the trajectories fulfilled the transport in the forward approach. The median age of the air was found to increase by 17 days at 15 km and 25 days at 17 km when the Flexpart convection scheme was not used so that vertical transport only relied on the vertical winds from ERA-Interim. In particular, the percentage of the air at 17 km that is younger than 10 days decreased from 11.1 % to 0.9 %.

The climatological median age of air in 30°S - 30°N was found to be 26 days at 15 km and 50 days at 17 km. At 15 km, the seasonal variability in age was relatively small; the median age varied by 1-2 days. At 17 km, more seasonal variability in the age was found; the air is youngest in December-February (DJF) and March-May (MAM), with a median age of ∼45 days, and oldest in June-August (JJA), with median age of ∼59 days. The age, both at 15 km and 17 km, was considerably lower near the equator than closer to the subtropics, and in particular it was low above the western Pacific, the Maritime Continent and Indian ocean. In a separate analysis for the trajectories released above the tropical western Pacific the median age was 16 days at 15 km and 30 days at 17 km; at 17 km varying between ∼27 days in DJF and ∼37 days in JJA.

The climatological BL-origins of the air was found to be similar at 15 km and 17 km and to correspond to the main areas of deep convection in the tropics in each season, the western Pacific being the most striking source region. This, as well as the short lift-times to 15 km, confirms that convection is the most important process for transport from the BL to the TTL. At both altitudes, 40-50 % of the air that has been in contact with the BL during the last 30 days, ascended from the West and Central Pacific, including the Maritime Continent and the South China sea. Other regions of importance were the Indian ocean (10-20 %), India and Bay of Bengal (10 % in JJA) and the Caribean Sea and Central America (∼10 % in JJA and September-November (SON)), while Central Africa and South America also gave some contribution throughout the year.

A decrease over the period of the age of air was found, both at 15 km and 17 km. The decrease in the annual median age during 2003-2012 was 2.0 days per decade at 15 km and 9.7 days per decade at 17 km. Much of this decrease appeared to have taken place around 2009.

Relationships between the phase of the El Niño-Southern Oscillation (ENSO) and the trans-

port to the TTL were found in the DJF season. During El Niño events, the air was younger above the Pacific Ocean than during La Niña events, both at 15 km and 17 km, and there were shifts in the origins, eastward to the Central Pacific in El Niño and westward to the Maritime Continent in La Niña. Moreover, in the annual mean the air in 30°S - 30°N as a whole at 15 km, and even more at 17 km, was found to be anomalously young during the El Niño event in 2009-10, and anomalously old in the La Niña events before and after this, relative to the average decrease of the median age over the period. A long-term decrease combined with ENSO variability can therefore explain the step-like decrease of the median age around 2009 that was identified at both 15 km and 17 km. The decrease in the median age over the period could imply that there is a trend in the age of air in the TTL, which could indicate that the transport from the surface to the stratosphere is getting faster. However, a longer time period is needed to conclude that there is a trend.

Overall, this study confirms that deep convection is the most important process for the tropospheric part of the transport to the tropical tropopause, and that the western Pacific is the most important BL-source for this transport in all seasons. The climatological median age of air in the middle TTL is estimated to 26 days, and to ∼50 days at the tropical tropopause, for the tropics as a whole. Above the tropical western Pacific, these number are 16 and ∼30 days.

For future work, the model setup used in this study could be extended to the whole ERA-Interim period (from 1979). This would enable the identification of a possible trend in the age of air in the TTL, and more cases of El Niño and La Niña could be studied to see if the relationships between ENSO and the timescales found in this study also appear in earlier ENSO events.

Appendix A

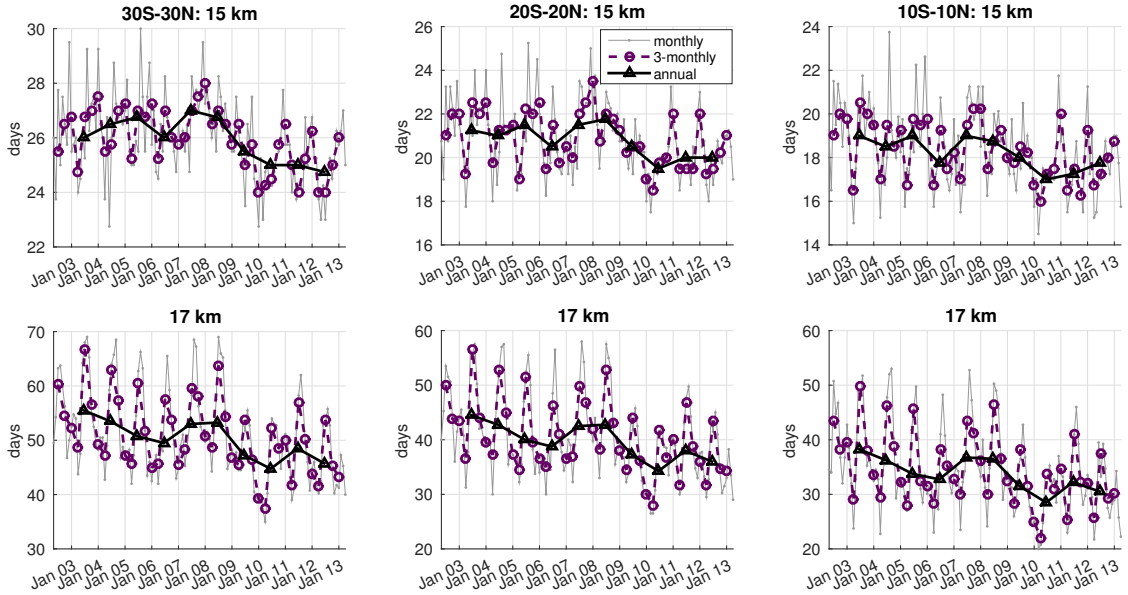

Figure A.1: Time series of median age of trajectories released between 30°S - 30°N (left), 20°S - 20°N (middle) and 10°S - 10°N (right), at 15 km (above) and 17 km (below). Time series of median age for each (monthly) release (thin, grey line). The position on the x-axis indicates the month at the end of which the trajectories were released. Also shown is the time series of seasonal (thick, dashed line) and annual (thick, solid line) samples (see Table 5.4).

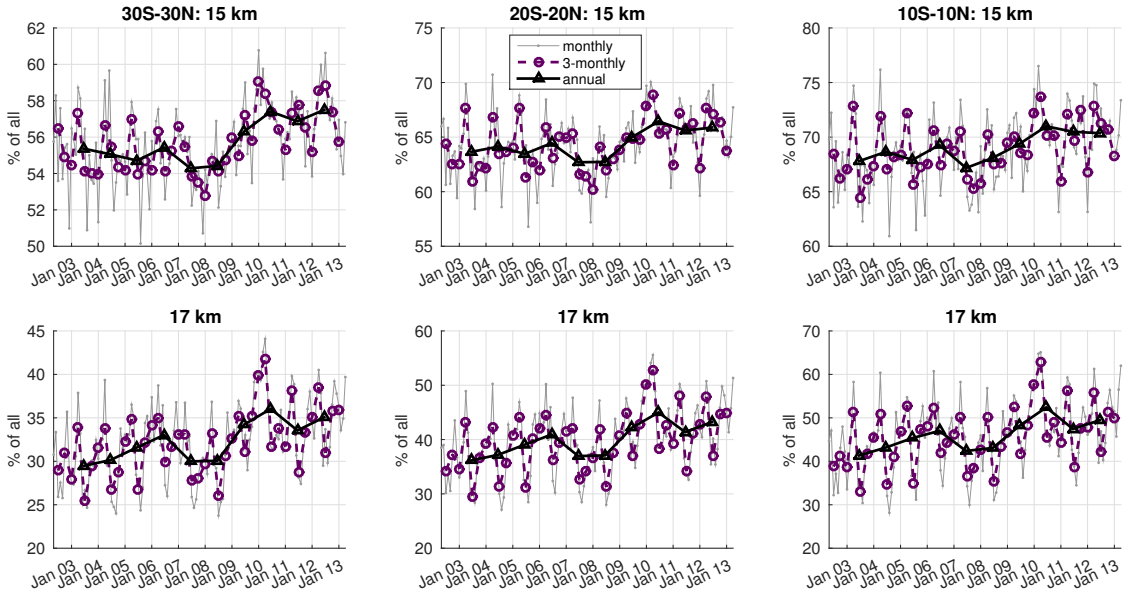

Figure A.2: Time series of the percentage of the trajectories that are younger than 30 days, shown for the same samples as in Figure A.1. The percentage is relative to all trajectories released within the respective latitude band at the respective altitude.

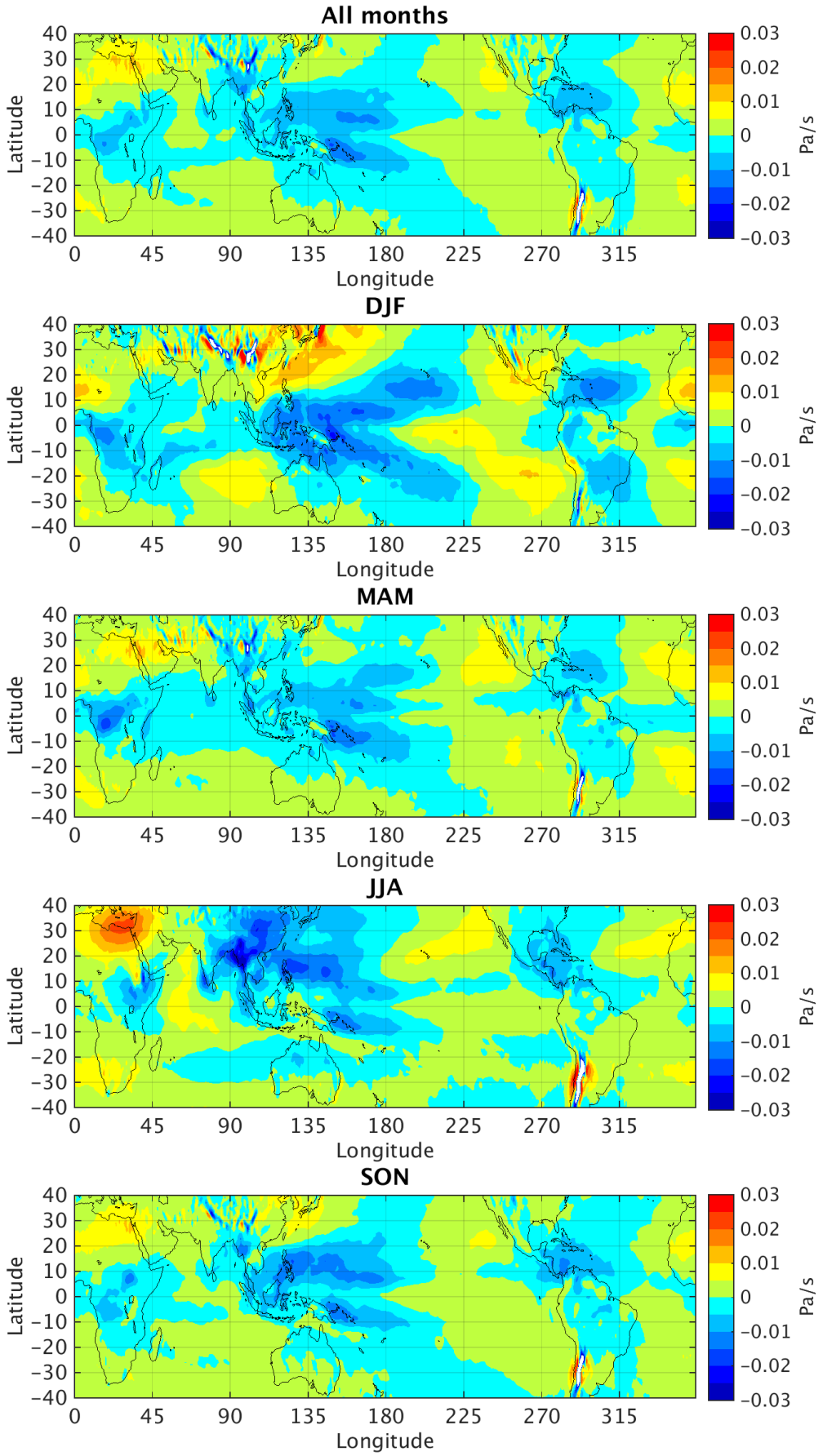

Figure A.3: Vertical velocity (Pa/s) at 125 hPa from ERA-Interim: Mean for the period May 2002 - April 2013. Top: All months. Below: For each season. Note that the velocity is in pressure coordinates, so negative values indicate ascent.

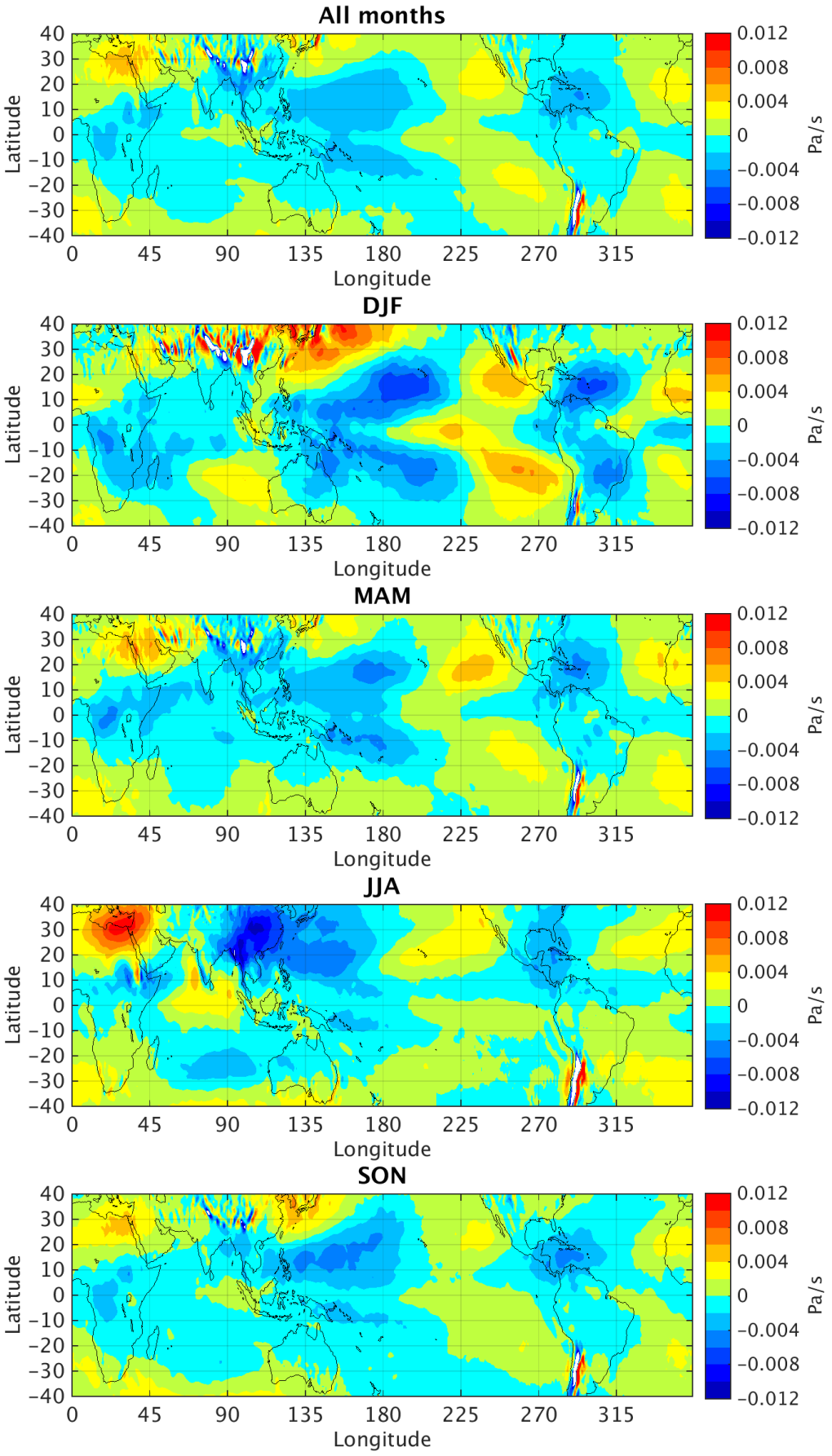

Figure A.4: Vertical velocity (Pa/s) at 100 hPa from ERA-Interim: Mean for the period May 2002 - April 2013. Top: All months. Below: For each season. Note that the velocity is in pressure coordinates, so negative values indicate ascent.

List of acronyms

BDC	Brewer-Dobson Circulation
CAPE	Convective available potential energy
CDF	Cumulative (probability) distribution function
CIN	Convective inhibition
COLA	Center for Ocean-Land-Atmosphere Studies
CPT	Cold point tropopause
DJF	December, January and February
ECMWF	European Center for Medium-range Weather Forecasts
ENSO	El Niño-Southern Oscillation
ITCZ	Intertropical Convergence Zone
JJA	June, July and August
LCL	Lifting condensation level
LFC	Level of free convection
LMS	Lowermost stratosphere
LNB	Level of neutral buoyancy
LZRH	Level of Zero Radiative Heating
MAM	March, April and May
NH	Northern Hemisphere
NILU	Norwegian Institute for Air Research
PDF	Probability distribution function
PR	Precipitation radar
SH	Southern Hemisphere
SLP	Sea level pressure
SOI	Southern Oscillation Index
SON	September, October and November
SST	Sea surface temperature
TRMM	Tropical Rainfall Measurement Mission
TST	Troposphere-to-stratosphere transport
TTL	Tropical tropopuase layer
UTC	Coordinated Universal Time
VSLS	Very short-lived substances
WMO	World Meteorological Organization

Acknowledgements

I want to thank my supervisor Kirstin Krüger for her assistance in understanding the topic of this thesis and for her large efforts in giving me constructive and detailed feedback on my results and on the scientific writing. I will also thank the Norwegian Institute for Air Research (NILU) for providing the pre-processed ERA-Interim data used in Flexpart. My co-supervisor Ignacio Pisso (NILU) has also given me valuable help with understanding the model. The efforts of Anne Fouilloux (University of Oslo) on setting up the Flexpart model and making it work have also been crucial for me to be able to carry out the model runs. I thank my fellow master students at Metos for the good studying environment and for helping me with technical issues.

I also thank my father, and the rest of my family in Norway and Denmark, for supporting me through the years of my study. A great thanks also goes to my fellow residents in the Acem student home; it has been important for me to have the social environment in the house, and I appreciate all the tasty dinners I have been served during the busy months of the thesis work.

Bibliography

Aschmann, J., Sinnhuber, B.-M., Atlas, E., and Schauffler, S. (2009). Modeling the transport of very short-lived substances into the tropical upper troposphere and lower stratosphere. *Atmospheric Chemistry and Physics*, 9(23):9237–9247.

Australian Government: Bureau of Meteorology. Soutern Oscillation index. `http://www.bom.gov.au/climate/current/soi2.shtml`. Accessed: 2014-09-12.

Berthet, G., Esler, J., and Haynes, P. (2007). A Lagrangian perspective of the tropopause and the ventilation of the lowermost stratosphere. *Journal of Geophysical Research: Atmospheres (1984–2012)*, 112(D18). doi:10.1029/2006JD008295.

Bonazzola, M. and Haynes, P. (2004). A trajectory-based study of the tropical tropopause region. *Journal of Geophysical Research: Atmospheres (1984–2012)*, 109(D20).

Brewer, A. (1949). Evidence for a world circulation provided by the measurements of helium and water vapour distribution in the stratosphere. *Quarterly Journal of the Royal Meteorological Society*, 75(326):351–363.

Dee, D., Uppala, S., Simmons, A., Berrisford, P., Poli, P., Kobayashi, S., Andrae, U., Balmaseda, M., Balsamo, G., Bauer, P., et al. (2011). The ERA-Interim reanalysis: Configuration and performance of the data assimilation system. *Quarterly Journal of the Royal Meteorological Society*, 137(656):553–597.

ECMWF. European Center for Medium-Range Weather Forecasts website. `http://old.ecmwf.int/`. Accessed: 2015-04-08.

Emanuel, K. A. and Živković-Rothman, M. (1999). Development and evaluation of a convection scheme for use in climate models. *Journal of the Atmospheric Sciences*, 56(11):1766–1782.

Forster, C., Stohl, A., and Seibert, P. (2007). Parameterization of convective transport in a Lagrangian particle dispersion model and its evaluation. *Journal of Applied Meteorology and Climatology*, 46(4):403–422.

Fueglistaler, S., Bonazzola, M., Haynes, P., and Peter, T. (2005). Stratospheric water vapor predicted from the Lagrangian temperature history of air entering the stratosphere in the tropics. *Journal of Geophysical Research: Atmospheres (1984–2012)*, 110(D8). doi:10.1029/2004JD005516.

Fueglistaler, S., Dessler, A., Dunkerton, T., Folkins, I., Fu, Q., and Mote, P. W. (2009). Tropical tropopause layer. *Reviews of Geophysics*, 47(1). doi:10.1029/2008RG000267.

Fueglistaler, S., Wernli, H., and Peter, T. (2004). Tropical troposphere-to-stratosphere transport inferred from trajectory calculations. *Journal of Geophysical Research: Atmospheres (1984–2012)*, 109(D3). doi:10.1029/2003JD004069.

Gettelman, A., Forster, P. M. d. F., Fujiwara, M., Fu, Q., Vömel, H., Gohar, L. K., Johanson, C., and Ammerman, M. (2004). Radiation balance of the tropical tropopause layer. *Journal of Geophysical Research: Atmospheres (1984–2012)*, 109(D7). doi:10.1029/2003JD004190.

Gettelman, A., Salby, M., and Sassi, F. (2002). Distribution and influence of convection in the tropical tropopause region. *Journal of Geophysical Research: Atmospheres (1984–2012)*, 107(D10):ACL–6. doi:10.1029/2001JD001048.

Hartmann, D. L. (1994). *Global Physical Climatology*. Elsevier Academic Press.

Holton, J. R., Haynes, P. H., McIntyre, M. E., Douglass, A. R., Rood, R. B., and Pfister, L. (1995). Stratosphere-troposphere exchange. *Reviews of Geophysics*, 33(4):403–439.

Ivanova, A. (2013). The tropopause: Variety of definitions and modern approaches to identification. *Russian Meteorology and Hydrology*, 38(12):808–817.

Jacob, D. J. (1999). *Introduction to Atmospheric Chemistry*. Princeton University Press, New Jersey, 266pp.

Kim, W., Yeh, S.-W., Kim, J.-H., Kug, J.-S., and Kwon, M. (2011). The unique 2009–2010 El Niño event: A fast phase transition of warm pool El Niño to La Niña. *Geophysical Research Letters*, 38(15).

Krüger, K., Tegtmeier, S., and Rex, M. (2008). Long-term climatology of air mass transport through the tropical tropopause layer (TTL) during NH winter. *Atmospheric Chemistry and Physics*, 8(4):813–823.

Levine, J., Braesicke, P., Harris, N., and Pyle, J. (2008). Seasonal and inter-annual variations in troposphere-to-stratosphere transport from the tropical tropopause layer. *Atmospheric Chemistry and Physics*, 8(13):3689–3703.

Levine, J. G., Braesicke, P., Harris, N. R. P., Savage, N. H., and Pyle, J. A. (2007). Pathways and timescales for troposphere-to-stratosphere transport via the tropical tropopause layer and their relevance for very short lived substances. *Journal of Geophysical Research: Atmospheres (1984–2012)*, 112(D4).

Liu, C. and Zipser, E. J. (2005). Global distribution of convection penetrating the tropical tropopause. *Journal of Geophysical Research: Atmospheres (1984–2012)*, 110(D23). doi:10.1029/2005JD006063.

Liu, C., Zipser, E. J., and Nesbitt, S. W. (2007). Global distribution of tropical deep convection: Different perspectives from TRMM infrared and radar data. *Journal of Climate*, 20(3):489–503. doi:10.1175/JCLI4023.1.

Marshall, J. and Plumb, R. A. (2008). *Atmosphere, Ocean and Climate Dynamics: An Introductory Text*. Elsevier Academic Press.

Monge-Sanz, B., Chipperfield, M., Simmons, A., and Uppala, S. (2007). Mean age of air and transport in a CTM: Comparison of different ECMWF analyses. *Geophysical Research Letters*, 34(4).

Montzka, S. A., Reimann, S., Engel, A., Krüger, K., O'Dothery, S., Sturges, W. T., et al. (2010). Chapter 1: Ozone-depleting substances (ODSs) and related chemicals. In *Scientific Assessment of Ozone Depletion: 2010, Global Ozone Research and Monitoring Project-Report No. 52*. World Meteorological Organization, 516pp.

Newell, R. E. and Gould-Stewart, S. (1981). A stratospheric fountain? *Journal of the Atmospheric Sciences*, 38(12):2789–2796.

Park, S., Jiménez, R., Daube, B., Pfister, L., Conway, T., Gottlieb, E., Chow, V., Curran, D., Matross, D., Bright, A., et al. (2007). The CO_2 tracer clock for the tropical tropopause layer. *Atmospheric Chemistry and Physics*, 7(14):3989–4000.

Patra, P., Takigawa, M., Dutton, G., Uhse, K., Ishijima, K., Lintner, B., Miyazaki, K., and Elkins, J. (2009). Transport mechanisms for synoptic, seasonal and interannual SF_6 variations and "age" of air in troposphere. *Atmospheric Chemistry and Physics*, 9(4):1209–1225.

Pisso, I., Haynes, P., and Law, K. S. (2010). Emission location dependent ozone depletion potentials for very short-lived halogenated species. *Atmospheric Chemistry and Physics*, 10(24):12025–12036.

Ploeger, F., Konopka, P., Günther, G., Grooß, J.-U., and Müller, R. (2010). Impact of the vertical velocity scheme on modeling transport in the tropical tropopause layer. *Journal of Geophysical Research: Atmospheres (1984–2012)*, 115(D3).

Rex, M., Wohltmann, I., Ridder, T., Lehmann, R., Rosenlof, K., Wennberg, P., Weisenstein, D., Notholt, J., Krüger, K., Mohr, V., et al. (2014). A tropical West Pacific OH minimum and implications for stratospheric composition. *Atmospheric Chemistry and Physics*, 14(9):4827–4841.

Sabin, T., Babu, C., and Joseph, P. (2013). SST–convection relation over tropical oceans. *International Journal of Climatology*, 33(6):1424–1435.

Santer, B. D., Wehner, M. F., Wigley, T., Sausen, R., Meehl, G., Taylor, K., Ammann, C., Arblaster, J., Washington, W., Boyle, J., et al. (2003). Contributions of anthropogenic and natural forcing to recent tropopause height changes. *Science*, 301(5632):479–483.

Seidel, D. J., Ross, R. J., Angell, J. K., and Reid, G. C. (2001). Climatological characteristics of the tropical tropopause as revealed by radiosondes. *Journal of Geophysical Research: Atmospheres (1984–2012)*, 106(D8):7857–7878.

Stohl, A., Sodemann, H., Eckhardt, S., Frank, A., Seibert, P., and Wotawa, G. (2011). The Lagrangian particle dispersion model FLEXPART version 8.2. *FLEXPART user guide, url: http://zardoz. nilu. no/flexpart/flexpart/flexpart82. pdf (March 14, 2012)*.

Stull, R. B. (1988). *An Introduction to Boundary Layer Meteorology*. Kluwer Academic Publishers.

Waliser, D. E. and Gautier, C. (1993). A satellite-derived climatology of the ITCZ. *Journal of Climate*, 6(11):2162–2174.

Waliser, D. E. and Graham, N. E. (1993). Convective cloud systems and warm-pool sea surface temperatures: Coupled interactions and self-regulation. *Journal of Geophysical Research: Atmospheres (1984–2012)*, 98(D7):12881–12893.

Wallace, J. M. and Hobbs, P. V. (2006). *Atmospheric Science*. University of Washington, 483pp, 2 edition.

Waugh, D. and Hall, T. (2002). Age of stratospheric air: Theory, observations, and models. *Reviews of Geophysics*, 40(4):1–1.

Wohltmann, I. and Rex, M. (2009). The Lagrangian chemistry and transport model ATLAS: validation of advective transport and mixing. *Geoscientific Model Development*, 2:153–173.

Yeh, S.-W., Kug, J.-S., Dewitte, B., Kwon, M.-H., Kirtman, B. P., and Jin, F.-F. (2009). El Niño in a changing climate. *Nature*, 461(7263):511–514.

Zhang, C. (1993). Large-scale variability of atmospheric deep convection in relation to sea surface temperature in the tropics. *Journal of Climate*, 6:1898–1913.

Zhang, W., Jin, F.-F., Li, J., and Ren, H.-L. (2011). Contrasting impacts of two-type El Niño over the western North Pacific during boreal autumn. *Journal of the Meteorological Society of Japan*, 89(5):563–569.